Seasonal Underground Heat Storage

B.P. Ter Meulen

Sustainable Energy Technology Student nr. 4255054 TU-Delft Supervisor: C.A. Infante Ferreira

ISBN 000-00-0000-000-0



Seasonal Underground Heat Storage

by

B.P. Ter Meulen

to obtain the degree of Master of Science at the Delft University of Technology, to be defended publicly on Friday May 29, 2020 at 14:30 pm.

Student number: 4255054

Project duration: March 1, 2019 – May 29, 2020

Thesis committee: Dr. Ir. C.A. Infante Ferreira, TU Delft, supervisor

Dr. Ir. M. Randin, TU Delft Dr. Ir. S. C. Jansen, TU Delft

This thesis is confidential and cannot be made public until May 29, 2025.

An electronic version of this thesis is available at http://repository.tudelft.nl/.





i

Abstract

This study aims to assess the role and need of (seasonal) thermal energy storage in the next generation renewable, and sustainable central heating systems for the built environment in the Netherlands. Specifically, the neighbourhood "Karwijhof" in the city Nagele which is transitioning to a collective renewable district heating network incorporating 24 users. The emphasis of this study lies on the technology for storing thermal energy and two different heat collection technologies. The storage of heat is done using an underground seasonal thermal energy storage (USTES), in this case an underground sensible heat storage tank using water as storage medium. The system relies on a small scale district heating network (DHN) for the distribution of heat.

For this research two heat collection technologies are considered resulting in two systems to be compared, both incorporating the USTES as main system component. The first system relies on heat collection by solar thermal collectors, the second on an air-water heat pump. Both systems are modelled in the Matlab-Simulink software environment and back tested on historic (publicly available) weather data provided by the Royal Dutch meteorological institute (KNMI).

Different system sizes are tested on their key performance indicators through an iterative process. System sizes depend on the capacity of the main components which include: volume of the USTES, surface area of the solar thermal collectors, and air-water heat pump capacity. Key performance indicators include the levelised cost of heat (LCOH) and the seasonal coefficient of performance of the system which gives an indication on the autonomy of the system. To increase the autonomy of the systems a photo-voltaic (PV) array is considered for both systems to offset the electricity use. However, the systems are allowed to exchange electricity with the grid translating into the goal of "zero on the meter" autonomy.

The model results show a mismatch between heat demand and generation. Demand peaks during winter from December-March while generation peaks during the summer months May-August. The USTES is needed to overcome this mismatch and ensure access to heat throughout the year.

The results show that both systems can ensure heat throughout the year for the users considered during this study. However, systems cannot compete with traditional natural gas heating systems based on the LCOH. This is partly due to the high cost of the district heating network. The systems including a PV array show a LCOH that can compete with the traditional natural gas HR-boiler but are constraint by the rooftop area available during this study leading to a non competitive LCOH. Though, even with enough rooftop area for a PV array the systems cannot pay them self back relative to the base scenario due to the financing costs. During the study no subsidies were taken into account. Subsidies will be needed to make the renewable energy systems presented in this study financially more attractive in the short term. When considering the environmental benefits it can be argued that the systems are already competitive to the traditional natural gas heating systems.

Further studies should focus on efficiency gains in the district heating network and the control mechanism of the air-water heat pump. It is expected that the LCOH of systems as proposed in this study will decline in the future as a result of cost reductions and/or efficiency increases of the system components. Also, a lower LCOH is deemed achievable for neighbourhoods with simpler district heating networks (i.e. less meters of DHN piping per user).

List of Abbreviations

BoS Balance of System

BTES Borehole Thermal Energy Storage

CAPEX Capital Expenditures

CBS (Dutch) Central Bureau of Statistics

COP Coefficient of Performance

DHI Diffuse Horizontal Irradiation

DNI Direct Normal Irradiation

DHN District Heating Network

ETC Evacuated Tube Collector

EPDM Ethyleen-Propyleen-Dieen-Monomeer

FPC Flat Plate Collector

GHG Green House Gas

GHI Global Horizontal Irradiation

GWP Global Warming Potential

HP Heat Pump

IAM Incidence Angle Modifier

KNMI Royal Dutch Meteorological Institute

KPI Key Performance Indicator

LCOH Levelised Cost of Heat

OPEX Operational Expenditures

PIR Polyisocyanurate

PUR Polyurethane

PV Photo-voltaic

R600a Iso-butane

SCOP Seasonal Coefficient of Performance

STES Seasonal Thermal Energy Storage

TEWI Total Equivalent Warming Impact

USTES Underground Seasonal Thermal Energy Storage

WACC Weighted Average Cost of Capital

XPS Extruded Polystyrene



Nomenclature

 \boldsymbol{A} Surface area [m²] Altitude [-] a_s Azimuth [-] A_s Heat capacity $[Jkg^{-1}K^{-1}]$ c_p dThickness [m] EEnergy [J] Long wave irradiance [Wm⁻²] E_L Zero loss efficiency [-] $F'(\tau \alpha)_{en}$ FFFill factor [-] GIrradiation [Wm⁻²] Direct (beam) radiation [Wm⁻²] G_b Diffuse radiation [Wm⁻²] G_d Enthalpy [Jkg⁻¹] hElectric current [A] Ι Incident angle modifier for the direct (beam) radiation [-] $K_{\theta b}$ Incident angle modifier for the the diffuse radiation [-] $K_{\theta d}$ l Length [m] L Leak rate [kga-1] Mass flow [kgs⁻¹] ṁ Mass [kg] mNumber of operating hours [-] Diode quality factor [-] Number [-] N Pressure [bar] Power [W] Elementary charge [C] q Q Heat [J] Heat flow [kW] Radius [m] Interest rate [%] Heat transfer resistance [m²KW⁻¹] R

t Time [hour]

T Temperature [K]

U Overall heat transfer coefficient $[Wm^{-2}K^{-1}]$

w Wind speed [ms⁻¹]

x Width bottom of USTES

X Width top of USTES

y Length bottom of USTES

Y Length top of USTES

z Height [m]

Greek Symbols

 Δ Difference [-] η Efficiency [-]

 θ Angle of module [°]

 κ Temperature coefficient [-/° C] λ thermal conductivity [Wm⁻¹K⁻¹]

 λ_S Sun's ecliptic longitude [°]

 ϕ_0 Location latitude [°] $\tau \alpha$ Zero loss efficiency [-] γ Angle of incidence [°]

 ϵ Axial tilt [°]

 σ Stefan Boltzmann constant in [Wm $^{-2}$ K $^{-4}$]

 ρ Density [kgm⁻³]

Subscripts

ambAmbientBeam

BoS Balance of system

C Source

compCompressorcondCondenserdDiffuseeffEffective

env Environment

end End of life evap Evaporator

hp Heat pump

hx Heat exchanger

 $egin{array}{ll} H & {
m Sink} \\ i & {
m Inside} \\ in & {
m In} \\ \end{array}$

is Isentropic L Long wave

m MeanM Modulemax Maximum

mpp Maximum power point

NOCT Nominal operating cell temperature

OC Open circuit

out Out

ref Refrigerant

S Sun

SC Short circuit

STC Standard test conditions

y Year



Contents

	Ab	ostrac	t	ii
I	Int	trodu	ction to the Problem Statement	1
	oduction	3		
	2	Scop	oe e	5
			Thesis Description	5
			Research Goals	6
			Methodology	8
		2.4	Limitations of the Study	9
	3		e of the Art	11
		3.1	Current Heating Systems	11
		3.2	The Need for Storage	12
			6, 1 de 1, 1 d	12
			3.2.2 Solar Thermal Collectors	13
			0, 0,	15
			3.2.4 Heat Pumps	19
			Cost Outlook of System Components	21
			Key Performance Indicators	
		3.5	Modelling Environment	24
	4	Heat	t Demand of Dutch Households	25
		4.1	Demand Profile	25
		4.2	Climate Effect on Energy Demand	25
		4.3	Modelling the Heating Demand	28
П	N/	lodolli	ing the System Components	29
"				
	5			31
			Underground Seasonal Thermal Energy Storage	
			5.1.1 Structural Layout of the USTES	
			U	33
			· · · · · · · · · · · · · · · · · · ·	33
			5.1.4 Heat Losses	33
			8,	34
			5.1.6 Auxiliary Heating	
			District Heating Network	
			5.2.1 Thermal Losses	
			5.2.2 Pump Electricity Consumption	
			Solar Thermal Collector	
			5.3.1 European Standard EN 12975-2	39
			5.3.2 Incidence Angle Modifier	39
			5.3.3 Positioning of the Solar Thermal Collectors	40
			5.3.4 Solar Resource	41
			5.3.4 Solar Resource	41 41
			5.3.4 Solar Resource Solar Resource 5.3.5 Shading Data Acquisition	41 41 42
			5.3.4 Solar Resource	41 41 42 44

Contents xi

		5.4.2 Temperature Effects	5
		5.4.3 Balance of System	6
		5.4.4 Power Output	6
	5.5	Heat Pump	7
		•	17
		•	18
			19
		r - J	60
			51
		•	52
			52
		<u> </u>	
		5.5.8 Expansion Device	52
6	Syst	tem design 5	3
	6.1	System Design 1: Solar Collector Based System	3
	6.2		
		6.2.1 Control Sequence	
	6.3	•	57
	6.4	Modelling the System Components	
	0.1		61
			61
		6.4.3 Solar Collector	
		6.4.4 Angle of Incidence	
		6.4.5 Heat Pump	ю
7	Cos	t of Components 6	7
	7.1	Cost of the USTES	7
		Cost of the Heat Pump	7ز
		<u>-</u>	67
	7.4	·	8
	7.5		8
	7.6		8
	7.7	=	8
	7.8	Cost of Electricity	
		Levelised Cost of Heat.	
	1.3	Levelised Cost of fleat.	J
ш	Evalu	ation 7	1
8	Vali	•	3
	8.1	Demand Validation	3
	8.2	Solar Collector Validation	3
	8.3	PV Array	4
	8.4	USTES	4
	8.5	Air-Water Heat Pump	8
0	Doo	ماريد	1
9	Res		1
			31
	9.2		33
		•	33
		1 1	34
		1 1	86
	9.3	0 , 1	88
		9.3.1 Optima of the Solar Collector Based System	88
		9.3.2 Optima of the Air-Water Heat Pump Based System	0
	9.4	CAPEX of the Systems	92
	9.5		93
	9.6	· · · · · · · · · · · · · · · · · · ·	96

Contents xii

0 Discussion	97
10.1 Determining the Optimal System Configurations	97
10.2 Simulation of the Optimal System Sizes	98
10.3 Cost Competitiveness	01
10.4 Payback Period	01
10.5 Research Limitations	03
10.5.1 Limitations in the Data Analysis	03
10.5.2 Limitations of the Model	04
10.6 Recommendations	04
1 Conclusion 1	05
ibliography 1	09



I

Introduction to the Problem Statement

Introduction

In recent years climate change has gained more awareness among the public and has become an everyday important topic in regional and world politics. Due to the Paris climate agreement of 2016 the pressure to transition to a sustainable and renewable energy future has been increasing.

Since the Paris agreement countries have been moving towards even more ambitious goals on reducing their greenhouse gas emissions and increase energy efficiencies. In Europe this resulted in the proposition of the 'European Green Deal' setting ambitious goals for various energy consuming sectors including the energy efficiency of the built environment. On this topic the European Commission stated:

"The Commission will rigorously enforce the legislation related to the energy performance of buildings [10]."

The Netherlands as part of the European Union will take part in the efforts to increase energy efficiency of buildings. However, the Dutch government has more incentives to start the transition from fossil fuels to renewable energy. Historically buildings in the Netherlands are heated by fossil resources extracted from the Dutch subsurface. This started in the late 19th century with the burning of coal mined in the Limburg province. With the discovery of the largest natural gas field of Europe - the Groningen gas field - in 1959, the heating of buildings transitioned from burning of coal to central heating systems relying on natural gas. However, lately resistance to the gas drilling is growing due to earthquakes as a result of the extraction of natural gas. Politicians are forced to close down the Groningen gas field making the Netherlands dependent on foreign natural gas for its buildings heating demand.

These factors result in the fact that the Netherlands is accelerating its efforts to transition the heating demand of buildings towards renewable energy. The government offers incentives and is funding innovative projects to investigate what solutions are available. The transition is not only enforced by providing subsidies but also in new legislation. For instance, as of the first of July 2018 newly built houses are prohibited to rely on gas for heating purposes. However, the main challenge lies in the transition of the roughly 6-7 million existing buildings with low energy efficiency that are still relying on natural gas for space heating.

For existing buildings the transition is more difficult compared to new built homes since systems that are already in place need to be altered to sustain the same level of comfort at a cost competitive price. Another challenge in the transition is the "dunkelflaute" period, a period in which little energy can be generated with renewable resources due to lack of wind and/or sunlight. The company HoCoSto proposes a method to overcome such periods by introducing a seasonal sensible heat storage tank installed underground. This storage is able to store heat during periods where energy can be generated for instance during summer and use this heat later to serve the heating demand through a small scale district heating network.

This research aims to investigate whether a neighbourhood can rely on a small scale district heating network with local seasonal heat storage and to compare two different thermal energy harnessing methods to charge the storage tank and find the most cost effective solution. The first system relies on solar collectors for its heat generation. The second uses an air-water heat pump to move energy/heat from ambient air to the storage tank.

The research starts with a literature study in chapter 3. Next the heating demand of Dutch households will be discussed in chapter 4. The system components will be discussed in chapter 5. Based on these system components a system design is presented in chapter 6. Cost estimates of the components are given in chapter 7.

The model is validated for its reliability in chapter 8. Then results of the model are presented in chapter 9 which are discussed in chapter 10. Finally conclusions of the study are presented in chapter 11.

2

Scope

2.1. Thesis Description

In cooperation with the Dutch government a feasibility project is started to evaluate the opportunity for heating of existing buildings with renewable energy. This project carries the name 'Energiek Nagele'. The houses were built in the 1950's and currently rely on natural gas for their space heating. Due to climate agreements and the pledge to reduce carbon dioxide emissions, the Dutch government seeks to transition the built environment of the Netherlands from fossil fuel energy to renewable energy during the coming decade.

The main goal of renewable central heating systems is the reduction of greenhouse gas (GHG) emissions. The advancements in renewable energy technologies and cost reductions enable the start of the transition to renewable and sustainable central heating for the built environment in the Netherlands. Though, due to the intermittent nature of renewable energy sources, an energy storage solution is needed to ensure energy availability at all times.

The work presented in this thesis aims to compare two approaches to facilitate seasonal (renewable) thermal energy storage systems. This study proposes two system configurations using thermal energy harnessing technologies in combination with the central component which is the underground seasonal thermal energy storage (USTES). The first system is relies on solar thermal collectors for thermal energy collection. The second system will use an air-water heat pump to collect heat. Both systems have an USTES to overcome "Dunkelflaute", a period where due to lack of wind or sunshine no renewable energy can be generated. The solar collectors experience this effect during cold periods with little sunshine, the heat pump is effected during times with low ambient temperatures.

Thermal energy storage in combination with solar thermal collectors

This system, presented in figure 2.1, starts by collecting heat in solar thermal collectors during summer. The collector arrays are installed on the rooftop of buildings and connected with the USTES by a district heating network (DHN). With an insulated district heating network heat, generated by the collectors, will be collected into the USTES. Here the energy will be stored as sensible heat in water for later use during winter. A water-water heat pump will be installed using the USTES as its source medium to increase the exergy of the USTES.

2.2. Research Goals 6

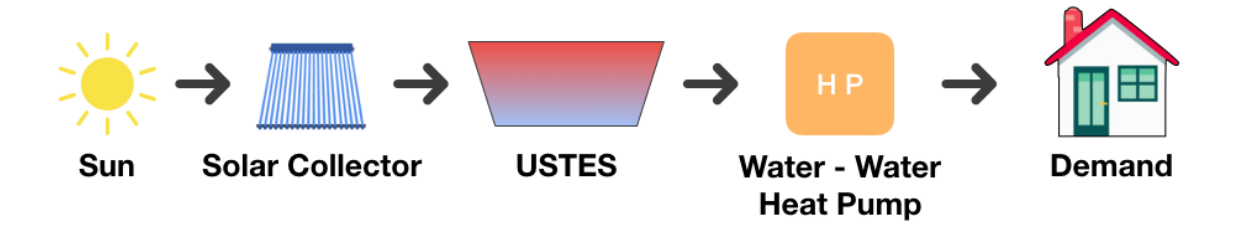


Figure 2.1: System one, with a solar collector array as main heat source. A USTES is used as heat storage and a water-water heat pump is installed in order to increase the exergy of the USTES.

Thermal Energy Storage using a Central Heat Pump

The alternative system presented in figure 2.2 relies on a central air-water heat pump extracting heat from ambient air and delivering this heat to a heat sink, in this case the USTES. The heat pump will only operate during periods where its coefficient of performance is above a certain threshold. This means the heat pump is turned off during periods of low ambient temperature. During these periods the USTES will cover the heating demand of the households. In this system also a water-water heat pump will be installed to increase the exergy of the USTES. Photo-voltaic (PV) panels will deliver electricity for the heat pump when possible. However it will not be a fully autonomous system since exchange of electrons with the grid will be allowed resulting in a "zero on the meter" system.

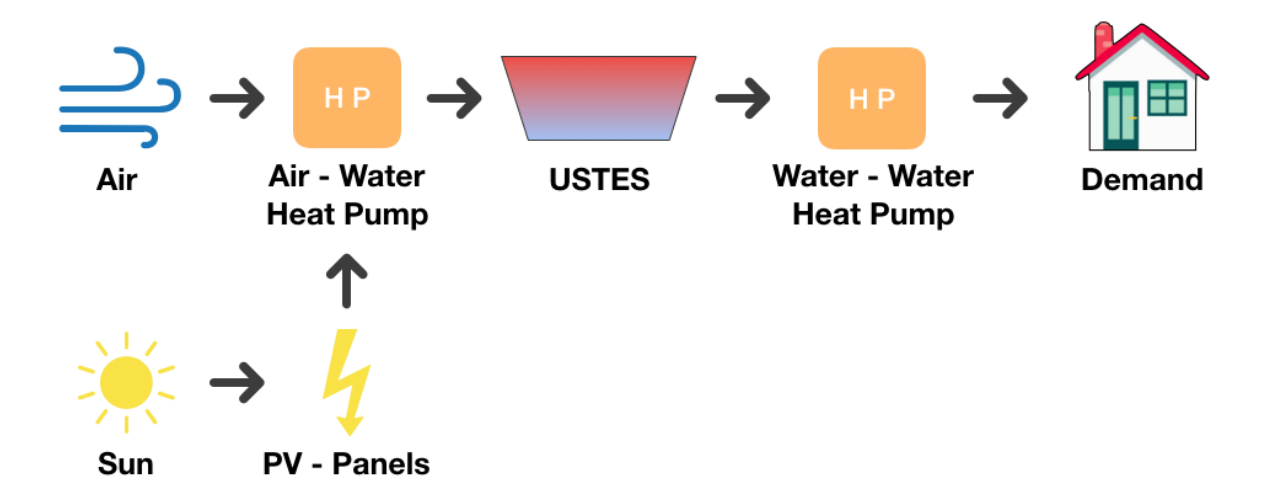


Figure 2.2: System two, with an air-water heat pump as main heat source. An USTES is used as heat storage and a water-water heat pump is installed in order to increase the exergy of the USTES.

2.2. Research Goals

The work in this thesis is based on a real life test case in the Dutch neighbourhood Karwijhof in the city Nagele. The main question is:

"Can a small scale district heating network operate year round based on renewable energy combined with a local seasonal heat storage?"

The secondary goal of this research is to determine the preferred method for harnessing energy to provide heat to the households during winter.

The research is done to evaluate the best possible solution for the particular set of households at Karwijhof Nagele. All systems are modelled in Simulink in combination with Matlab. The models are used to achieve the following goals:

2.2. Research Goals 7

• Develop a model representing the neighbourhoods energy consumption related to the local climate, i.e. the local temperature, throughout the year (degree days).

- Develop a model to present the location of the sun in the sky. This is linked to a model of a solar collector array resulting in an energy output throughout the year based on open source weather data. The same will be done for the electricity generation using PV panels.
- Develop a model of an USTES with in- and output of energy flows while considering heat losses and conduction.
- Develop a model of an air-water heat pump optimised for the application of moving heat into the USTES at high temperatures.
- Combine all model components to create a simulation of the two proposed systems so that both can be compared.
- Determine what energy harnessing technology is preferred for the application of delivering heat to the USTES considering the key performance indicators proposed in this study.

and give answer to the following research questions:

- What efforts have been undertaken on the subject of seasonal heat storage?
- What modelling environment can be used to simulate a district heating network system?
- Can a small scale district heating network which relies on seasonal energy storage fully replace a natural gas fired heating infrastructure?
- Does the system perform better by harnessing heat through use of solar collectors or by using a heat pump in combination with PV-panels?
- What is the optimal size of the systems components based on cost per unit of energy?
- Is the system cost competitive with alternative heating options like the standard heating system based on natural gas or a large scale district heating network? Which of the systems is the most cost competitive? This will be based on the levelised cost of heat of the systems (LCOH).
- What is the payback time of the systems.
- What is the future outlook of the proposed USTES systems in terms of technology improvement and market opportunities.

2.3. Methodology 8

2.3. Methodology

This study investigates an alternative to conventional fossil fuel powered central heating systems for the Dutch built environment. It is a quantitative research partly based on public data and partly based on data provided by the participating stakeholders.

The study incorporates a Simulink/Matlab model description of the systems introduced. The simulations of these systems generate results on both thermodynamic and financial aspects, which will be used to discuss the validity of the proposed central heating systems. The historic data used are from the years 2015-2020. Hence, the systems are back tested for a five year time period.

Figure 2.3 gives an outline of the structure of the study. It can be broken down into three parts: the first part covers the problem statement, state of the art, system components, and the key performance indicators. The second part describes models of the components and the combined system model. The third and final part evaluates the work in this study and concludes whether the systems proposed will be able to deliver renewable energy in a cost competitive and sustainable way.

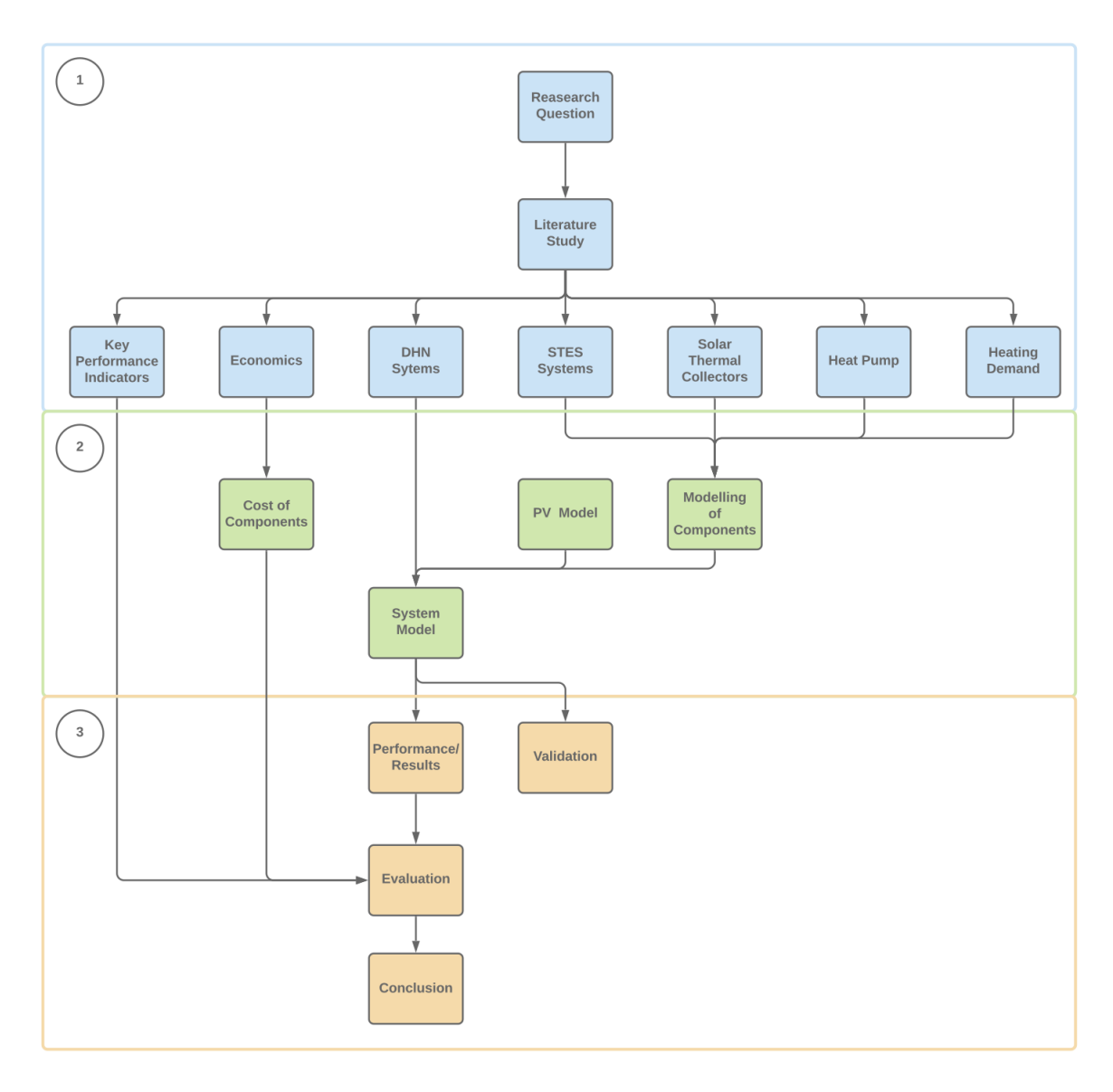


Figure 2.3: Presented is an overview of the study's structure, broken down into three parts. The first part consists of the problem statement, literature study and introduction to the system components. Part two covers the heating demand and the Matlab-Simulink model. The third part describes the models performance and evaluates the systems based on the key performance indicators.

2.4. Limitations of the Study

This thesis brings no generally applicable solution on the subjects covered and therefore has limitations in its outcomes.

- This thesis is specifically focused on the case study 'Karwijhof Nagele' and therefore other similar or different systems in other neighbourhoods may vary in outcome.
- The storage tank model is a simplified model. This model has to be validated with real life measurements of similar USTES implementations to perform an accurate error analysis.
- The financial comparison today may be off in the future due to the rapid development and cost reduction in renewable energy systems. Heat pumps, PV panels and solar collectors are increasingly more researched and implemented which may lead, and according to current trends this is likely, to significant future cost reductions.
- The Karwijhof Nagele is a protected monumental neighbourhood which limits the design of the system in some areas. For instance, it is hard to apply insulation to the buildings to lower the heating demand. Also, the solar collectors and PV-array need to be installed at a predetermined angle since they are not allowed to be seen from street level. This leads to sub-optimal conditions for some components in the systems which, in other scenarios, may be further optimised.

3

State of the Art

The goal of this research is to investigate fossil fuel free space heating systems relying on a seasonal thermal energy storage (STES). The research is built around a case study 'Energiek Nagele' of the neighbourhood Karwijhof in the city Nagele in the Netherlands. This is a Dutch residential area which aims to be no longer relying on natural gas for space heating.

The underground seasonal thermal energy storage (USTES) system considered during this study is developed by the Dutch company HoCoSto. The storage medium in the heat buffer is fresh water and energy is stored in the form of sensible heat. Two heat generation methods are considered. The first is heat collection through evacuated tube collectors (ETC). The other method uses a central air-water heat pump for the collection of heat.

The state of the art will start with an introduction to Dutch central heating systems and provide a state of the art on the subject of seasonal (sensible) heat storage and heat collection. Relevant components of the systems are discussed and cost indications are presented. Finally a modelling approach will be defined.

The state of the art evaluates what actions have been undertaken on the subject of renewable energy central heating systems with an emphasis on the seasonal nature of the heating demand.

3.1. Current Heating Systems

To understand the transition to renewable energy for existing buildings in the Netherlands it is important to understand the current central heating systems.

Currently Dutch residential houses and large buildings rely on a central heating system powered by natural gas which is transported by pipeline into each building. Inside the building a natural gas boiler is installed providing the house with hot tap water and hot water for its central heating. These natural gas boilers are so called high efficiency boilers which can theoretically reach efficiencies just over 100%. In reality the seasonal efficiency is lower, around 90%.

There are cases where households do not rely on natural gas for their central heating. For instance, in the city Utrecht a district heating network (DHN) is installed. This network of pipelines delivers hot water from central heat factories for instance, an incineration plant, through the DHN towards households using a 'delivery set' which includes a heat exchanger in order to separate the mass flows of the DHN and the heating system of the household. The DHN of Utrecht is operating on a large scale with around 55.000 households depending on the DHN. The total number of households connected to a DHN in the Netherlands was 316.200 in 2017 [31]. This DHN principle is also well established in Germany and Denmark. Since this study covers only a small neighbourhood the DHN considered will be smaller though the basic principle will remain the same.

Sustainable Heating Systems in the Netherlands

Currently there are some efforts towards sustainable heating systems in the Netherlands. For instance, waste heat from incineration plants is used in the district heating network of Utrecht, heating homes in the city centre. Another example is geothermal heat. The 'Delft Aardwarmte Project' at the Technical University Delft is planning on using the concept where heat is extracted from the subsurface and used to heat university buildings. The same concept has been applied to heat greenhouses in the Dutch Westland area which before relied on vast amounts of natural gas.

3.2. The Need for Storage

There are various technologies able to supply sustainable and renewable heat. However, these technologies are: either not constant due to the intermittent nature of the source otherwise known as 'Dunkelflaute', or the technology is not able to quickly increase capacity in case of a certain peak in demand. For instance, geothermal energy is able to deliver a constant supply of heat but is unable to account for sudden spikes in demand.

To overcome the problem of intermittency or the lack of flexibility in energy supply an energy storage solution is needed. An energy storage acts as a buffer in periods of dunkelflaute where renewable sources cannot deliver sufficient heat to meet demand. The storage can also be used to ensure delivery of heat during peak demands in systems that do not have sufficient flexibility.

There are several options to store heat. For instance, heat storage in the form of sensible heat where heat is stored by heating a material and heat is released by cooling that same material down e.g. Water. Another method is heat storage in the form of latent heat where phase changes of a material are used to store energy e.g. wax. The final option is chemical energy storage where heat or energy is stored in molecules that can release the energy or heat by burning or other chemical reactions e.g. hydrogen. In this research the focus lies on heat storage in the form of sensible heat.

3.2.1. Seasonal Thermal Energy Storage Systems

Research on (solar) heat energy storage systems has a long history. A wide variety of systems are described due to the many different applications of heat. Studies in the past focus both on short term- and seasonal sensible heat storage. Many underground storage methods are considered. For instance, aquifer heat storage, duct heat storage, gravel/sand put storage, borehole thermal energy storage and hot water tanks. Also different storage media are considered - although water is most common.

Not only the storage duration and different system components have been considered, also different loads have been assessed. For instance, USTES systems have been modelled for single family homes by Sweet and McLeskey [37], large urban residential buildings by Terziotti et al. [38], and Rezaie et al. [26] described a system for small housing areas. Chung et al. [7] and Schmidt et al. [29] predicted both thermal performances and economic aspects of USTES systems.

At present there are several sensible thermal energy storage projects in operation. For instance, in the Netherlands borehole thermal energy is increasingly used to heat greenhouses. In Denmark several gravel pit thermal energy storage projects have been conducted to heat households. In Germany several concrete hot water tanks have been installed to store sensible heat. The interest in systems able to store heat is increasing and it is expected that in the coming decade the frequency of deployment of such systems will increase.

Novo et al. [25] and Xu et al. [40] reviewed and compared operating seasonal and diurnal hot water storage tanks for their thermal performance and cost. Some relevant projects comparable in storage tank size to the aim of this study are presented in table 3.1. These systems all rely on solar thermal energy for heat collection. However, the systems use auxiliary heat to cover the mismatch between generation and demand. This is described by the solar fraction, the total fraction of demand that can be supplied with solar thermal energy generated by the system.

As seen in table 3.1 these existing systems operate with solar fractions all below 50%. These heating systems still use auxiliary heating and are designed only to replace a part of the conventional domestic heat generation. Moreover, many systems are designed for diurnal storage instead of seasonal storage.

Table 3.1: Heat storage systems in operation as described by [25, 40]. Different district heating network projects in northwest Europe relying on solar collectors in combination with a heat storage.

Project	Heated living area (m²)	Demand by district heating (GJ/a)	Solar collector area (m²)	Storage volume (m^3)	Solar fraction (%)	Reference
Hamburg, DE	14,800	5796	3000	4500	49	Schmid et al. 2004 [30]
Hannover, DE	7365	2496	1350	2750	39	Schmid et al. 2004 [30]
Munich, DE	24,800	8280	2900	5700	47	from Dalenbäck, 2012 as by [40]
Eggenstein, DE (Pit)	12,000		1600	4500	37	(Schmidt and Mangold, 2006) [28]
Rise, DK	115 buildings		3575	5000		from Dalenbäck, 2012 as by [40]
Herlev, DK		4520	1025	3000	35	(Heller, 2000) [13]
Ingelstad, SE	50 houses	1320	5000			from Dalenbäck, 2012 as by [40]
Lambohov, SE	50 houses	2700	10,000			from Dalenbäck, 2012 as by [40]

Another interesting renewable central heating project was conducted in Canada. This project is the Drake Landing Solar Community and is for a large part similar to the proposed system of this study. It is located in Okotoks, Canada at a latitude of 50.7°. It is an example of a seasonal thermal energy storage heating network with consistent solar fraction over 90%. The community consists of 52 houses installed with flat plate solar collectors. However, this system as described by Sibitt et al. [33], uses borehole thermal energy storage (BTES) for its seasonal energy storage instead of a USTES system. The Drake Landing project is similar in latitude, scale and solar fraction to the Energiek Nagele - Karwijhof project which is located at a latitude of 52.6°.

3.2.2. Solar Thermal Collectors

The basic principle of solar collector technology is the "collecting" of solar radiation and transporting the energy as heat in water for later use. This is achieved by using materials that heat up when exposed to sunlight by absorbing solar irradiation. This generated heat is then used to heat up a liquid that flows through the solar collector. The collected heat is used directly or stored in a water tank for later use. There are multiple solar collector technologies that use this principle for the collection of energy from the sun. The most commonly used for residential purpose are further elaborated in the following sections.

Flat Plate Collector

The Flat Plate Collector (FPC) (figure 3.1) is the most basic solar collector on the market. It is designed to absorb as much heat as possible at the lowest possible cost. The FPC is made of an insulated housing with a glass plate cover. This glass plate has a high transmittance for sunlight but a very low transmittance for long wave thermal radiation which is emitted by the heated absorbing layer in the solar collector. This creates a greenhouse effect in the solar collectors housing, maximising the retained energy. The inside of the housing consists of a highly light absorbing collector plate designed to absorb as much irradiation as possible while losing as little heat as possible to its surroundings. This plate heats up and transfers the heat to the liquid that runs through the collector and transports the heat.

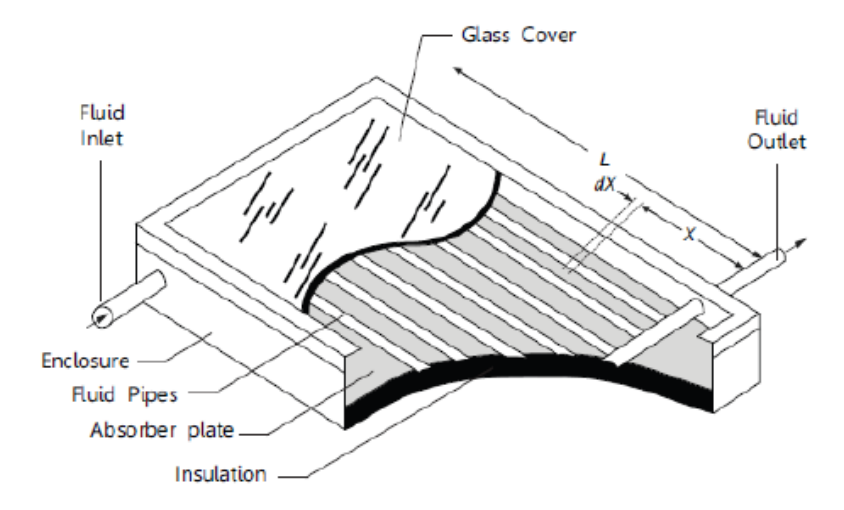


Figure 3.1: Schematic view of the components of a flat plate solar collector. The collector consists of a glass cover covering the enclosure. Inside the enclosure is the absorber plate heating up by the solar irradiation. Subsequently the fluid pipes containing the heat transfer fluid are heated. Taken from Jazlan [15].

Flat plate collectors are designed for installation in warm and sunny climates. When operating in a cold climate with more wind, rain, and clouds the FPC's performance will be significantly lower compared to warmer climates [16], [27]

Evacuated Tube Collector

Evacuated Tube Collectors (ETC) (figure 3.2 are made of a glass vacuum sealed tube with a heat pipe inside. Thanks to this vacuum, the collector is able to operate at higher temperatures since there are lower convective and conductive losses. The advantage of the ETC is that its efficiency is higher at lower incident angles. This is especially beneficial in winter months and at higher latitudes where the sun stays low on the horizon during the colder winter months.

The process of capturing solar radiation and converting it to heat is different for the ETC to that of a FPC. An ETC uses liquid-vapour phase change materials to transfer the heat. Inside the evacuated tube is a highly thermal conductive copper heat pipe. Attached to this heat pipe is a black fin that acts as the absorber plate conducting heat to the heat pipe. At the top of each heat pipe a metal tip is attached which acts as the condenser. Inside the heat pipe is a small amount of fluid that undergoes an evaporating-condensing cycle. Solar radiation heats up the absorber fin which heats up the heat pipe and subsequently the fluid inside causing it to evaporate. This vapour travels to the condenser tip where it condenses and gives off its latent heat to a fluid flow (water or glycol), after which the condensate returns to the heat pipe to repeat the process [27].

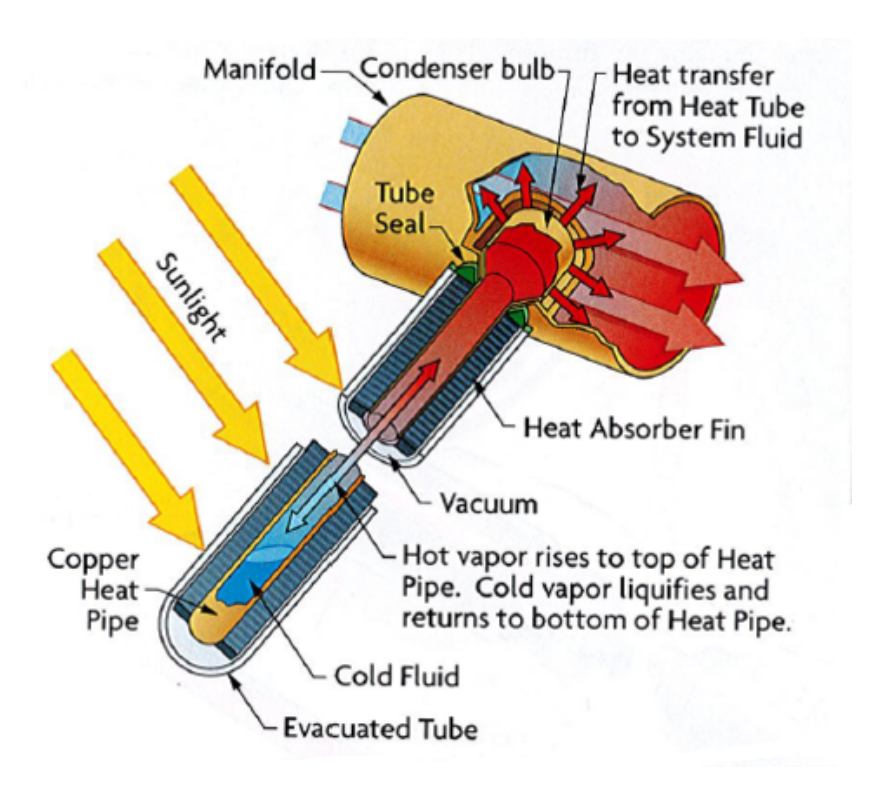


Figure 3.2: Schematic view of the components of an evacuated tube solar collector. Inside the evacuated tube is a copper heat pipe with an absorber fin attached. As the absorber fin heats up the heat pipe heats up too. This causes a fluid inside the heat pipe to evaporate after which it condenses in the condenser bulb transferring heat to the heat transfer fluid. Taken from Hydrosolar.ca [14].

An ETC is able to generate more power per unit area compared to the FPC and is therefore favoured during this research project since limited rooftop area is available. Also the collectors will be installed at 50 degrees latitude in a cold climate where the ETC will be the most efficient choice. From this point on only the ETC will be considered.

Thermal Performance

The amount of thermal energy collected relative to the solar irradiance incident on the collector describes the thermal performance of a solar collector array. The energy output can be tested in a laboratory or in real world conditions, though the outcomes are dependent on the conditions of testing and may fluctuate between test setups. Therefore the European Union provides a general testing method to describe solar collector performance called the 'European Standard EN 12975-2' which is further elaborated in section 5.3.

3.2.3. Underground Seasonal Thermal Energy Storage

Until recently most large scale seasonal hot water heat storage tanks were made of reinforced concrete tanks. However, HoCoSto has in recent years installed multiple modular USTES systems. The HoCoSto USTES in theory is very similar to the concrete storage tanks mentioned before. Yet there are some differences. For instance the geometric shape of the HoCoSto USTES is an upside down obelisk as seen in figure 3.3 instead of a cylindrical or square basin. Also, the HoCoSto USTES is placed entirely underground. The aluminium framework enables utilisation of the overlying surface resulting in minimal land use.

USTES Capacity

According to Schmidt et al. 2003 [29] supply- and return temperatures of the heating network are very important for the usable capacity of the USTES (exergy). When the USTES is designed to operate from $40^{\circ}C$ and the supply temperature of the heating network is $70^{\circ}C$ it means the USTES can only be discharged to $70^{\circ}C$ without use of auxiliary heating. When the USTES temperature is below the supply temperature auxiliary heating is needed reducing the efficiency of the system. For this reason it is important to design a system with low supply and return temperatures.

The scaling of system components is important since this effectively reduces the cost of capital expenditures and the cost of heat. This subsequently increases the likeliness of implementation. HoCoSto claims the storage tank is the most expensive part of the system which is confirmed by Schmidt et al. [30]. Scaling the system with the priority of minimising storage tank size could therefore result in significant cost reductions of the total system.

Sweet and McLeskey [37] found that at a fixed solar collector surface area a "practical optimum" occurs where from a certain storage size a further increase in volume did not have a positive effect on the reduction of auxiliary heating. Sweet and McLeskey believe this is due to the fact that as storage mass increases, more energy is required to raise the temperature. Thus although the larger bed has the potential to store more energy, the final temperature of the bed is not as high. This results in a decrease of exergy content in the storage medium.

Heat Losses

As mentioned before, the USTES has the geometric shape of an obelisk. The volume of the USTES is described by equation 3.1 and figure 3.3

$$V = \frac{z}{6}(Xy + xY + 2(xy + XY))$$
 (3.1)

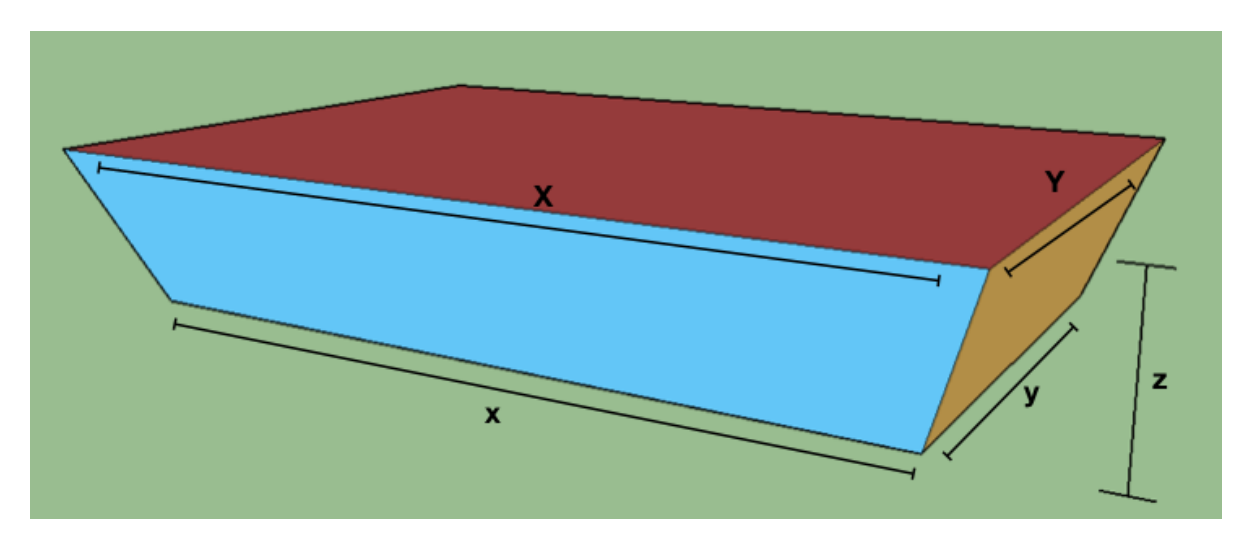


Figure 3.3: Geometric shape of the USTES in 3-D. x, X, y, Y, and z describe the length, width, and height of the USTES respectively according to equation 3.1.

Heat losses occur on every surface area of the USTES. These surface areas are broken down into three parts. The top, sides and bottom. Sorknæs [35] defines three types of thermal losses (\dot{Q}_{loss}) for the heat storage tank using the basic equation 3.2 presented in figure 3.4 .

$$\dot{Q}_{loss} = \frac{\lambda}{d} * A * \Delta T \tag{3.2}$$

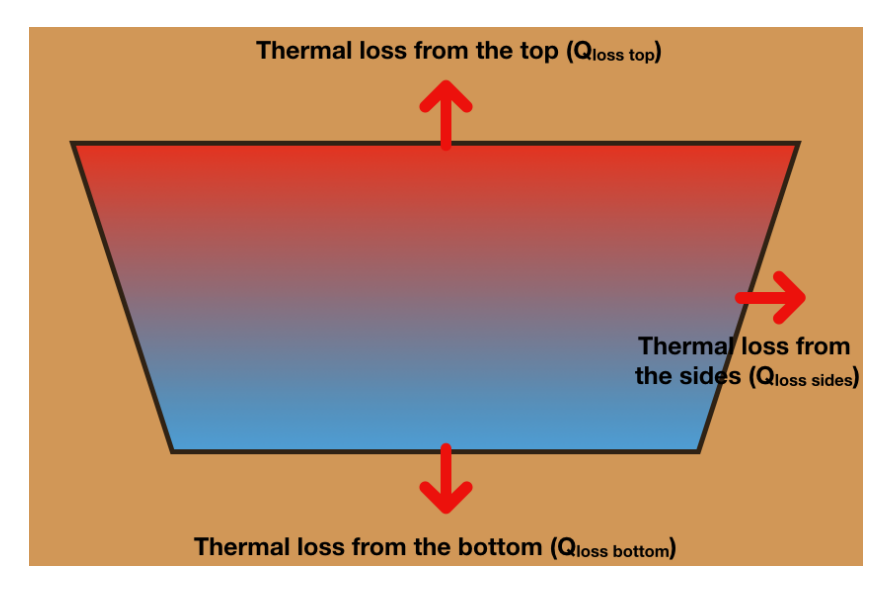


Figure 3.4: Thermal losses in a pit seasonal thermal energy store in two dimensions. Heat losses occur at the top, sides and bottom of the USTES.

Where λ is the material thermal conductivity of the insulation material in [W/(mK)], d is the thickness of the material in [m], A is the materials surface area in [m²], and ΔT is the temperature difference in between the tank and the surrounding soil in [K].

Shelton [32] found that the heat loss to surrounding soil depends greatly on the type and humidity of the soil and is therefore site specific. He also found that the time required for the average heat loss rate of the underground storage tank to approach a steady state value is in the order of one year. Also he states that the ground surrounding a storage tank contributes little to storage capacity of the system [32].

A borehole sample from DINOloket presenting the stratigraphy of the soil near Karwijhof is given in figure 3.5 [9]. From this profile can be seen that the subsurface consists of three soil types, clay, fine sand and peat. The buffer is four meters tall and installed approximately 1-1.5 meters underground. This means the tank will be at 5.5 meters below the surface in the sand layer, and the tank walls will have 3 different soil types each with a different thermal conductivity. According to Dinoloket the groundwater level is at approximately 1 meter. This means the water saturation of the soil is expected to be high and subsequently the thermal conductivity will be high as well.

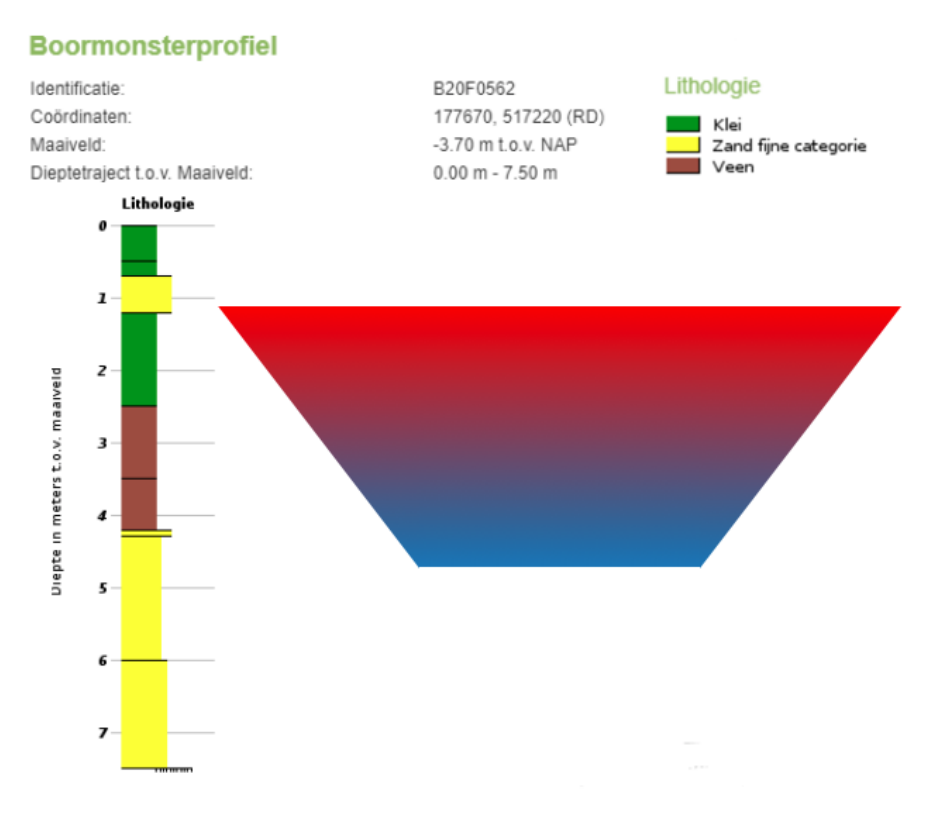


Figure 3.5: Borehole profile of the first 7 meters of the subsurface near Karwijhof, Nagele [9]. The borehole shows a subset of clay, peat, and fine sand for the interval the USTES will be placed.

Modelling Approach

Sensible thermal energy storage in water has been widely researched in tanks of different sizes and shapes like hot water boilers and cylindrical tanks. The shape of the USTES used in this study is different but the principles remain the same. In literature the most common approach to model hot water storage tanks is the use of nodes, both Cadafalch et al. [1] and Cruickshank and Baldwin [8] among others use this approach. The tank is divided vertically into N nodes which all have their own mass and energy balance. Mass and energy transport are described for each node and communication between nodes is updated every timestep of the simulation. This process will be discussed in more detail in section 5.1.

3.2.4. Heat Pumps

Heat pumps are used to collect heat from a source and deliver this heat at a sink. The concept of large scale central heat pump systems is already implemented in large projects in the Netherlands. For instance, canal heat pumps are installed in Amsterdam-north to collect heat for central heating of buildings. In the municipality Utrecht the biggest heat pump of the Netherlands (25 MW) is planned for installation by Eneco to recover heat from waste water in a water treatment plant to deliver heat to the district heating system of the city Utrecht [11].

Working Principle of the Heat Pump

A heat pump transports heat against a temperature gradient. The working principle of a heat pump exploits the physical property that the boiling point of a fluid increases with increasing pressure. At low pressure a 'working fluid' can be evaporated at low temperatures while by increasing pressure the boiling point of that working fluid increases. Therefore, the working fluid in heat pump applications is selected by the temperature range of its thermodynamic cycle.

A heat pump consists of four main components: the evaporator, compressor, condenser and expansion valve. Kiss and Infante Ferreira [17] describe a typical cycle in a mechanical vapour compression heat pump as the following.

- At the evaporator (heat exchanger) heat is extracted from an external heat source e.g. ambient air. This causes the working fluid to heat up, boil and evaporate.
- In the compressor the heated working fluid (now in gaseous phase) is compressed which causes it to further heat up.
- At the condenser the gas condenses releasing the now useful heat to the hot side of the DHN in a heat exchanger and cools down until it turns back into a liquid at moderate temperature.
- In the expansion valve the liquid flashes causing it to cool down and partially evaporate. Since the refrigerant delivered heat in the condenser it is now cooler and able to start the cycle over again, starting in the evaporator extracting energy from the external heat source.

In the evaporator a heat flow \dot{Q}_{in} is added to the system. In the compressor work is delivered by the compressor which results in a power added to the system \dot{W}_{comp} . The heat delivered by condensation of the working fluid in the condenser is described by \dot{Q}_{out} resulting in the energy balance of the system as given by equation 3.3.

$$\dot{Q}_{out} = \dot{Q}_{in} + \dot{W}_{comp} \tag{3.3}$$

Selection of the Working Fluid

Heat pumps are increasing in popularity due to the fact that they have the potential to drastically reduce the use of fossil fuels and therefore have a positive impact on climate change. However, the refrigerants used in the heat pump need to be selected carefully for each application. This means its performance in the operating temperature range needs to be considered.

The working fluid will be selected on multiple criteria. The first important factor is whether the working fluid is chemically stable and inert. Also, health, safety and environment need to be taken seriously. The fluid

should therefore be non-toxic, non-flammable, should have a minimal impact on the environment, and low global warming potential (GWP).

Furthermore, a low vapour heat capacity, low viscosity, and high thermal conductivity are favourable. Other important considerations are a low freezing point, easy leak detection and low cost.

Health, Safety and Environment

Since often refrigerants have a global warming potential (GWP) it is an important factor to take into account. The global warming potential of the refrigerant is expressed as the total equivalent warming impact (TEWI). Equation 3.4 gives the TEWI for a refrigerant used in a heat pump.

$$TEWI = GWP * m_{ref} * (L_y * n + L_{end}) + \frac{\dot{Q}_{out}}{COP_{hp}} * N_{operating} * \frac{CO_2 \ emission}{kWh}$$
 (3.4)

where, m_{ref} is the refrigerant content, L_y is the leak rate, n is the number of operating years, L_{end} is the end life leak percentage, and $N_{operating}$ represents the number of operating hours during the lifetime of the system.

Not only the GWP is important to consider. Health and safety are two other factors that are increasingly more important in current society. Some refrigerants can be toxic or flammable which in certain situations can be of serious concern.

For the project Nagele the selected refrigerant is iso-butane (R-600a) due to its high performance at high temperature applications. Also, the low GWP of 4 indicates it is of little impact on the environment which is important in a project that seeks to lower the GWP of a neighbourhood. One thing to consider is the high flammability of iso-butane which, when handled properly, should not be of any concern.

Ambient Air as a Heat Source

The most widely installed heat pump type is the air sourced vapour compression heat pump. It is inexpensive and relatively easy to install. However, there are some downsides to ambient air as a heat source. During periods of extreme cold the increase in temperature differential causes the coefficient of performance (COP) to drop significantly. According to Kiss and Infante Ferreira [17] for a standard air sourced heat pump in mild weather, the COP may be around 4.0, but when temperatures drop below zero the COP may be only 2.5. the average seasonal COP (SCOP) is estimated at 2.5-2.8.

Hence, the COP is largely dependent on the temperature differential and therefore the ambient air temperature. The graph seen in figure 3.6 shows the hourly temperature occurrence throughout the year and visualises which temperatures are most common in the Netherlands.

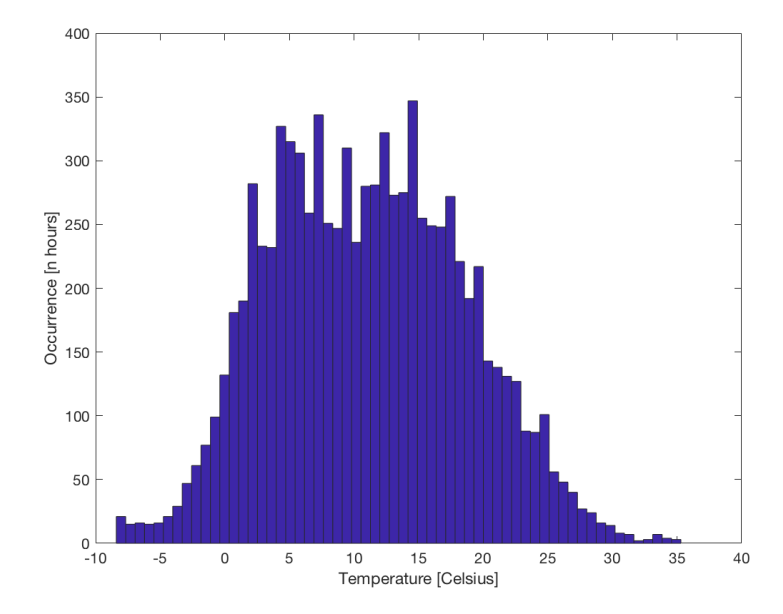


Figure 3.6: Hourly ambient air temperature frequency during the year 2018 at Marknesse weather station located near the city Nagele (approximately 15 km in direct line).

3.3. Cost Outlook of System Components

The cost of system components is an important metric since it determines the competitiveness against traditional systems. The costs consist of two parts: the capital costs (CAPEX) and the operational costs (OPEX). Sustainable autonomous systems tend to have a large CAPEX since no import of energy is needed over the lifetime of the system which results in a low OPEX. A system that relies on energy import generally has a low CAPEX but a very high OPEX since all energy needs to be imported during the systems lifetime.

New technologies generally show a decline in cost over the years. For instance PV technology has been extensively researched and produced resulting in drastic declines in cost per Wp.

Seasonal heat storage is known to be be an expensive concept but has declined in price/m³ storage volume over the years. Schmidt et al. [29] compared several seasonal heat stores for their investment costs as visualised in figure 3.7.

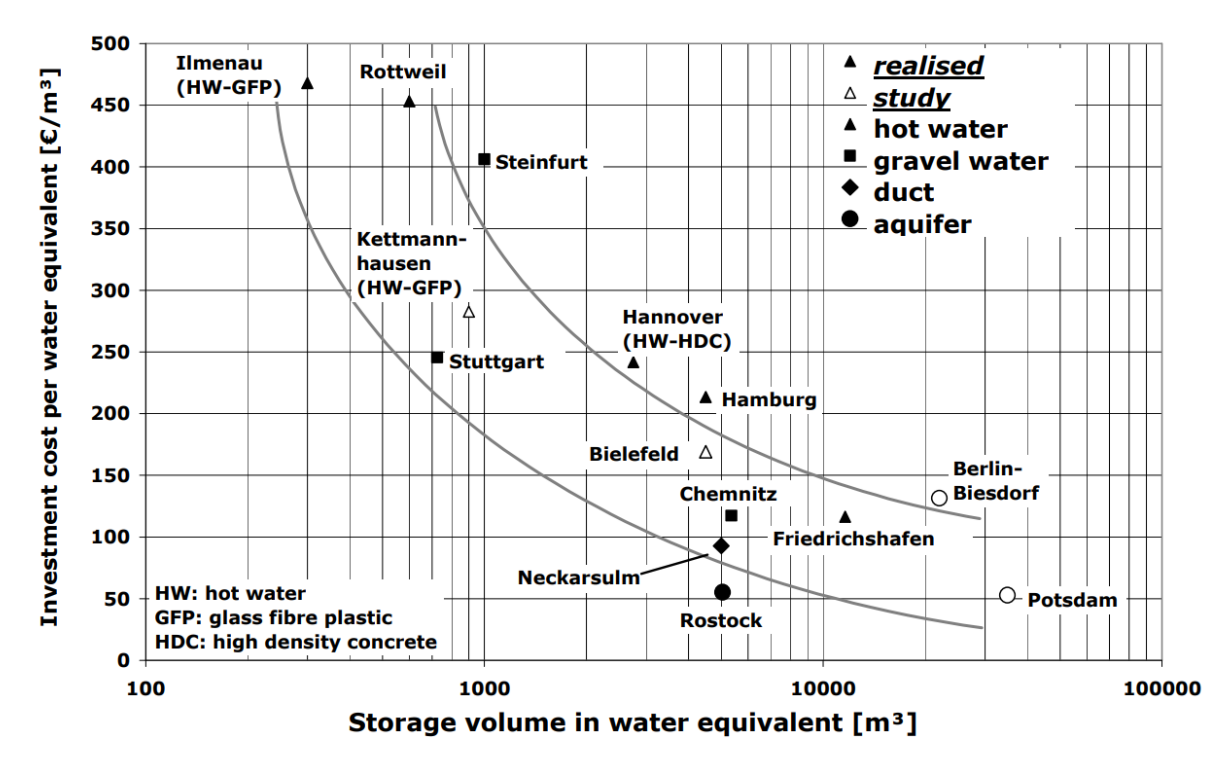


Figure 3.7: Investment costs of different seasonal heat store technologies as function of total storage volume taken from Schmidt et al. [29].

From figure 3.7 can be seen that with increasing storage volume the investment costs/m³ decreases.

The company HoCoSto managed to reduce the cost of thermal storage significantly with the introduction of their innovative modular aluminium spaceframe based storage. The cost for a m^3 of storage capacity declined to as low as $150 \in /m^3$ for storage tank sizes of 800 m^3 and larger. Costs are expected to decrease further in the future with increasing frequency of deployment.

The costs per component are discussed in more detail in chapter 7.

3.4. Key Performance Indicators

The performance of a seasonal energy storage system can be assessed using key performance indicators (KPI). The preferred system will be determined based on the following KPI's:

- Levelised cost of heat (LCOH)
- System seasonal coefficient of performance (SCOP)

The KPI's are not equally important in determining the preferred system and size. Therefore the KPI's are weighed. Table 3.2 presents the weight given to the KPI's.

Table 3.2: Weight given to the different key performance indicators (KPI). The weight represents the importance of the KPI in determining the eventual preferred system and its size. The total weight makes up 1.

KPI	Weight	
LCOH	0.8	
SCOP	0.2	

Levelised Cost of Heat

In this study the LCoH is deemed the most important metric since this determines whether it is economically feasible to install the proposed systems in future projects in the Netherlands.

The levelised cost of heat is defined as the cost per unit of energy that is delivered to the demand. The lower this levelised cost the more financially competitive the system is compared to existing central heating systems.

Seasonal Coefficient of Performance

The SCOP is a measure of the level of autonomy and describes the system efficiency and its dependence on other sources than those of the systems own. For instance, a system that relies on natural gas is not at all autonomous since all energy needs to be imported through gas pipelines. Subsequently a system that relies on the electricity grid can already achieve a higher level of autonomy. A system is only fully autonomous when it does not require to exchange any energy with other systems than its own. In other words, all energy consumed is locally produced and all energy produced is locally consumed.

The two key performance indicators mentioned above are not the only consideration when transitioning towards sustainable central heating. The performance of the systems and the impact on the comfort of users should also be taken into account.

System Performance

Sweet and McLeskey [37] define the internal system efficiency as the ratio of the heat provided to the users and the total solar energy collected as given by equation 3.5. This is only valid for systems that have a solar fraction of 100%

$$Internal \, System \, Efficiency = \frac{Heat \, Provided \, to \, Users}{Solar \, Energy \, Collected} * 100\% \tag{3.5}$$

The solar fraction of a system describes what fraction of the total heat delivered at the user end is generated by the solar collectors as given by equation 3.6.

$$Solar fraction = \frac{Solar Energy Collected}{Heat Provided to Users} * 100\%$$
(3.6)

The efficiency of the solar collector array describes how efficiently the system captures all available solar energy and is defined as Eq. 3.7 [37].

$$Solar \, Efficiency = \frac{Heat \, Provided \, to \, Users}{Total \, Energy \, Incident \, Upon \, Collectors} * 100\% \tag{3.7}$$

The system performance is also based on the seasonal coefficient of performance (SCOP). This represents the ratio between the energy that is delivered to the households and the total electric energy consumed by the system as described by equation 3.8

$$SCOP = \frac{\sum E_{delivered}}{\sum E_{electric\ consumed}}$$
(3.8)

Ease of Installation in Existing Homes

The ease and impact of installation is of great importance when transitioning existing buildings to a renewable heating system. Often houses need to be insulated and complex systems need to be installed in and around the house to be able to provide the home with renewable heating while maintaining a certain comfort level. This can have a great impact on the building and its residents. Also the cost of such a process can be significant. Ideally as little as possible renovations/alterations are needed in the household to save trouble and reduce costs. However, the energy efficiency of the building needs to be sufficient resulting in the fact that in reality some form of additional insulation is almost always beneficial. Another benefit with little installed hardware in the household is that little servicing is needed reducing operating costs of the system.

3.5. Modelling Environment

The components described earlier will be modelled to simulate their operation. These components will be part of a larger system that back-simulates hourly operation over 5 years. The components are modelled in the Matlab environment. The Matlab components will be imported to the Simulink environment in which the total system model will be constructed.

The Matlab - Simulink environment was chosen based on the broad nature of the research. Other - more specialised - software tools are also available for instance, TRNSYS. However, these software tools are often in a 'black-box' environment where the underlying physics are not always open to alteration. This limits the understanding and freedom of the model in such a way that these modelling environments are not sufficient to obtain the understanding and goals of this research study. The Matlab - Simulink environment is therefore the preferred software for this research.

Heat Demand of Dutch Households

According to the Dutch Central Bureau of Statistics (CBS) [3] in 2018 the total yearly natural gas demand for an average Dutch household was $1300~\mathrm{m}^3$. Natural gas accounts for roughly 75% of the total energy demand of the average household. Of this natural gas 80% was used for space heating while 20% was used for hot water and cooking [2]. This comes down to a total energy demand of $1040~\mathrm{m}^3$ of natural gas for space heating.

4.1. Demand Profile

The natural gas demand for the participating households in the case study 'Karwijhof, Nagele' is known and displayed in figure 4.1. The graph visualises the natural gas demand of the neighbourhood for one year. However, the natural gas demand profile is not consistent year over year. For instance, demand depends on the demography of the neighbourhood which changes slowly over the years. More significantly does the energy demand depend on the ambient temperatures in winter which may vary greatly over the years. This effect will be discussed in section 4.2. The energy demand of the users considered during this study is without any additional measures to improve the energy efficiency of the household. It is not yet known what additional measures can be taken due to the monumental status of the buildings.

The monthly energy demand of households in the Netherlands also varies within one year due to seasonal changes. In winter more energy is required for space heating. This results in a higher energy consumption during the cold winter months compared to the warmer summer months. From figure 4.1 a demand profile can be obtained. The figure shows that natural gas consumption peaks in the months November - March and follows a sinusoidal profile. Table 4.1 provides the natural gas consumption of the individual users in the year 2018.

4.2. Climate Effect on Energy Demand

As stated before, climate has a large effect on energy demand for space heating. Therefore, the Dutch meteorological institute (KNMI) uses a definition called "degree days" to account for this climate effect on energy demand. This method is also widely used in literature, for instance by Niessink [24] and Sorknæs [35] among others.

Niessink [24] describes a degree day as a day in the year where the outside air temperature is below $18^{\circ}C$, since only below this temperature a building is assumed to require space heating, otherwise known as the heating limit. Every degree Celsius below this 18 degrees is counted as one degree day. To give an example: for a given day the outside temperature averaged over 24 hours is 8 degrees, then this accounts for 18-8=10 degree days [24].

The number of degree days gives an indication of the severity of the winter and therefore the need for space heating and its related energy demand. The number of degree days varies greatly over the years. For instance,

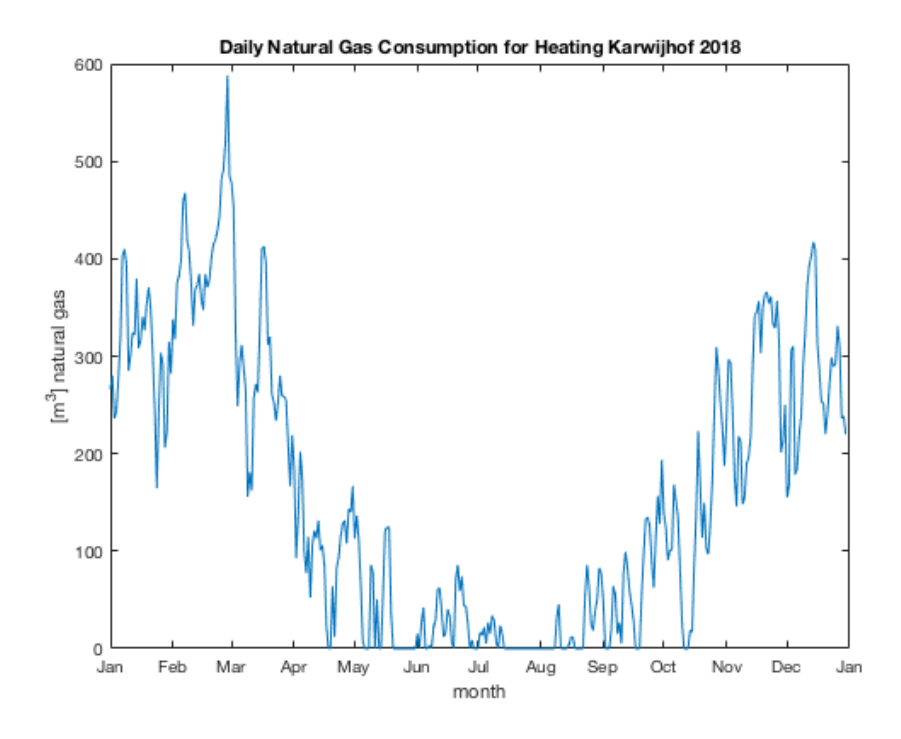


Figure 4.1: Gas consumption of the participating 24 users at 'Energiek Nagele' coupled to the outdoor daily mean air temperature measured by the KNMI at Marknesse weather station along the year 2018. The consumption is per day with a total annual gas consumption of $58448 \ m^3$.

 $Table \ 4.1: Overview \ of the \ natural \ gas \ consumption \ during \ the \ year \ 2018 \ for \ the \ users \ taking \ part \ in \ the \ 'Energiek \ Nagele' \ project.$

Adress	m ³ natural gas	
Ring 1 (former school)	11000	
Ring 98	98 1355	
Ring 100	1355	
Ring 102	1355	
Ring 104	1355	
Ring 106	1355	
Ring 108	1355	
Ring 110	1355	
Ring 112	1355	
Zuiderpoort 2	oort 2 1500	
Zuiderpoort 4	1500	
Zuiderpoort 10-low	3500	
Zuiderpoort 10-high	3500	
Karwijhof 33	1500	
Karwijhof 34	2000	
Karwijhof 35	2100	
Ploegstraat 7	4500	
Ploegstraat 9	1933	
Ploegstraat 11	2925	
Ploegstraat 13	2442	
Ploegstraat 15	4200	
Ploegstraat 17	1258	
Ploegstraat 19	1750	
Ploegstraat 21	2000	
Total	58448	

the (unweighted) difference between 2013 (3078) and 2014 (2385) is 693 degree days where the KNMI climate expectation was 2779 - 2769 degree days respectively. This is a deviation of +11% and -14% respectively from the KNMI expected number of degree days for those years [4]. The effect of these deviations becomes even more severe since 2014 had less degree days while 2013 had more. The change in degree days between these adjacent years is 22.5%.

The degree days are weighted to account for the seasonal changes in solar insolation which contributes to the space heating of a house. Degree-days from November-February are weighted with a factor of 1.1, degree-days in March and October have a weight factor of 1 and April-September get a weight factor of 0.8 [24].

Figure 4.2 shows the number of degree days since the year 2000. Figure 4.3 visualises the distribution of degree days throughout the year 2018.

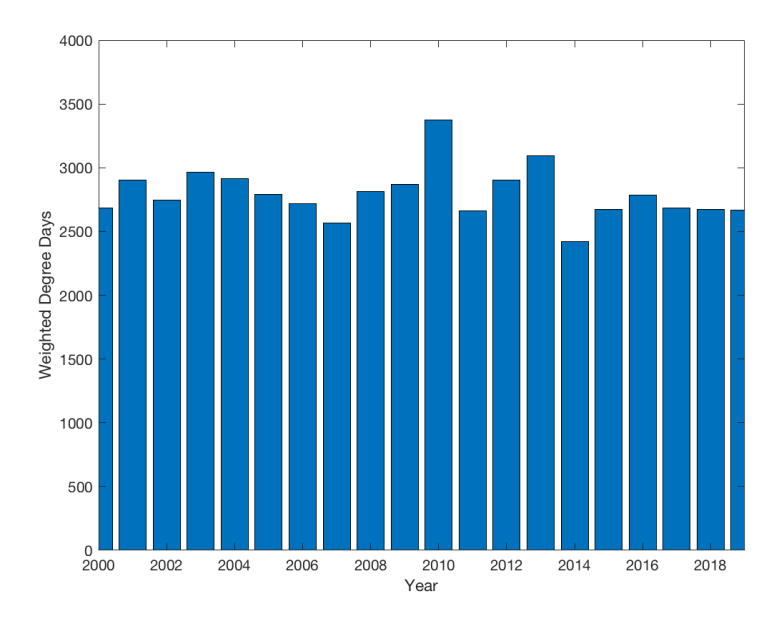


Figure 4.2: Cumulative annual weighted degree days from 2000-2018. Temperature measurements were performed by the KNMI at Marknesse weather station [19].

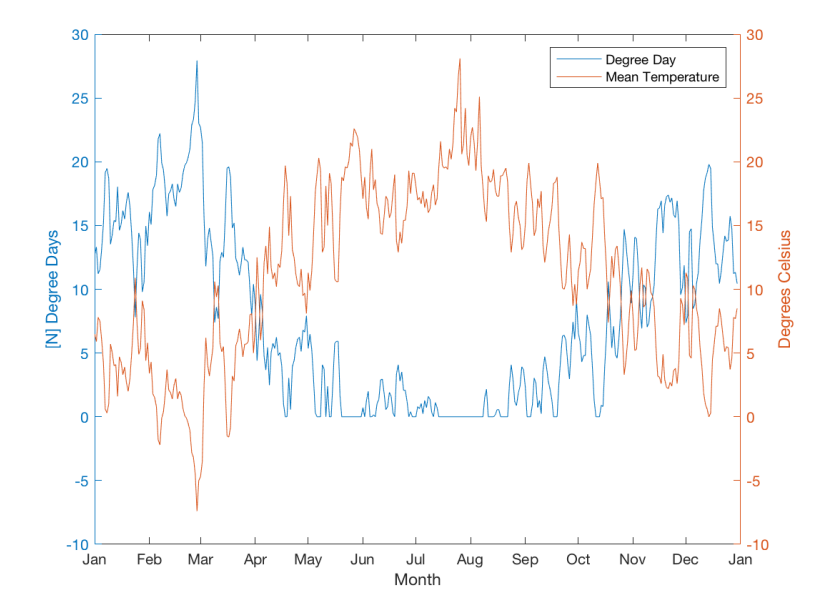


Figure 4.3: Daily degree days and mean temperature during 2018. The heating limit is taken at 18° C. Temperature measurements were performed by the KNMI at Marknesse weather station [19].

Niessink [24] also describes some downsides by relating the heating demand directly to the outside temperature or degree days. For instance, the number of degree days are directly related to the chosen heating limit (in this case $18^{\circ}C$). A different heating limit may drastically influence the total number of degree days. Generally houses with different building types from different building periods do not have the same heating limit. Increased insulation can lower the heating limit. Also the energy demand of a household in reality is intermittent. The house is only heated during hours that the occupant is at home, which is generally around 08:00 in the morning and from 17:00-23:00 in the evening.

4.3. Modelling the Heating Demand

Since the model will have a simulation time step of one hour, degree hours will be used instead of degree days but this is essentially the same. The natural gas consumption of the households is known for the year 2018. For this year the degree hour distribution can be obtained from historical temperature data provided by the KNMI. These two data-sets are linked to get an accurate understanding of the natural gas consumption of the households per degree hour. The KNMI has been continuously measuring the hourly ambient air temperatures for decades. The gas consumption per degree hour are linked to the temperature data over the previous years to simulate multiple years of energy demand with its natural variations.

II

Modelling the System Components

System Components

5.1. Underground Seasonal Thermal Energy Storage

The USTES, in essence, is an artificial underground tank in which a fluid can be stored. What sets the system designed by HoCoSto apart from other designs is the structural framework and the fact that it is modular. The basin draws it structural strength from an aluminium space-frame inside the water tank.

5.1.1. Structural Layout of the USTES

The USTES is installed 4-5 meters underground in an excavated pit. This pit is first lined with EPDM foil to ensure it is watertight. On this EPDM foil insulation is added. The floor and walls of the USTES are insulated using XPS foam blocks. On top of the XPS another layer of EPDM foil is added. This results in a watertight fit around the insulation keeping the material from moisture ensuring its insulating properties over time.

Inside the now watertight and insulated pit the aluminium space-frame is placed as shown in figure 5.1.



Figure 5.1: HoCoSto USTES being placed in a prepared insulated pit. The picture was taken at a project with a 250 m^3 USTES for a newly built school in Boekel. The USTES is part of a central heating and cooling system that is relying on solar collectors instead of the traditional natural gas.

The top of the pit is sealed with the same subset of materials as the floor only thicker for increased insulation. Finally the USTES is covered with 1-1.5 m of soil.

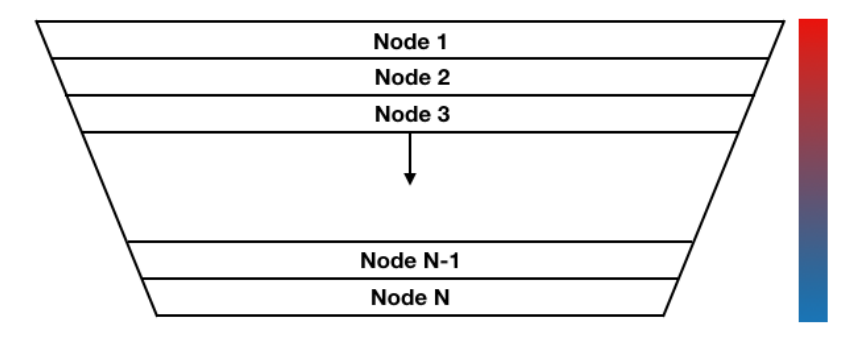
5.1.2. Storage Material

The material used in the storage vessel is water for environmental reasons and simplicity. Water is a non-toxic harmless fluid which causes no concern when a leakage of the tank may occur. Furthermore, water is low cost, easily available, extensively researched as a heat storage material, and has a high specific heat capacity (4.1813 J/gK). This is translated to 1.16 kWh/m³K. Novo et al. [25] favour water as a storage medium from a thermodynamic point of view due to its high specific heat and high capacity rates for charge and discharge.

Other storage materials such as phase change materials like paraffin have been considered. Though due to logistic, regulatory, and environmental reasons the preferred storage material remains water.

5.1.3. Temperature Stratification in the USTES

Research has shown that in liquid-based, sensible heat storage systems high degrees of stratification can be achieved. This stratification is mostly described using simplified one dimensional models. Cruickshank and Baldwin [8] present a way to define a model of a stratified thermal storage by dividing the tank into N constant volume sections or "nodes". Figure 5.2 visualises the node approach applied to the USTES. The nodes are assumed to be fully mixed and at uniform temperature. The resolution of the temperature stratification depends on the number of nodes used. The more nodes the higher the resolution will be, but also the longer the computation time. Cruickshank found that 10 nodes result in an accurate resolution with acceptable computation times, this is therefore the number of nodes used during this study. For each node an energy balance is introduced accounting for the thermal losses to its surroundings and for instance, conduction between the nodes. Each node will represent a physical thermocouple installed inside the USTES spaced uniformly in the vertical direction at a distance $\Delta z = z/N_{nodes}$.



 $Figure 5.2: Visualisation of the node model approach applied to the USTES. The number of nodes can be increased to increase resolution. \\ However, this increases computation times.$

5.1.4. Heat Losses

The heat losses of the USTES need to be taken into account to determine the efficiency of the USTES over time. Table 5.1 provides values for the insulating properties of the materials used in the USTES. The overall heat transfer coefficient (U) can be obtained from the thermal conductivity (λ) and the thickness of the material (d) used as seen in equation 5.1. The lower the value for the overall heat transfer coefficient the lower the heat conduction is through that medium. R is the heat transfer resistance of the material in [m^2K/W].

$$U = \frac{1}{R} = \frac{1}{\frac{d}{\lambda}} = \frac{\lambda}{d} \tag{5.1}$$

The overall heat transfer of a subset of materials is calculated differently and is described by equation 5.2

$$U = \frac{1}{\frac{d_1}{d_1} + \frac{d_2}{d_2}} \tag{5.2}$$

Table 5.1: Insulation properties of the materials used in the USTES for the top, sides, and bottom. The top consists of a subset of materials which are presented separately. The 'Top full subset' presents the insulating properties of the subset of material in the top of the USTES.

Location	Insulation type	Thermal conductivity (λ) [W/m K]	Thickness (d) [m]	Heat transfer coefficient (<i>U</i>) [W/m ² K]
Bottom	XPS	0.027	0.15	0.18
Sides	PUR	0.028	0.25	0.112
Top	PIR	0.023	0.24	0.095
Top	Air	0.026	0.15	0.17
Top	Air with high humidity	0.16	0.15	0.10
Top	full subset		0.39	0.088

resulting in an overall heat transfer coefficient of 0.088 $[W/m^2K]$ for the top of the USTES using high humidity air

5.1.5. Energy Balance

The energy balance incorporates the heat flows in and out of the USTES as well as some processes that occur inside the USTES such as conduction resulting in the temperature stratification as discussed in section 5.1.3. The energy balance consists of multiple contributions which will be described below.

Heat Losses

The extent of heat loss is dependent on the insulating properties of the USTES and the temperature difference between the medium and its environment. Equation 5.3 describes this heat loss.

$$\dot{Q} = UA(T_{USTES} - T_{amb}) \tag{5.3}$$

where \dot{Q} is the heat loss in [W], U is the overall heat transfer coefficient in [W/m²K], A is the surface area subject to heat loss, T_{USTES} is the temperature inside the USTES in [K], and T_{amb} is the temperature of the surrounding environment in [K].

Conduction

Heat conduction, also known as Fourier's law, describes the rate of heat transfer through a material. This is dependent on the negative gradient in temperature (ΔT), the materials thermal conductivity (λ) and surface area (A) as seen in equation 5.4.

$$\dot{Q} = -\frac{\lambda}{d} A \Delta T \tag{5.4}$$

According to the node approach conduction between nodes is present in two directions, upwards to the node above and downwards to the node below. To account for both equation 5.5 is implemented.

$$\dot{Q} = -\frac{\lambda}{\Delta z} A(T_{node\ above} - T_{node}) - \frac{\lambda}{\Delta z} A(T_{node\ below} - T_{node})$$
(5.5)

Heat Transfer in/out

Heat transfer in and out of the USTES occurs through open flow represented by equation 5.7

$$\dot{Q} = \dot{m}_{in} c_p (T_{node} - T_{in}) \tag{5.6}$$

$$\dot{Q} = \dot{m}_{in} c_p T_{node} - \dot{m}_{out} c_p T_{in} \tag{5.7}$$

where \dot{m}_{in} and \dot{m}_{out} are the mass flows in and out of the USTES in [kg/s] respectively, c_p is the thermal capacity of water, T_{node} is the temperature of the node out of which water is extracted, and T_{in} is the temperature at which water is injected into the USTES

Final Energy Balance

The final energy balance for a node combines the previous terms. This energy balance is valid for every node except for the top and bottom node. These nodes do not have either a node below or above. Also, the heat loss term is larger since a larger surface area subject to heat loss to the environment is present. Equation 5.8-5.10 presents the final energy balance of a node n.

$$\dot{Q} = UA(T_{USTES} - T_{amb}) - \frac{\lambda}{\Delta z} A(T_{node\ above} - T_{node}) - \frac{\lambda}{\Delta z} A(T_{node\ below} - T_{node}) + \dot{m}_{in}c_p T_{node} - \dot{m}_{out}c_p T_{in}$$
(5.8)

with,

$$\dot{m}_{in} = \dot{m}_{out} \tag{5.9}$$

giving,

$$\dot{Q} = UA(T_{USTES} - T_{amb}) - \frac{\lambda}{\Delta z} A(T_{node\ above} - T_{node}) - \frac{\lambda}{\Delta z} A(T_{node\ below} - T_{node}) + \dot{m}_{out} c_p(T_{node} - T_{in}) \quad (5.10)$$

A time derivative of this equation will be introduced in section 6.4.2 which describes the temperature change per unit of time of each node in the USTES.

5.1.6. Auxiliary Heating

The USTES can be cooled down to a minimum temperature of 5 degrees due to forming of ice at lower temperatures. In cases of shortage of energy, when the temperature in the USTES reaches below 5 °C, an auxiliary heat source adds heat to the USTES. This auxiliary heat source is an electric resistance that is assumed to transfer electric energy to sensible energy at 100% efficiency.

When the auxiliary heating is needed this effects the autonomy of the system since the electricity is imported from the electricity grid. The SCOP will also be affected since the electricity consumption can be significant depending on the duration of the auxiliary heating. Finally the LCOH of the system will be affected since the electricity used will add to the operating costs. However, cases could occur where it is more cost efficient to occasionally rely on auxiliary heating instead of upsizing the entire system because the increase in operating costs may not be as high as the increase in capital costs to ensure full autonomy.

5.2. District Heating Network

The households will be part of a district heating network (DHN). This DHN will be used to transport the hot water from the heat storage to the houses for space heating and tap water. For this study a traditional two-line network is considered with a supply and return line. The water in the supply line needs to be at a minimum temperature in order to transport enough energy to meet the heating demand, to ensure a certain comfort level, and to ensure the Legionella legislature is met. This translates in the need for a minimum supply or service level temperature of the DHN.

The supply temperature is dependent on the energy demand of the households. In general a minimum supply temperature of 70 ° $^\circ C$ is pre-defined. However, the space heating demand is largely dependent on the outdoor temperature as discussed in section 4.2. This implies that during Autumn and Spring a lower supply temperature may be sufficient. A heating district will benefit from a variable supply temperature since this will increase the overall efficiency of the district heating network and lower the total energy need. Therefore, during this study a variable supply temperature will be considered. The supply temperature is related to the ambient air temperature (figure 5.3). Usually the heating temperature is variable from the heating threshold at $18^\circ C$. Though, due to Dutch Legionella bacteria legislature it is required for the households to be supplied with water of at least $55^\circ C$ for hot tap water production. Since there is a ΔT of about 5 K at the supply side and some heat losses in piping and the DHN. This results in a relatively flat variable service level with a base temperature of $63^\circ C$.

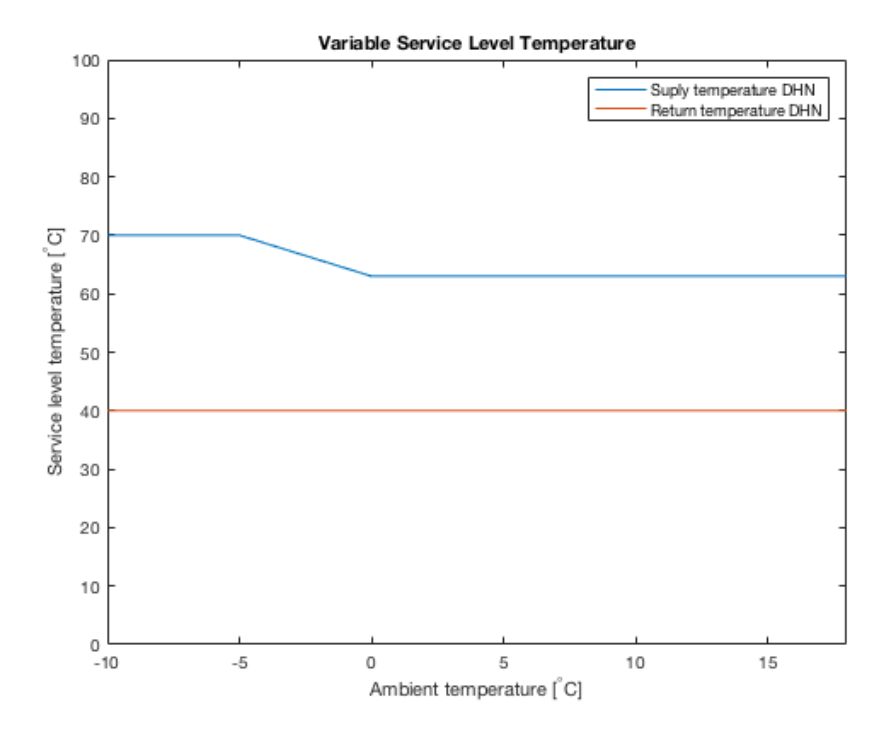


Figure 5.3: Supply and return temperatures of the DHN relative to the ambient air temperature. Minimum supply temperature is determined at 63° C due to Dutch Legionella legislation. The return temperature is fixed at 40° C.

The households do not use all energy the DHN delivers to them. When the household is supplied with heat the DHN return water is cooled down, resulting in a return flow. This flow is assumed constant in temperature. This return flow temperature is constant since with increasing demand the DHN flow rate will increase such that the return temperature remains constant at $40^{\circ}C$.

The DHN model will be simplified since the emphasis of this study is on the storage and generation of heat. The two systems compared will contain the same DHN. However it is important to describe the DHN accurately to obtain a realistic LCOH. The thermal losses in the pipe network and the electricity consumption of pumps are important parameters since they have impact on the LCOH and the SCOP of the system.



Figure 5.4: Layout of the 2-line district heating network (DHN). Participating buildings are indicated in blue, the USTES is indicated in red, and the DHN is indicated by the black lines. Total length of the DHN is roughly 700 meters.

5.2.1. Thermal Losses

The thermal losses in the piping network are described in W/m. The total length of the DHN is around 700 meters. Since most of the year the DHN is operating at constant temperatures of 63 $^{\circ}$ C supply and 40 $^{\circ}$ C return, the thermal losses are considered as a constant power loss of 10 W/m. With a total length of the DHN at 700 meters this comes down to 7 kW.

The separate DHN that connects the solar collectors to the USTES is also subject to heat losses. Since this DHN operates at a higher temperature, heat losses will be slightly higher. However, the length of this DHN

is shorter (50-100 m). The heat loss per meter of the solar collector loop is assumed at 12~W/m with a total length of 75 meters.

5.2.2. Pump Electricity Consumption

Electric pumps are used to circulate water through the DHN. The electricity used by these pumps affects the seasonal coefficient of performance (total electricity used relative to the total energy delivered).

According to Miltenburg [22] the relative pump electricity demand of the system is generally considered to be 0.5% of the total energy demand/heat delivery. In this case this is approximately 4600 kWh/year.

5.3. Solar Thermal Collector

As mentioned earlier, solar collector output varies over the year. To accurately determine the amount of solar collectors needed to supply the users demand, a method to model the collection of heat of solar collectors throughout the year is presented in this section.

5.3.1. European Standard EN 12975-2

Since April 2001 an European standard for the performance of solar collectors is defined according to Fischer et al. [12]. This standard identified by the code EN 12975-2 is accepted by all members of the European Union. The standard describes three methods for estimating the performance of solar collectors. The most reliable for real life performance is the quasi dynamic approach. Other methods are more suitable to indoor laboratory testing. The quasi dynamic approach will be used to determine the solar collector thermal output during this study.

The quasi dynamic approach is expressed by a combination of equations (4 in total). Starting with the zero loss efficiency for beam radiation and diffuse radiation as seen in equation 5.11

$$\dot{Q}_1 = F'(\tau \alpha)_{en} K_{\theta h}(\theta) G_h + F'(\tau \alpha)_{en} K_{\theta d}(\theta) G_d \tag{5.11}$$

where $F'(\tau \alpha)_{en}$ is the zero loss efficiency [-], $K_{\theta b}$ [-] and $K_{\theta d}$ [-] are the incident angle modifiers (IAM) for the direct (beam) radiation (G_b) in [W/m⁻²] and the diffuse radiation (G_d) in [W/⁻²] respectively.

During this study the wind component will be neglected due to lack of accurate data and since ETC are used the effect on the final result will be less compared to other collector types.

Equation 5.12 describes the temperature dependent heat losses.

$$\dot{Q}_2 = -c_1(T_m - T_{amb}) - c_2(T_m - T_{amb})^2 \tag{5.12}$$

where, T_m is the mean fluid temperature in [K], T_{amb} is the ambient temperature in [K], c_1 is the heat loss coefficient at $(T_m - T_{amb}) = 0$ in $[\text{Wm}^2 \text{K}^{-1}]$ and c_2 is the temperature dependence of the heat loss coefficient in $[\text{W}(\text{m}^{-2}\text{K}^{-1}].$

The long wave irradiance dependence of the heat loss is described by equation 5.13

$$\dot{Q}_3 = c_4 (E_L - \sigma T_{amb}^4) \tag{5.13}$$

where c_4 is the sky temperature dependence of the heat loss coefficient [W/m⁻²], E_L is the long wave irradiance in [Wm⁻²], σ is the Stefan Boltzmann constant in [Wm⁻²K⁻⁴].

Combining these equations results in the final equation describing the output of the solar collector, equation: 5.14.

$$\dot{Q} = F'(\tau \alpha)_{en} K_{\theta b}(\theta) G_b + F'(\tau \alpha)_{en} K_{\theta d}(\theta) G_d - c_1 (T_m - T_{amb}) - c_2 (T_m - T_{amb})^2 + c_4 (E_L - \sigma T_{amb}^4)$$
 (5.14)

where \dot{Q} is the useful output power of the solar collector in Watt.

5.3.2. Incidence Angle Modifier

The German Institute for Solar Technologies [36] introduces the Incidence Angle Modifier (IAM) or angle factor which describes how the efficiency of a collector changes if the sun is found at a certain angle in respect to the collector.

Figure 5.5 visualises the concept of the increased efficiency at certain angles of incidence.

The absorber area of an ETC remains the same at an increasing angle of incidence up to the point where the tubes overshadow each other. It is only from this shadowing point that the absorber area decreases. The solar

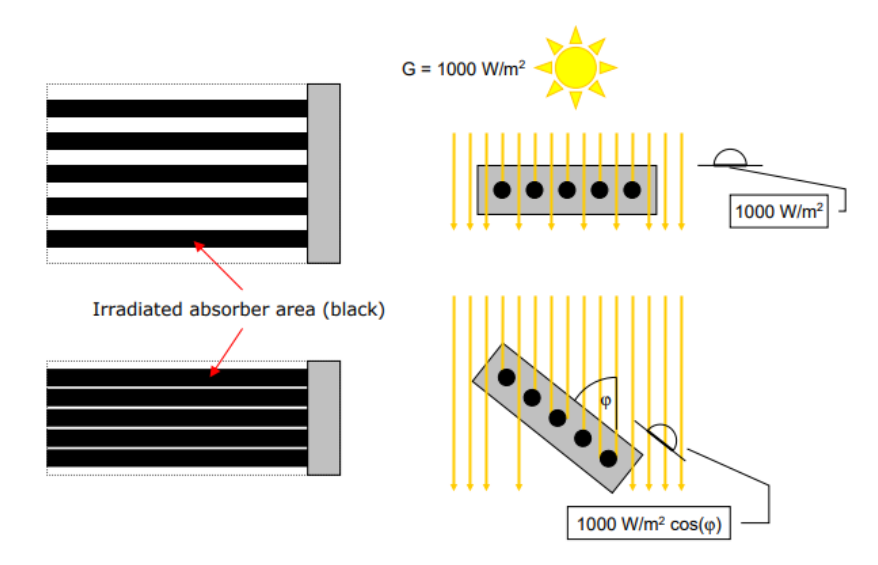


Figure 5.5: Angle factor for evacuated tube collectors [36]. The evacuated tube collector (ETC) facing the sun at an inclination has a larger effective surface area compared to the ETC facing the sun without inclination.

irradiation per square meter on a solar collector remains constant no matter the position of the collector. However, the area receiving sunlight becomes smaller and therefore the total received irradiation is smaller. Since the efficiency of the solar collector is determined by dividing the total captured solar energy by the total incident solar energy, the ETC will show higher efficiencies at increasing angles of incidence up to the point where the tubes start overshadowing [36].

Figure 5.6 shows the IAM factor at different angles of incidence of the irradiation.

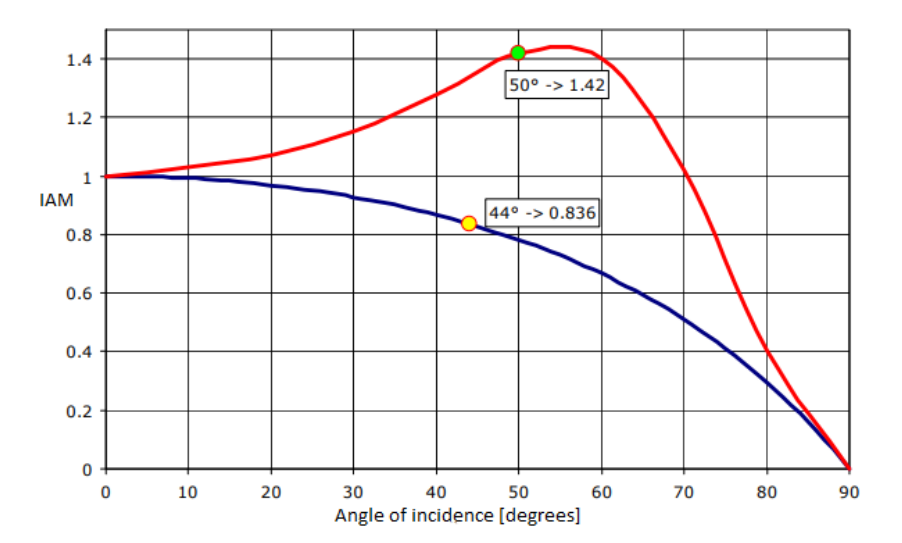


Figure 5.6: Beam IAM for an ETC at different angles of incidence for a flat plate solar collector (blue) and an evacuated tube solar collector (red) [36]. Note the increase in IAM for the ETC due to the increase in effective surface area as shown in figure 5.5.

5.3.3. Positioning of the Solar Thermal Collectors

The solar thermal collectors are installed in arrays on the rooftops of the buildings. The rooftops consist of 2 flat surfaces on buildings near the USTES. In this study a separate DHN pipe is assumed to collect heat from the solar collectors and to transport it to the USTES.

The solar collectors are installed at a fixed angle of 15° oriented 180° towards the south. 15° is not the ideal inclination angle but since the buildings have a monumental status, the collectors cannot be visible from

streetview resulting in a smaller inclination angle.

5.3.4. Solar Resource

To be able to determine the thermal performance of the solar collectors and PV panels accurate solar irradiation data are needed. The solar insolation is highly fluctuating in the Netherlands due to the seasonal variation related to the position of the earth with respect to sun. This also causes the angle of incidence to change throughout the year. To accurately incorporate all these variables into the solar collectors thermal performance the daily solar irradiation needs to be modelled in a site specific model.

5.3.5. Shading

Shading created by the collectors is an important parameter to consider when installing solar collectors or PV modules. The length of the shadow behind the collector determines the spacing between rows of modules. Using equation 5.15 the length of the shadow behind a solar collector or PV module can be determined. The angles are visualised in figure 5.7.

$$l_{shadow} = \frac{\sin(\theta_M) \times l_M}{tan(a_S)}$$
 (5.15)

where, l_{shadow} is the length of the modules shadow in meters, l is the vertical length of the module, θ_M is the modules tilt angle in degrees and, a_S is the sun elevation. To be sure no modules are in each others shading the spacing between modules should be sufficient.

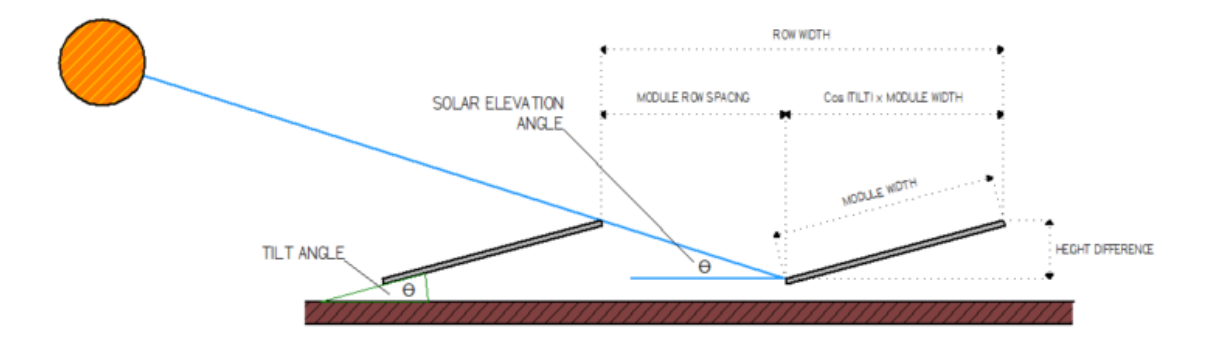


Figure 5.7: Inter row spacing between solar collectors or PV modules on a horizontal surface [6]

5.3.6. Data Acquisition

The weather data used during this research are provided by the Dutch Meteorological Institute (KNMI) and climate data was provided by the computer software METEONORM. Hourly data on the global horizontal solar irradiation (GHI) and other weather parameters are available, also climate data on the irradiation components direct normal irradiation (DNI) and the diffuse horizontal irradiation (DHI). This data-set is used as input for the Matlab - SIMULINK model. The weather data contain hourly temperature data as well as daily mean temperatures.

Solar irradiation data comes in three parts. It is broken down in the Direct normal irradiation component which describes the irradiation directly coming from the sun normal to the module. Diffuse Horizontal Irradiation describes the diffuse irradiation as a result of clouds or haziness of the sky with high turbidity in other words, all forms of light that are scattered by the atmosphere in some way. Finally the global horizontal irradiation (GHI) is the sum of the two prior components as shown in equation 5.16 and figure 5.8 [34]. Figure 5.9 presents the solar irradiance at Marknesse weather station near the city Nagele.

$$GHI = DNI \times \sin a_S + DHI. \tag{5.16}$$

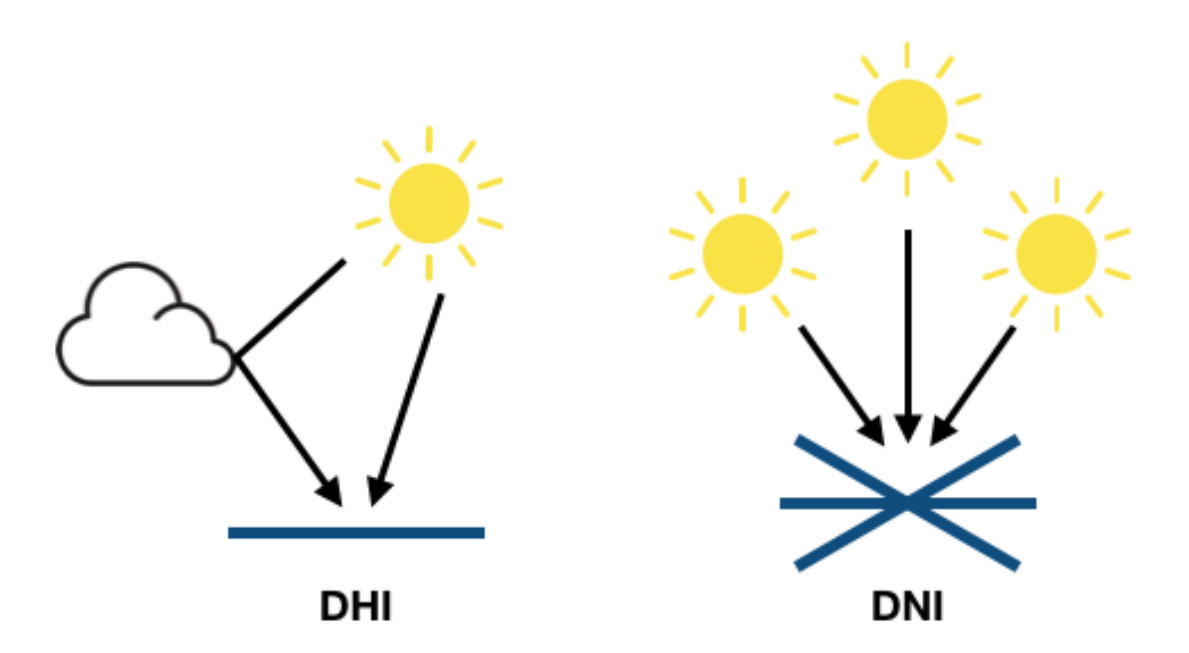


Figure 5.8: Visualisation of the direct normal irradiance (DNI) and the diffuse horizontal irradiance (DHI). The sum of the DNI and DHI make up the global horizontal irradiance (GHI).

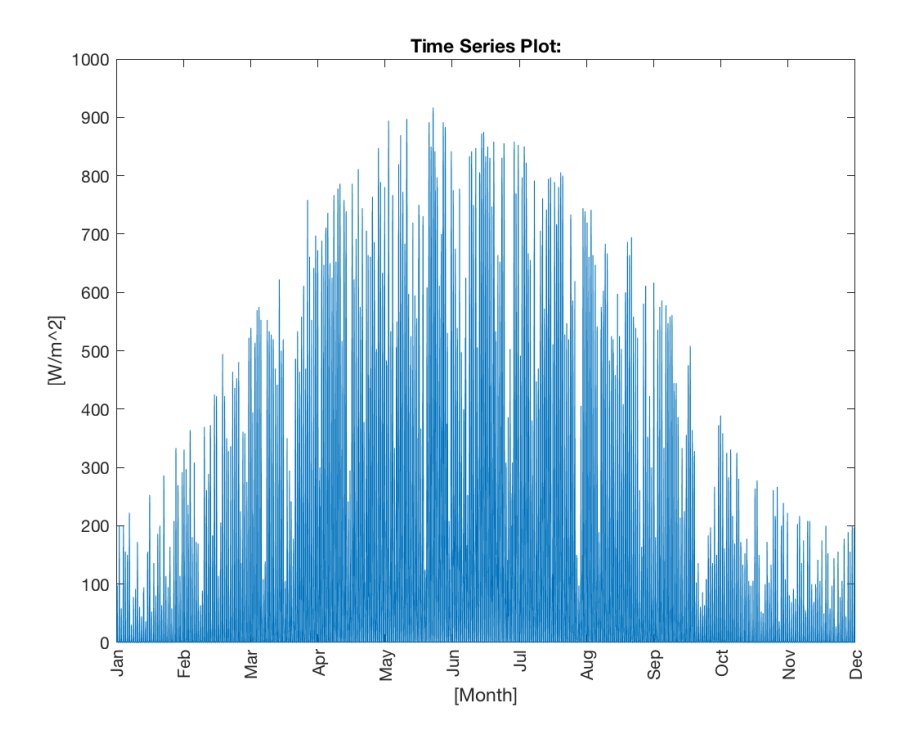


Figure 5.9: Daily solar insolation (GHI) measured at Marknesse weather station during the year 2018 [19]. The total annual irradiance for 2018 is $1079\,\mathrm{Wm}^{-2}$

The typical ratio between the DNI and DHI at the location of the city Nagele is determined using METEONORM and is presented in figure 5.10. The sum of the two components totals to the GHI. The graph shows the diffuse part of the global radiation.

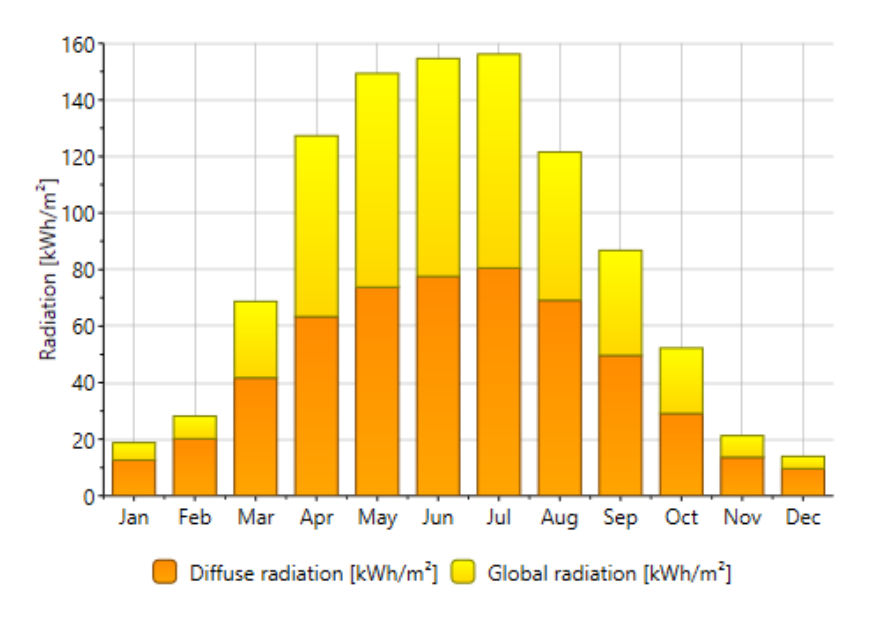


Figure 5.10: Diffuse radiation as part of the global radiation. The global radiation minus the diffuse radiation gives the direct normal radiation. The figure shows that during summer the diffuse component is about 50% of the GHI, during winter its share increases to around 75%.

5.3.7. Rooftop Area Availability

Since the solar collectors will be installed on the rooftops of the users there is a limit to the amount of solar collector area installed. The total available rooftop area of the users is 2800 m². Not all area can be used effectively, meaning some area is lost due to shading. The effective usable surface area is assumed at 80% of the roof top area giving 0.8*2800 m² = 2240 m². The panels are installed in rows resulting in inter-row shading as described in section 5.3.5. The spacing is not optimised for the shortest day in the year $(23^{rd}$ December) where the sun is at its lowest point and therefore the shadow of the collector the longest. Instead, some shading during the winter months is allowed in order to be able to increase the amount of solar collectors and PV panels. Depending on the system configuration this may be necessary. The inter-row spacing translates into an effective surface area loss of 60%. The total available rooftop area becomes 0.6*2240 m² = 1344 m².

5.4. Photo-Voltaic Array

To increase the autonomy of the heating systems introduced, PV panels are installed to account for the electricity of the heat pump(s) and other components. Since limited rooftop area is available high efficiency mono-crystalline PV modules are considered. Modules range in conversion efficiency from 15-24% depending on the manufacturer. Generally higher efficiency panels are more expensive.

With the findings on the sun position from section 5.3, calculations can be made to find the output of the PV-array throughout the year.

5.4.1. Module Specifications

The specifications of the PV module considered during this study, the Trina Solar Duomax 144 half-cell module [39], are presented in table 5.2.

Table 5.2: PV module specifications under standard test conditions from the manufacturers data sheet [39]

"Trina Solar Duomax 144 half-cell Module"		
Peak Power (P_{max})	405	Wp
Max Power Voltage (V_{mpp}	41.4	V
Max Power Current (I_{mpp})	9.79	A
Open Circuit Voltage (V_{OC})	50.8	V
Short Circuit Current (I_{SC})	10.23	A
Module Efficiency (η_M)	19.7	%
Annual Degradation	0.5	%
Length	2031	mm
Width	1011	mm
Surface area	2.05	m^2

The modules on the rooftops are installed oriented 180° south with a tilt angle of 15° . These limitations are the result of the protected status of the Karwijhof as discussed in section 2.4

5.4.2. Temperature Effects

The efficiency of a PV-module is presented in the datasheet provided by the manufacturer [39]. This efficiency is tested under standard test conditions and does not represent the efficiency in real world conditions. For instance, the efficiency of a PV-module is affected by the temperature of the module. With increasing temperature of the module the efficiency drops. The temperature of the module can be approximated using the Duffie-Beckman approach given by equation 5.17 [34].

$$T_M = T_{amb} + (\frac{T_{NOCT} - 20^{\circ}}{I_{NOCT}}) G_M (\frac{9.5}{5.7 + 3.8 \times w}) (\frac{1 - \eta_M}{0.9})$$
 (5.17)

where, T_M is the temperature of the PV module, T_{amb} is the ambient temperature, T_{NOCT} and I_{NOCT} are the temperature and irradiance at nominal operating cell temperature, respectively. G_M is the irradiance incident on the module in Wm⁻², w is the wind speed in ms⁻¹, and η_M is the PV modules listed efficiency under standard test conditions.

Temperature Affected Efficiency

The efficiency corrected for the temperature of the module is calculated following equation 5.18 tot 5.22 [34]. The standard test conditions parameters needed are generally presented in the manufacturers datasheet.

$$V_{\rm OC}(15^{\circ}, G_M) = V_{\rm OC}(STC) + \frac{n \kappa T_{\rm STC}}{q} \ln \frac{G_M}{G_{\rm STC}}$$
 (5.18)

$$I_{SC}(15^{\circ}, G_M) = I_{SC}(STC) \frac{G_M}{G_{STC}}$$
(5.19)

$$FF = \frac{P_{\text{max}}}{V_{\text{OC}}(15^{\circ}, G_{\text{STC}}) I_{\text{SC}}(15^{\circ}, G_{\text{STC}})}$$
(5.20)

$$P_{\text{mpp}}(15^{\circ}, G_M) = FF \ V_{\text{OC}}(15^{\circ}, G_M) \ I_{\text{SC}}(15^{\circ}, G_M)$$
 (5.21)

$$\eta(15^{\circ}, G_M) = \frac{P_{\text{mpp}}(25^{\circ}, G_M)}{G_M A}$$
(5.22)

where, (15°, G_M) represent the operating conditions (tilt angle and solar irradiance respectively), n the diode quality factor, κ the temperature coefficient, q the elementary charge, FF the fill factor, and A the surface area of the module. For crystalline silicon modules the diode quality factor is around 1.5 and κ is around -0.0035 [-/°C] depending on the module. Using equation 5.22 the temperature specific efficiency can be obtained:

$$\eta(T_M, G_M) = \eta(15^\circ, G_M) \left[1 + \kappa \left(T_M - T_{STC} \right) \right]$$
(5.23)

Equation 5.23 results in the module efficiency as a function of the modules temperature and incident irradiance.

5.4.3. Balance of System

The balance of system (BoS) consists of all components of the PV system but the PV module itself. Generally the BoS contains the cabling, power optimisers, inverters, racking. The electrical components of the BoS result in additional efficiency losses which are generally about 8%. During this study the inefficiency related to the Bos is assumed at 8%.

5.4.4. Power Output

The final efficiency of the PV modules is lower than the efficiency presented by the manufacturer. Subsequently the power output of the PV array is also lower. The final efficiency is calculated according to equation 5.24:

$$\eta_{\text{total}} = \eta(T_M, G_M) \times \eta_{\text{BoS}}$$
(5.24)

$$P = \eta_{\text{total}} \times P_{\text{max}} \tag{5.25}$$

5.5. Heat Pump

5.5.1. Efficiency and Performance

Heat pumps are more efficient at heating than at cooling at a certain temperature difference between source and sink. This is due to the fact that the input energy of the compressor is also turned into useful heat and is moved together with the earlier harvested heat into the condenser as can be concluded from equation 3.3. When in cooling mode the dissipated work (or waste heat) from the compressor is transported outside and therefore the energy is lost to the environment. Since the application in this research covers only heating the COP of the heat pump will always be at least 1.

Coefficient of Performance

According to Kiss and Infante Ferreira [17] the ideal refrigeration/heat pump cycle is the reversed Carnot cycle, which consists of two isothermal and two isentropic processes, all processes being reversible. The COP of the Carnot cycle is given by equation 5.26.

$$COP_{hp} = \frac{T_H}{T_H - T_C} \tag{5.26}$$

Where, T_H is the sink temperature and T_C is the source temperature.

From equation 5.26 can be seen that, as the temperature difference between evaporation and condensation increases, the maximum achievable COP decreases. In practice this means that a heat pump has a higher COP when the source temperature and the sink temperature are close together (small temperature differential).

The theoretical Carnot cycle is not possible in real life since the real process always shows some degree of irreversibility and inefficiency.

Compressor Efficiency

Kiss and Infante Ferreira [17] state that the quality of the compressor is determined by its isentropic efficiency as stated in equation 5.27. This equation describes the factor of losses due to irreversibility including heat losses.

$$\eta_{is\,comp} = \frac{\dot{W}_{is}}{\dot{W}_{practical}} \tag{5.27}$$

or, by equation 5.28 in terms of enthalpy states.

$$\eta_{is\,comp} = \frac{\Delta h_{is}}{\Delta h} = \frac{h_{2\,is} - h_1}{h_2 - h_1} \tag{5.28}$$

The power of the compressor is obtained from equation 5.29 and is dependent on the mass flow \dot{m}_{ref} through the compressor and the desired enthalpy increase of the working fluid.

$$P_{comp} = \dot{m}_{ref}(h_2 - h_1) = \frac{\dot{m}_{ref}(h_{2is} - h_1)}{\eta_{is\,comp}}$$
 (5.29)

Heat Exchangers

A heat pump contains at least two heat exchangers. One at the source side (evaporator) and one at the sink side (condenser). The work that is required to provide a certain amount of heating or cooling is directly affected by the area of the heat exchanger and the temperature differential. This means that as the heat exchanger area increases the temperature difference decreases resulting in a more efficient system.

The performance of the heat exchanger is determined by the product of its surface area A in $[m^2]$ and the overall heat transfer coefficient U in $[W/m^{-2}K]$.

In the heat exchanger of a heat pump the source temperature at the outlet of the heat exchanger is lower compared to the source inlet. This is the result of heat being removed from the stream and into the working fluid. At the sink side the stream to be heated experiences a similar effect. Equation 5.30 takes this into account for determining the source temperature.

$$T_C = \frac{(T_{source\ in} - T_{source\ out})}{ln(\frac{T_{source\ in}}{T_{source\ out}})}$$
(5.30)

Similar for the sink temperature:

$$T_{H} = \frac{(T_{sink out} - T_{sink in})}{ln(\frac{T_{sink out}}{T_{sink in}})}$$
(5.31)

The pinch in the heat pump heat exchangers is assumed as 3 K. A low pinch is favourable since it will increase the overall performance of the heat pump cycle. An economic study should point out whether this weighs against the extra costs.

Operating Temperatures

Initially the heat pump will be specifically designed for the source temperature range of 10-30 degrees. This source temperature is based on the frequency of measured hourly temperatures. The most occurring temperature is 10 degrees Celsius. However, not only the occurrence is taken into account. The theoretical Carnot efficiency and the heating demand of the users is also considered.

The sink outlet temperature is set at $63 - 70^{\circ}C$ since this is the operating temperature and the charge temperature of the USTES. However during certain periods of the year a lower DHN temperature could suffice. During these moments the sink temperature may be lowered to achieve a higher COP.

Evaporation and Condensation Temperature

The condensation temperature is given by equation 5.32

$$T_{cond} = \frac{T_{sink\,out} - T_{sink\,in}e^{-\frac{UA_{cond}}{\dot{m}_H * c_{p_H}}}}{1 - e^{-\frac{UA_{cond}}{\dot{m}_H * c_{p_H}}}}$$
(5.32)

And the evaporation temperature is given by eq: 5.33

$$T_{evap} = \frac{T_{source\,out} - T_{source\,in}e^{-\frac{UAevap}{m_C*c_{p_C}}}}{1 - e^{-\frac{UAevap}{m_C*c_{p_C}}}}$$
(5.33)

5.5.2. REFPROP

To determine the relevant states of the refrigerant during the heating cycle the software program REFPROP is used. The software determines fluid properties of a refrigerant at a user defined input state like temperature and pressure. This enables calculations on the state of the working fluid before and after components in a heat pump cycle, for instance before and after the compressor. These thermodynamic properties of the refrigerant are needed to determine the overall performance of the heat pump.

The software contains the thermodynamic properties of fluids and is able to calculate among others, temperature, pressure, enthalpy, entropy and heat capacity. In Matlab the calculations are executed using the command 'refpropm' of which an example is given below:

$$p = refpropm('p', 'T', 373.15, 'Q', 0, 'water')$$

giving the vapour pressure of water at 373.15 K in [kPa] and with Q the quality, as described by Lemmon et al. [20].

REFROP also helps to visualise the thermodynamic properties of refrigerants by plotting for instance pressureenthalpy diagrams as shown in figure 5.11

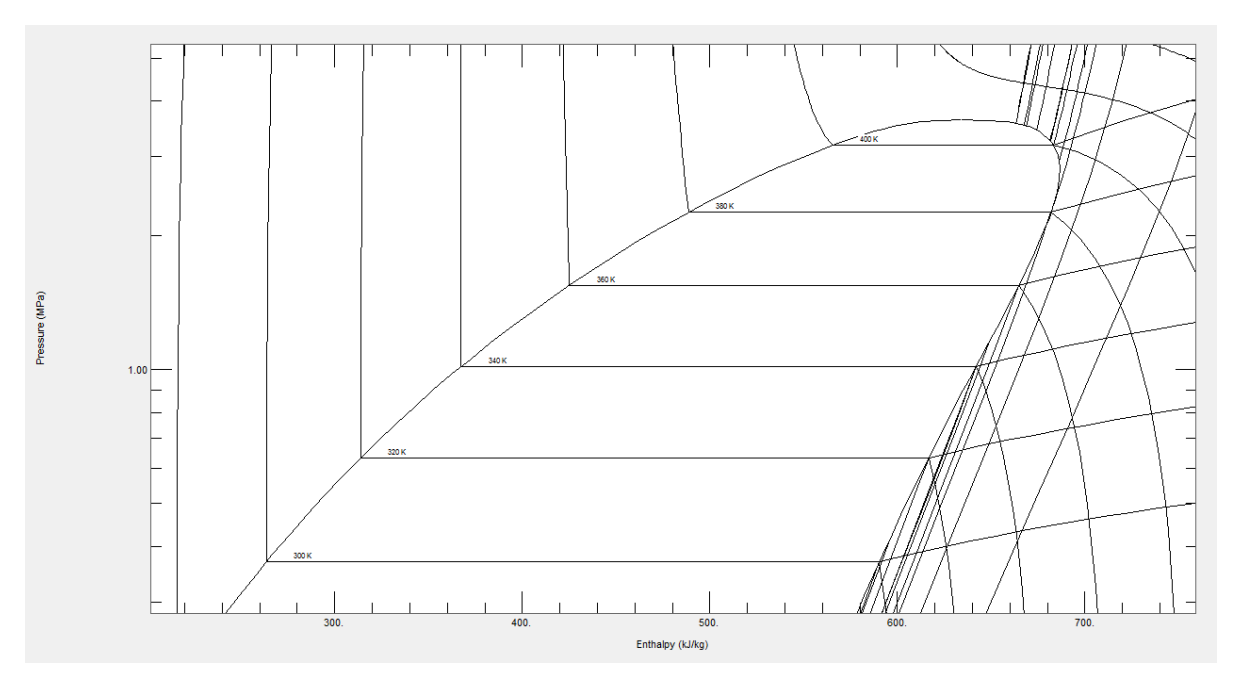


Figure 5.11: The pressure-enthalpy diagram for the refrigerant iso-butane (R600a) plotted using REFPROP.

5.5.3. Heat Pump Cycle

Below the heating cycle is described in detail and the states in each part of the cycle are mentioned and visualised in figure 5.12.

The refrigerant iso-butane (R600a) starts in a gas-liquid phase in the evaporator at T_9 where it evaporates at the source temperature, increasing the enthalpy and entropy until all liquid is turned into vapour, this is state 1 in the heat pump cycle and shown in figure 5.12 past the gas saturation line. After state 1 the refrigerant is slightly superheated to T_2 ,

The refrigerant now enters the internal heat exchanger where it is further superheated to state 3 by the condensate from the subcooler which is still at medium temperature.

Next the gas is compressed by the compressor increasing the pressure, temperature, enthalpy, and entropy. The refrigerant is now at state 4 as shown in figure 5.12 past the gas saturation line as it remains superheated at T_4 .

The superheated refrigerant enters the de-superheater and is cooled down by transferring heat to the sink. The refrigerant is now at the gas saturation line in state 5.

In the condenser the gas is condensed at $95^{\circ}C$ transferring heat to the sink. This causes the enthalpy and entropy to decrease while the temperature remains constant. The refrigerant is now at state 6 in the cycle as seen in figure 5.12 and is all liquid.

The fluid is still at the condensing temperature and therefore further cooled down in the subcooler to state 7 around the temperature of the sink inlet, which in this case is the DHN $(40^{\circ}C)$.

At this stage ($T = 43^{\circ}C$) the refrigerant is still containing usefull energy. Therefore it inters the internal heat exchanger where it further superheats the refrigerant flow before it enters the compressor. The now even further cooled down refrigerant at state 8 enters the throttling device where it is flashed decreasing the temperature, and pressure at constant enthalpy. This turns it into a gas-liquid mixture at state 9 at which the cycle starts over again.

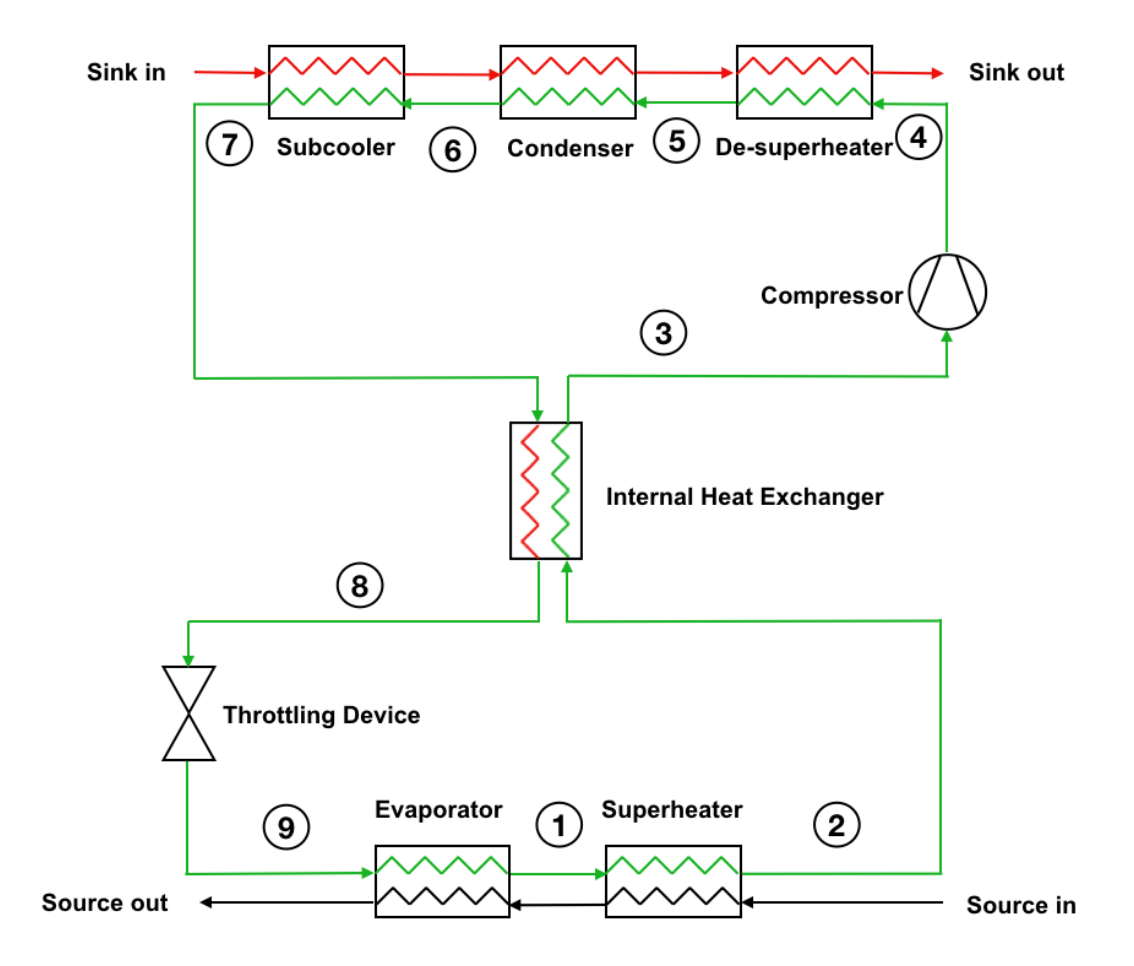


Figure 5.12: Schematic view of the 9 stages of the air-water heat pump incorporating an internal heat exchanger.

Figure 5.13 visualises the enthalpy, pressure, and temperature progression during the cycle.

5.5.4. Evaporation

The heat pump cycle starts at the evaporator by evaporating the refrigerant and thus adding energy to the heat pump cycle from an external energy source: ambient air. This source medium is assumed to be infinitely large since it will cause no constraints as long as enough air mass flow through the evaporators heat exchanger is realised by the fan.

Heat source

The heat source for the heat pump cycle is ambient air which is varying throughout the year. However, the heat pump is designed to be able to run at peak capacity at the lowest defined operating temperature which is $10\,^{\circ}C$.

The source temperature glide (ΔT_{source}) is assumed constant at 3 K for every source temperature input ($T_{source\,in}$). Using this assumption the source outlet temperature ($T_{source\,out}$) can be determined according to equation 5.34.

$$T_{source\ out} = T_{source\ in} - \Delta T_{source} \tag{5.34}$$

Evaporator

In the evaporator the refrigerant is evaporated by addition of energy from the ambient air. The ΔT_{hx} of the heat exchanger is defined at 3 K resulting in an evaporation temperature of $4^{\circ}C$ at an ambient air temperature

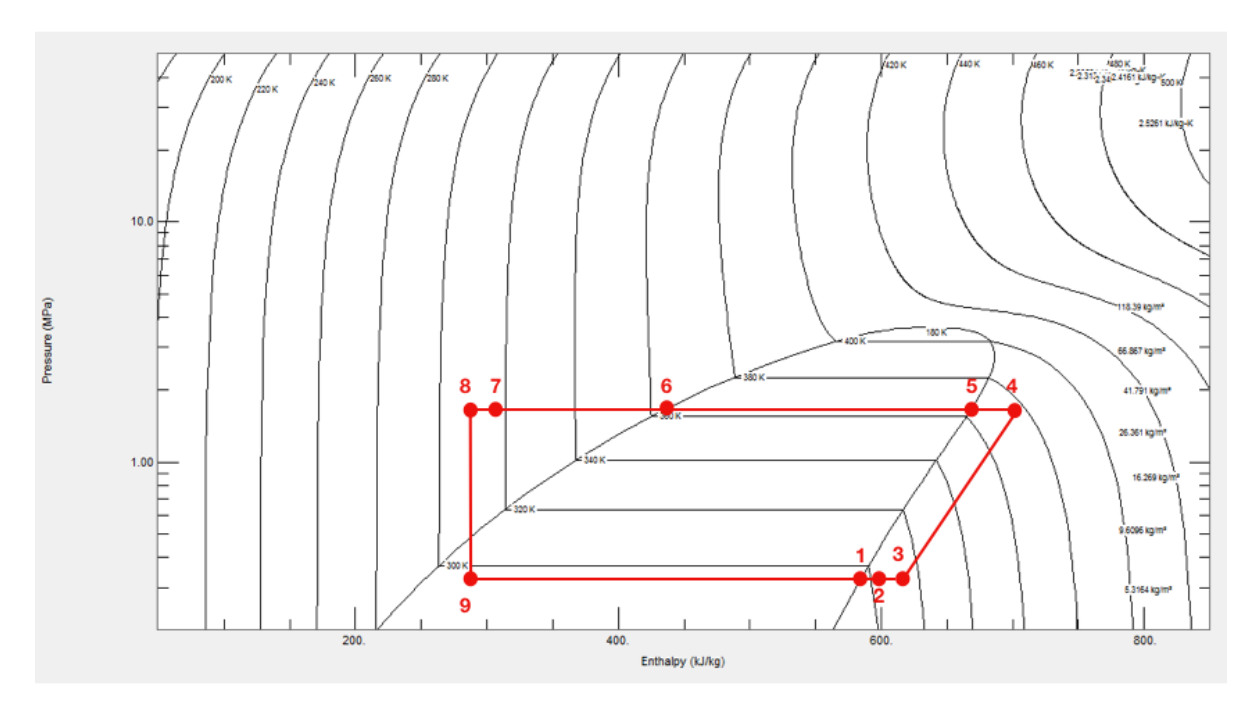


Figure 5.13: Heat pump cycle in the pressure-enthalpy diagram of iso-butane for a heat pump with internal heat exchanger as shown in figure 5.12 (with, $h_2 - h_3 = h_8 - h_7$).

of $10^{\circ}C$. The ΔT between source inlet and outlet is assumed constant at 3 K with a constant heat capacity of air.

The size and heat transfer coefficient UA of the heat exchanger is derived from equation 5.33 resulting in equation 5.35.

$$UA = ln(\frac{T_{source\,in} - T_{evap}}{T_{source\,out} - T_{evap}})\dot{m}_{source}c_{p\,air}$$
(5.35)

with \dot{m}_{source} resulting from equation 5.36

$$\dot{m}_{source} = \frac{\dot{Q}_{evap}}{c_p \Delta T_{source}} \tag{5.36}$$

Superheater

In the superheater the gaseous refrigerant is heated beyond the gas saturation line before entering the compressor. This is done to ensure the refrigerant is fully evaporated while increasing the enthalpy.

5.5.5. Compression

The evaporated refrigerant now runs into the compressor where it is compressed by a piston compressor increasing the pressure, temperature, and enthalpy. The mass flow through the compressor is important as it determines the amount of heat that is transported from the source to the sink, the amount of work that needs to be delivered by the compressor, and it determines the size of the compressor. The refrigerant mass flow (\dot{m}_{ref}) is given by equation 5.37.

$$\dot{m}_{ref} = \frac{\dot{Q}_{out}}{\Delta h_{cond}} = \frac{\dot{Q}_{out}}{h_4 - h_7} \tag{5.37}$$

The work delivered by the compressor is defined by the product of the refrigerant mass flow and the change in enthalpy before and after the compressor as shown in equation 5.38

$$\dot{W}_{comp} = \dot{m}_{ref} * (h_4 - h_3) \tag{5.38}$$

5.5.6. Condensation

The condensation side of the heat pump in reality consists of three stages. First the refrigerant passes the desuperheater, second it moves to the condenser where the gas condenses to a liquid and finally the now liquid passes through the subcooler where it cools down further. Figure 5.13 shows the condenser side of the heat pump and their states. All three stages are modelled separately from each other. During the three stages heat is transferred to the heat sink medium which in this case is water from the USTES.

Desuperheater

In the desuperheater the temperature of the refrigerant is reduced to the condensation temperature (T_{cond}). The enthalpy of the refrigerant is reduced from h_4 to the gas saturation line at state h_5 as seen in figure 5.13. By doing this the sink is heated further and results in the sink outlet temperature $T_{sink\,out}$. The temperature before and after the de-superheater is calculated using the 'refpropm' function in Matlab.

Condenser

In the condenser the refrigerant condenses while heating up the sink flow. The enthalpy states before and after the condenser are h_5 and h_6 respectively. The temperature of the refrigerant remains unchanged meaning only latent heat was transferred to the sink stream.

Subcooler

In the subcooler the refrigerant is further cooled down to the outlet temperature T_7 which is described by equation 5.39. It is assumed that the refrigerant and sink remain at a ΔT of 3 K as specified earlier for the heat exchanger.

$$T_8 = T_{sink\,in} + \Delta T_{sink} \tag{5.39}$$

5.5.7. Internal Heat Exchanger

The internal heat exchanger allows to cool the refrigerant further after the subcooler. The heat is transferred to the refrigerant just before the compressor. This further superheats the refrigerant resulting in a higher temperature after the refrigerant is compressed. The result is a higher COP than without this heat exchanger. Figure 5.13 shows the heat pump cycle in a pressure - enthalpy diagram incorporating this internal heat exchange [21]. The internal heat exchanger is simplified in the model. The difference in enthalpy between the states before and after the heat exchanger (state 7-8 and 2-3) are equal as seen in 5.13.

5.5.8. Expansion Device

In the expansion device the fluid is flashed reducing the pressure from high to low. This process is isenthalpic meaning the enthalpy states $h_9 = h_8$.



System design

This research is considering two systems which are to be simulated and compared. This section is dedicated to describe both systems in detail.

6.1. System Design 1: Solar Collector Based System

For the base case district heating network heat is generated by solar collectors, stored by a single USTES and has the possibility to use a water - water heat pump when the USTES temperature is below supply temperature level. A schematic overview of the system is given in figures 6.1 and 6.2.

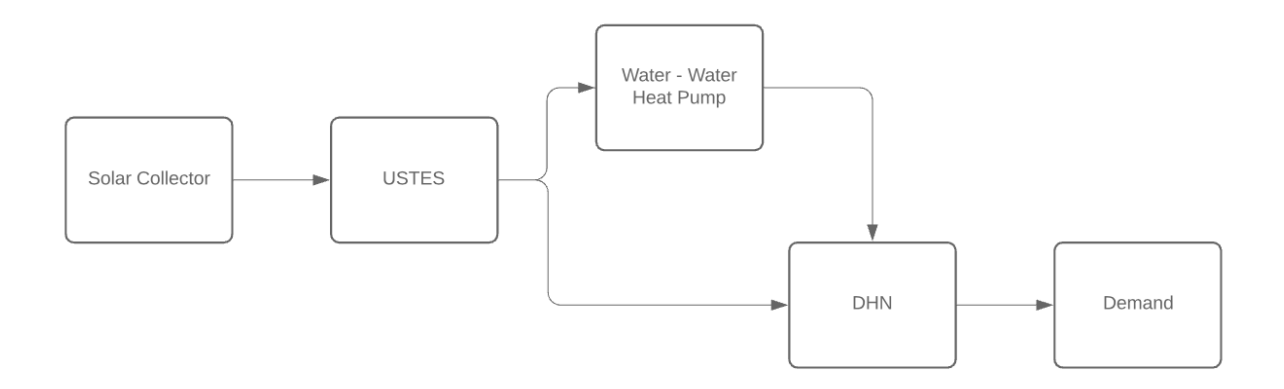


Figure 6.1: Flow chart overview of system design 1: solar collector based system. From the flow chart it becomes clear there are two options of discharging the USTES, directly into the DHN or through the water-water heat pump.

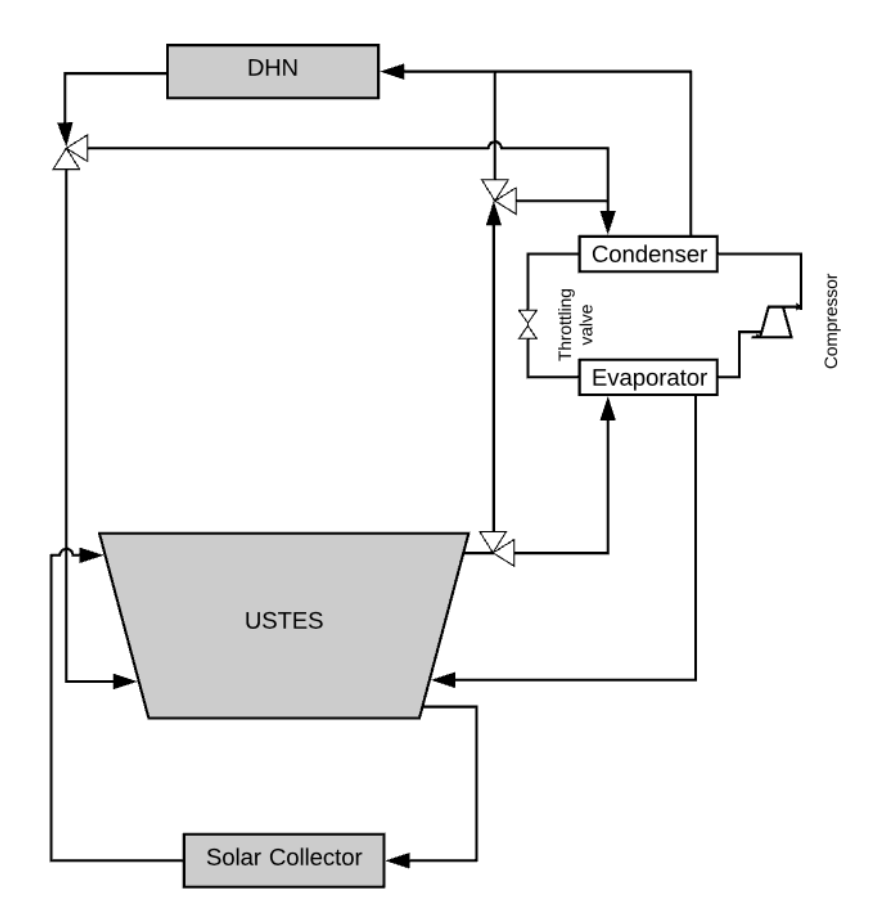


Figure 6.2: Technical overview of the components making up the solar collector based system. Arrows in the overview represent piping. The blank triangles represent valves.

The solar collector array consists of evacuated tube collectors. While in reality the collectors are likely to be decentralised, meaning the collectors will be installed on rooftops across the neighbourhood, during this study it is assumed that the collectors are centralised in one collector field. Collected heat is fed into the USTES after which it is transported into the DHN.

The model assumes centralised solar collector arrays since the DHN is not modelled in full detail. The assumption of centralised solar collectors does influence the output of the solar array. This is due to the fact that when decentralised solar collectors deliver heat to the DHN, the DHN will heat up. As more solar collectors deliver heat, the efficiency of heat exchange will decrease. Assuming the heat generation to be centralised and supplied directly to the USTES will therefore result in a more optimistic energy output of the solar collectors.

The size of the USTES is determined to ensure demand can always be supplied. This means the volume of the USTES must be sufficient to bridge the "Dunkelflaute" periods where no heat generation is possible. These are typically cold periods with low solar insolation. The USTES will be sized based on historical weather data.

Direct output from the USTES is limited to the supply service temperature $63-70^{\circ}C$. This means the output of the USTES is constrained by temperature and can only be cooled down to $70^{\circ}C$. To utilise an increased share amount of exergy an additional water-water heat pump is installed next to the USTES as seen in figure 6.1. This way the USTES functions as source for the heat pump while the DHN acts as sink. The water in the USTES can now be cooled down further in an efficient way since the heat pump operates at high COP's. This does require energy from the electricity grid and therefore the system will not be classified as fully self sustainable.

6.2. System Design 2: Air - Water Heat Pump Based System

This system consists of a central air - water heat pump for thermal energy generation, the USTES for thermal storage, a water - water heat pump to maximise exergy in the buffer, and the DHN to supply demand. A schematic overview of the system is given in figures 6.3 and 6.4.

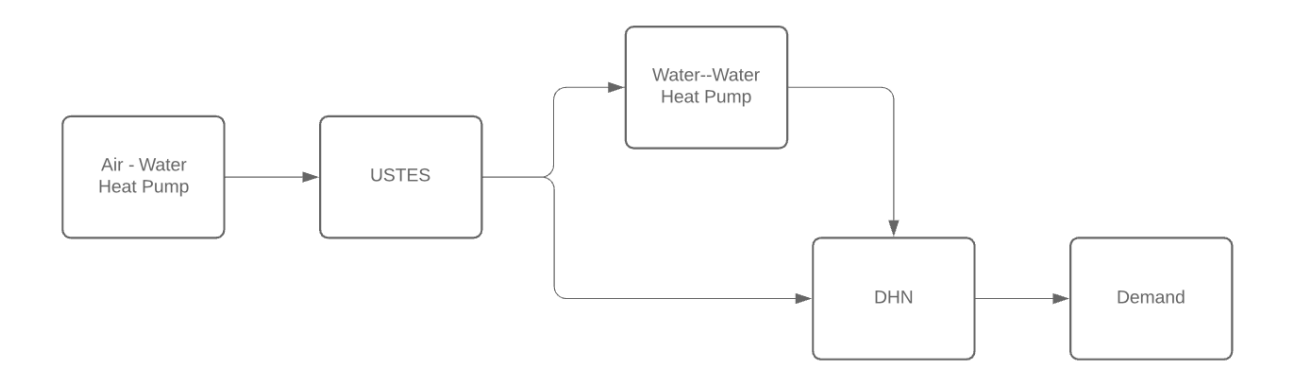


Figure 6.3: Flow chart overview of system design 2: air-water heat pump based system. The USTES can be discharged directly into the DHN or through the water-water heat pump.

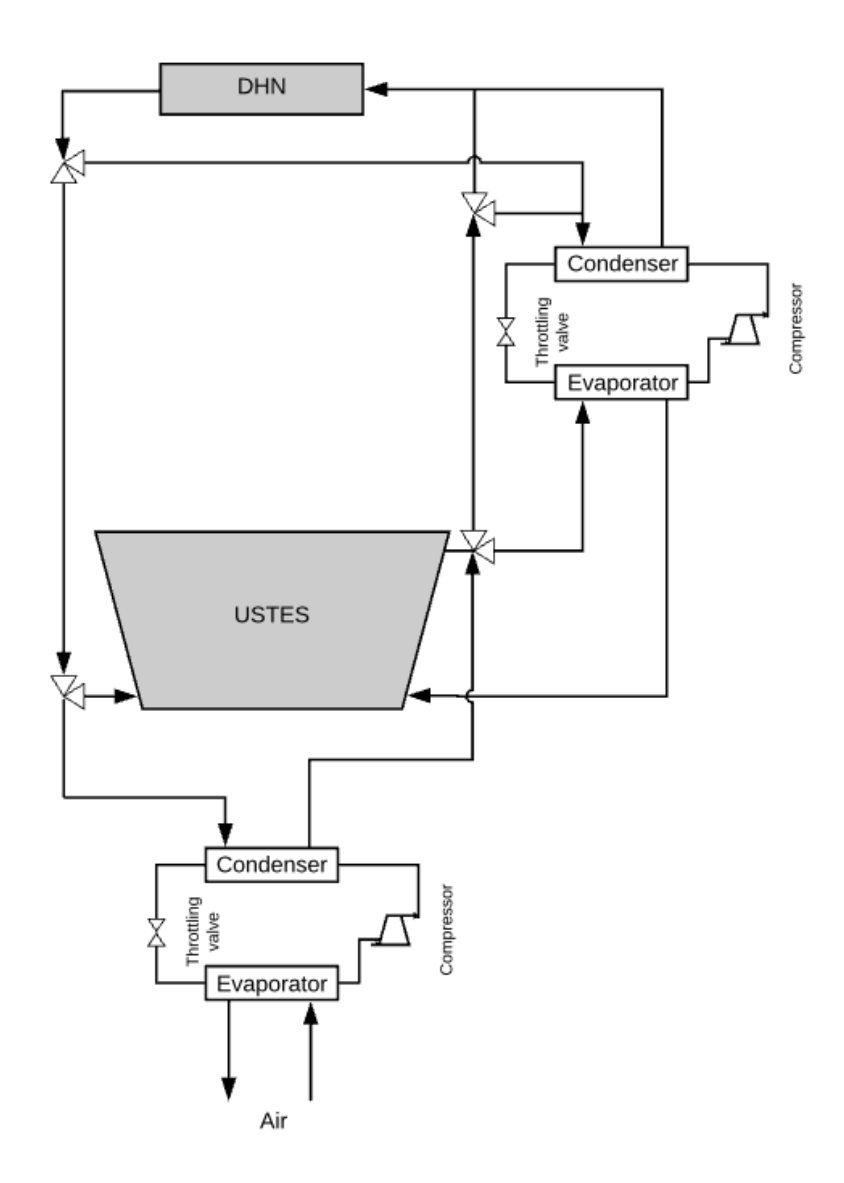


Figure 6.4: Technical overview of the components in the air-water heat pump based system. Arrows in the overview represent piping. The blank triangles represent valves.

System 2 uses a central air - water heat pump for heat generation. With the possibility to install multiple heat pumps for redundancy and to enable different power outputs. Water heated by the heat pump is fed into the top of the USTES.

Again the volume of the USTES needs to be sufficient to overcome the "Dunkelflaute" periods. Therefore the scaling of the USTES needs to be sufficient to overcome these periods. In this case the Dunkelflaute periods include periods with low ambient air temperature. It is expected that in this system the USTES volume will be smaller compared to system 1.

Like system 1 direct output from the USTES is limited to the supply service temperature $63-70^{\circ}C$. To utilise the full potential of the USTES an additional water-water heat pump is installed next to the USTES as seen in figure 6.3.

System 2 is not as self sufficient as system 1 (system 1 only uses some electricity to power pumps and the water - water heat pump). System 2 relies heavily on the electricity grid which can be seen as a disadvantage. This will be discussed in more detail later during this study.

6.2.1. Control Sequence

The system using an air-water heat pump has a control strategy based on the ambient air temperature. The different operating levels are described below.

Ambient temp ≥ $18^{\circ}C$

The heat pump will be operational while there is only some tap water demand by the households. The demand will be supplied by the USTES while simultaneously the heat pump is charging the USTES with hot water.

$10^{\circ}C \leq \text{Ambient temp} \leq 18^{\circ}C$

There is a space heating demand and the heat pump is operational. The heat pump is operational charging the USTES. Simultaneously the USTES is discharging into the DHN to meet demand.

Ambient temp ≤ min operating temperature Heat Pump

The heat pump is not operational at these ambient temperatures. Heat is supplied directly from the USTES. When the USTES is below supply service level $(63^{\circ}C)$ the water - water heat pump will "upgrade" the return heat with energy sourced from the USTES.

6.3. Discharging the USTES

The system can discharge into the DHN in three different modes depending on the temperature of the USTES. The schematic overview of the operation modes are presented in figures 6.5, 6.6, and 6.7.

1. $T_{USTES\ TOP} >= supply\ temperature$, the DHN return flow (m_4) mixes with the appropriate amount of mass from the top node of the USTES (m_1) (figure 6.5) to obtain the service level temperature. This is described by equations 6.1, 6.2, and 6.3.

$$\dot{Q}_2 = \dot{Q}_1 + \dot{Q}_4$$

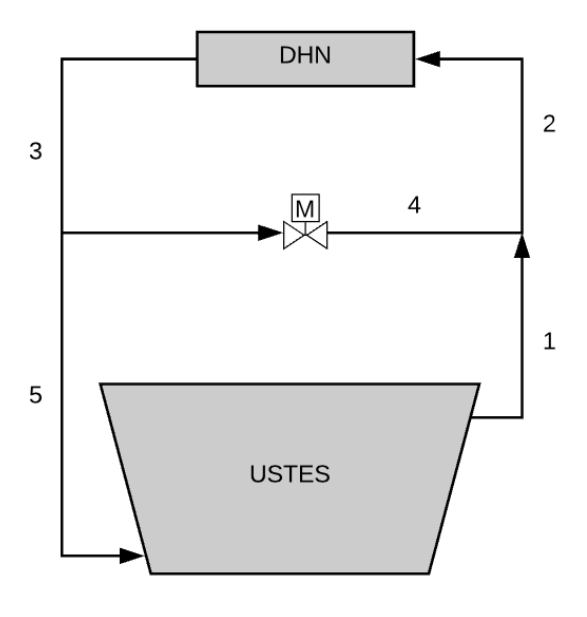
$$\dot{m}_2 c_p T_2 = \dot{m}_1 c_p T_1 + \dot{m}_4 c_p T_4$$
(6.1)

The mass balance follows as,

$$\dot{m}_2 = \dot{m}_1 + \dot{m}_4 \tag{6.2}$$

The mass flow needed from the top node of the USTES is described by equation 6.3. The DHN mass flow that re-enters the USTES in the bottom node can be derived from equation 6.2.

$$\dot{m}_1 = \dot{m}_2 * \frac{T_4 - T_2}{T_4 - T_1} \tag{6.3}$$

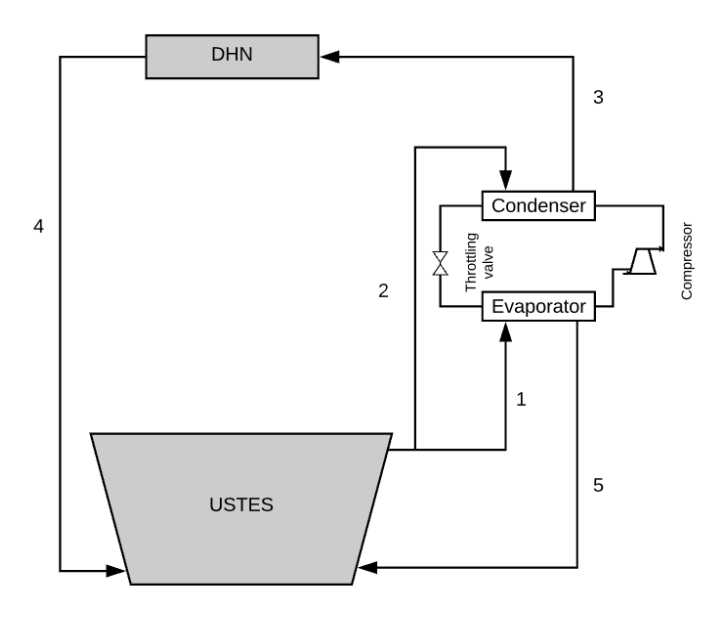


 $T_{USTES out} >= T_{supply}$

Figure 6.5: Discharging the USTES in mode one using the mixing valve. There is no need for use of the heat pump. Return water is mixed with water from the top of the USTES to achieve the desired supply temperature.

2. $T_{USTES\,(TOP)} >= T_{DHN\,(return)}$, $T_{USTES\,(TOP)} < supply temperature$, the water from the top of the USTES is not at the service level temperature and needs to be boosted by the heat pump. The mass flow from the top of the USTES acts both as sink and source for the heat pump as seen in figure 6.6. Equation 6.4 describes the mass flow through the evaporator, the mass flow through the condenser is equal to the mass flow of the DHN as $\dot{m}_2 = \dot{m}_3$.

$$\dot{m}_1 = \frac{(\frac{COP - 1}{COP})(T_3 - T_2)\dot{m}_3)}{(T_1 - T_5)} \tag{6.4}$$

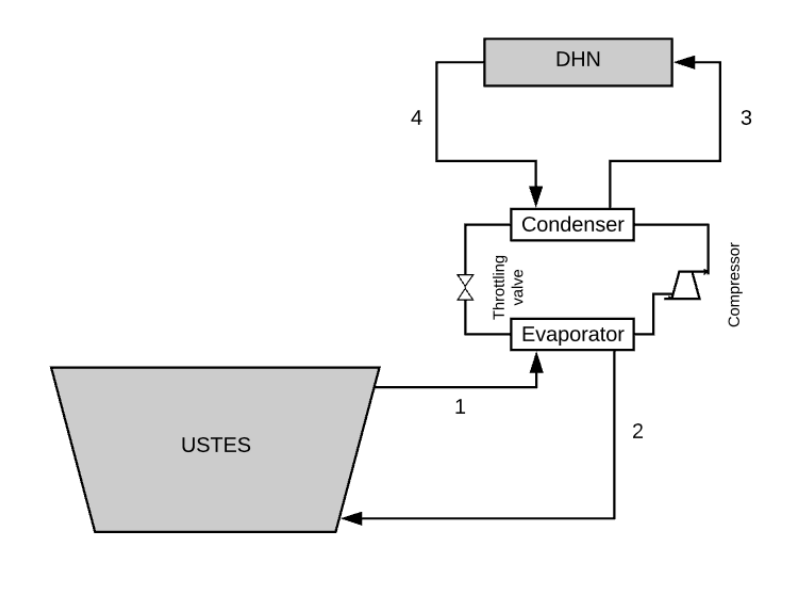


 $T_{return} < T_{USTES out} < T_{supply}$

Figure 6.6: Discharging the USTES in mode two. The heat pump is used to upgrade the heat from the USTES. Water from the top of the USTES is used both as sink and source for the water-water heat pump.

3. $T_{USTES\,(TOP)} < T_{DHN\,(return)}$, The water from the top of the USTES is below the return temperature of the DHN. In this case the DHN return flow will be directed to the sink of the heat pump where it will be reheated to the service level temperature. A mass flow from the top of the USTES will enter the evaporator of the heat pump and act as source as seen in figure 6.7. The mass flow \dot{m}_{evap} follows from equation 6.5. The mass flow through the condenser is equal to the mass flow in the DHN.

$$\dot{m}_1 = \frac{\dot{m}_3(T_1 - T_3)(\frac{COP - 1}{COP})}{(T_1 - T_2)} \tag{6.5}$$



T_{USTES out} <= T_{return}

Figure 6.7: Discharging the USTES in mode three. The return flow from the DHN is upgraded to the required supply temperature with the heat pump using water from the top of the USTES as its source.

6.4. Modelling the System Components

This section elaborates the modelling approach of all system components. All components are combined in the Simulink model. Finally the control mechanism as implemented in Simulink is discussed.

6.4.1. Demand

The demand is modelled from two input parameters. These are the hourly ambient air temperature provided by the KNMI, and the natural gas consumption of the households provided by the Energiek Nagele project. The two data sets are correlated to obtain the energy demand of the households per degree day, and subsequently degree hour. This is done according to equation 6.6. The space heating demand is corrected for the fact that households tend to lower the space heating during the night. This is done by multiplying the degree hours from 23:00 - 06:00 by 0.7. This lowers the total number of degree hours giving more weight (more gas consumption) to the degree hours during the day (the total annual energy demand is not affected)

$$E_{degree\,day} = \frac{E_{Gas\,total}}{N_{degree\,days}} \tag{6.6}$$

where $E_{Gas\ total}$ is the total energy of the natural gas in [J] using 35.17 MJm⁻3 natural gas, $N_{degree\ days}$ is the total number of degree days in one year with the heating demand threshold assumed to start at 18° C.

The hot tap water demand is assumed consistent throughout the year and is therefore considered as a base load on which the space heating demand is added. The gas consumption related to cooking purposes is accounted for by subtracting it from the total initial natural gas demand.

6.4.2. USTES

To model the USTES the energy balance needs to be considered. Mass flows leave and enter the USTES at different temperatures changing this energy balance. Also, the USTES is heated up by the solar collector array. The result is an energy balance with various components, these are: heat losses, heat conduction, mixing between nodes (convection), solar energy charging, and heat exchange with the DHN. The previous components are visualised in figure 6.8 and described in more detail below.

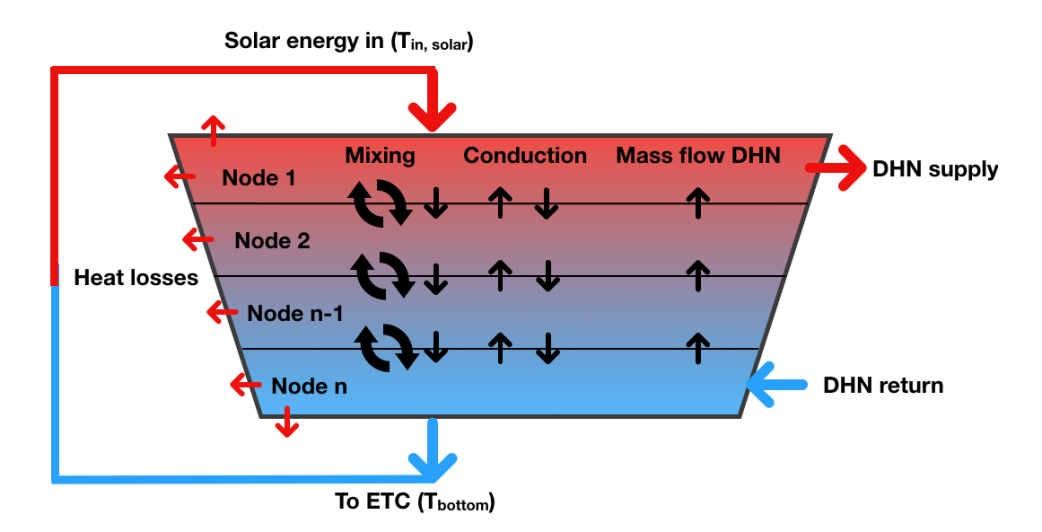


Figure 6.8: Energy flows in the USTES consisting of the heat losses to its surroundings, mixing between nodes, conduction between nodes, mass and heat transport due to solar charging, and mass and heat transport due to heat supply to the users through the DHN.

Heat Losses

The heat losses described in the model are broken down into three parts. The losses in the upper node (the top of the USTES), the losses to the walls of the USTES in all nodes, and the losses in the bottom node at the bottom of the USTES.

The heat loss coefficients can be found in table 5.1. For the top, walls and bottom of the USTES the U values are 0.088, 0.112, and 0.18 Wm⁻² K respectively. The change in energy of a node over time is described by Newtons law given by equation 6.7.

$$\frac{dQ}{dt} = UA_{loss}(T_{node} - T_{ground}) \tag{6.7}$$

where, U is the heat loss coefficient in [Wm⁻²K], A is the surface area subject to heat loss in [m²], T_{amb} is the ambient temperature surrounding the USTES in [K], and T_{node} is the temperature of the node in [K].

The temperature of the soil surrounding the USTES is not consistent since the soil on top of the USTES will cool faster due to contact with the environment, whereas the soil surrounding the USTES will show more constant temperatures.

Conduction

Heat conduction acts between adjacent nodes and is described by two equations. Equation 6.8 describes the change in temperature over time of a node due to conduction between the current node and the node above while equation 6.9 describes the same process for the interaction with the node below the current node.

$$\frac{dQ}{dt} = \frac{\lambda}{dz} A(T_{node\ above} - T_{node}) \tag{6.8}$$

$$\frac{dQ}{dt} = \frac{\lambda}{dz} A(T_{node} - T_{node \, below}) \tag{6.9}$$

where, λ is the thermal conductivity in $[Wm^{-1}K^{-1}]$, and dz is the distance between the centers of two nodes in [m].

Solar Energy Charging

Water from the bottom of the USTES is used as feed into the inlet of the solar collector array. The heated fluid from the outlet of the solar collectors is fed back into the top of the USTES as seen in figure 6.8. The mass flows of the DHN are schematically visualised in figure 6.9. The energy transport due to solar charging is described by equation 6.10.

$$\frac{dQ}{dt} = \dot{m}_4 c_p T_4 \tag{6.10}$$

$$\frac{dQ}{dt} = -\dot{m}_3 c_p T_3 \tag{6.11}$$

with $\dot{m}_4 = \dot{m}_3$

where, \dot{m}_4 is the mass flow from the ETC array in [kgs⁻¹], c_p is the heat capacity of water in [Jkg⁻¹K⁻¹], T_4 is the temperature from the ETC's into the USTES in [K], and T_3 is the temperature of the bottom node of the USTES going to the ETC's in [K].

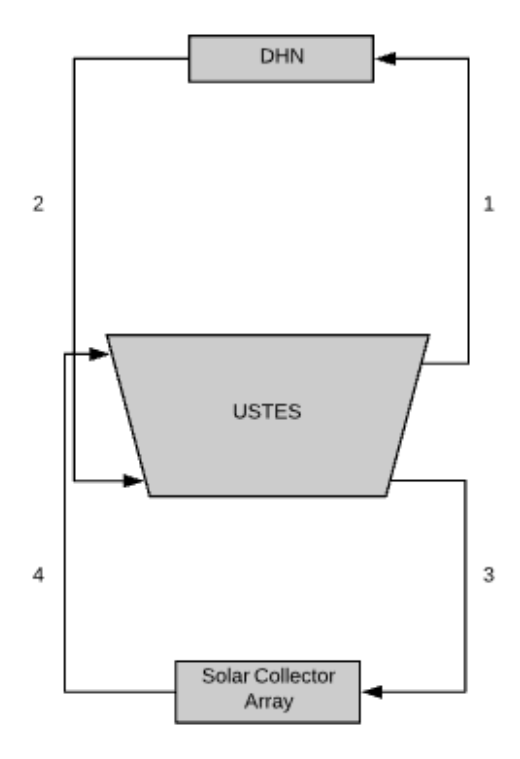


Figure 6.9: Mass flows from the USTES to the DHN and to the solar collector array.

Energy Exchange with the DHN

Energy exchange with the DHN occurs through a mass flow from the top node through the DHN back into the bottom node. Mass exiting the top node is described by equation 6.12. The DHN heat re-entering the bottom node of the USTES is described by equation 6.13.

$$\frac{dQ}{dt} = -\dot{m}_1 c_p T_1 \tag{6.12}$$

$$\frac{dQ}{dt} = \dot{m}_2 c_p T_2 \tag{6.13}$$

Due to this mass flow, mass transport occurs between nodes in the USTES. This mass flow is equal to that of the mass flow going out of the top node or into the bottom node since the mass balance of the USTES is constant and no increase or decrease of mass occurs in the USTES according to: $\dot{m}_1 = \dot{m}_2$. This results in a mass flow leaving node n at the temperature of node n. At the same time an equal amount of mass enters node n at the temperature of node n-1. This is described by equations 6.14 and 6.15

$$\frac{dQ}{dt} = -\dot{m}_1 c_p T_n \tag{6.14}$$

$$\frac{dQ}{dt} = \dot{m}_1 c_p T_{n-1} \tag{6.15}$$

however, the mass flow due to solar charging changes the balance when both the DHN mass flow and the solar charging mass flow are positive. The mass flow up/down between two nodes of the USTES follows from equations 6.16

$$\dot{m}_{un/down} = \dot{m}_2 - \dot{m}_3 \tag{6.16}$$

when $\dot{m}_{up/down}$ is positive the mass flow between two adjacent nodes is up while a negative value indicates a downward mass flow.

Inversed Thermocline Mixing

The nodes have different temperatures, generally the warmest nodes are in the top of the USTES while it becomes cooler going down. Due to this temperature differences between nodes a thermocline with a positive gradient exists. When the gradient shifts and becomes negative, i.e. when a node below another node is warmer, we speak of an inversed thermocline. Since the density of water decreases when heating up (only exception below 4°*C*) mixing based on density difference will occur. The warmer water will flow upwards creating mixing between nodes. This process has been researched by Cadafalch et al. [1] and Austin et al. [23]. Cadafalch et al. found that to model the mixing between nodes the thermal conductivity can be assumed infinite such that any inversed thermocline in the water column is eliminated. Cadafalch et al. also found that when, after mixing between nodes, still an inversed thermocline exists the process must be repeated until the entire inversed thermocline is eliminated.

In reality an inversed thermocline will be rare, however it must be taken into account for the model to work under all conditions.

Final Energy Balance

The total differential equation describing the time derivative of temperature is given by equation 6.17.

$$\frac{dQ}{dt} = -UA_{loss}(T_{node} - T_{ground}) + \frac{\lambda}{dz}A(T_{node\,above} - T_{node}) - \frac{\lambda}{dz}A(T_{node} - T_{node\,below}) + \dot{m}_3c_p(T_3 - T_4) - \dot{m}_1c_pT_1 + \dot{m}_1c_pT_2 - \dot{m}_1c_pT_n + \dot{m}_1c_pT_{n-1}$$

$$(6.17)$$

where the final step consists of calculating the temperature of each node. This is done according to equation 6.18

$$T_{node} = \frac{Q_{node}}{\rho c_p V_{node}} \tag{6.18}$$

6.4.3. Solar Collector

The solar collector is modelled using the quasi dynamic approach as discussed in section 5.3. This model does not describe the suns position or the angle of incidence over the year. This is necessary to obtain an accurate estimate of the collector output. The suns position and the angle of incidence are discussed in the following section.

6.4.4. Angle of Incidence

The angle of incidence describes the angle between the surface normal to the solar collector and the sunlight direction. Before the angle of incidence can be described the position of the sun must be known. The position of the sun depends on the time of the day and year due to the changing position of the earth relative to the sun.

Smets et al. [34] tell us that the suns position at a certain moment in time relative to the horizon is described by the angular elevation of the sun a_s as seen in figure 6.10 with a range of -90° - 90° where $a_s > 0$ describes the sun above the horizon and 90° describes the suns position normal to the earth surface.

The azimuth A_s as seen in figure 6.10 describes the suns position in the horizontal direction ranging from 0° - 360° corresponding to North (0°) - East (90°) - South (180°) - West (270°).

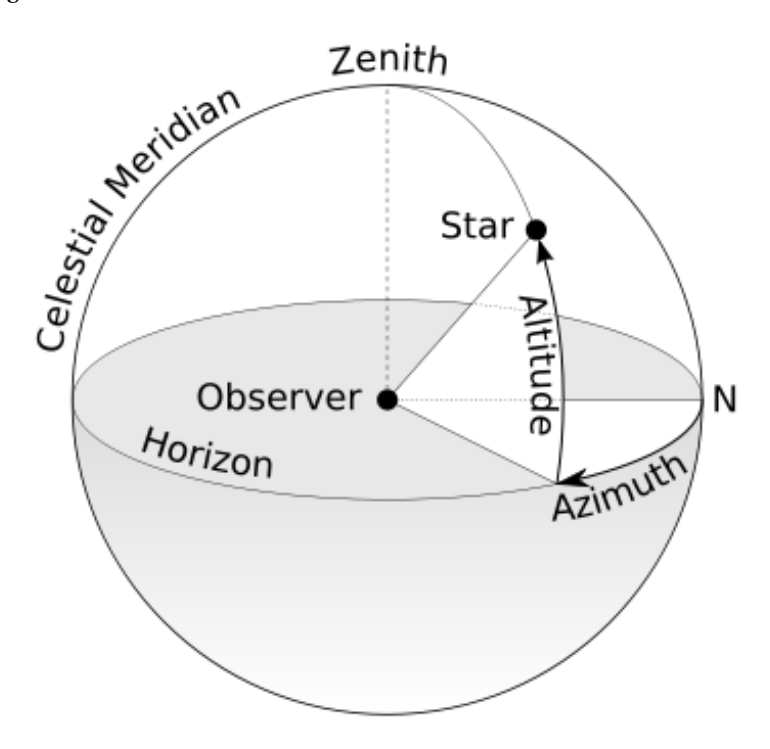


Figure 6.10: Visualisation of the suns angle relative to the observer point with the azimuth A_s and altitude a_s .

Smets et al. give a method to describe the suns position on the ecliptic circle at a certain time and place given by Equation 6.19 and 6.20

$$\tan A_{s} = \frac{-\sin \theta_{L} \cos \lambda_{S} + \cos \theta_{L} \cos \epsilon \sin \lambda_{S}}{-\sin \phi_{0} \cos \theta_{L} \cos \lambda_{S} - (\sin \phi_{0} \sin \theta_{L} \cos \epsilon - \cos \phi_{0} \sin \epsilon) \sin \lambda_{S}}$$
(6.19)

$$\sin a_{s} = \cos \phi_{0} \cos \theta_{L} \cos \lambda_{S} + (\cos \phi_{0} \sin \theta_{L} \cos \epsilon + \sin \phi_{0} \sin \epsilon) \sin \lambda_{S}$$
 (6.20)

Where the angle of the module is described as (θ_L) , the suns ecliptic longitude as λ_S , axial tilt ϵ , and the locations latitude ϕ_0 .

Now the position of the sun from a certain point on earth is known, this position can be translated into the angle of the sun to this point. This angle of incidence γ is described as the angle between the direction of sunlight and the surface normal of the panel. The scalar product of the normal vector of the module and the sun can be used to calculate $\cos \gamma$ as seen in equation 6.21

$$\cos \gamma = \vec{n}_M \times \vec{n}_S \tag{6.21}$$

where \vec{n}_M is the normal vector of the module and \vec{n}_S is the normal vector of the sun given by

$$\vec{n}_M = \begin{pmatrix} \cos a_M \cos A_M \\ \cos a_M \sin A_M \\ \sin a_M \end{pmatrix}, \tag{6.22}$$

$$\vec{n}_M = \begin{pmatrix} \cos a_M \cos A_M \\ \cos a_M \sin A_M \\ \sin a_M \end{pmatrix}, \tag{6.22}$$

$$\vec{n}_S = \begin{pmatrix} \cos a_S \cos A_S \\ \cos a_S \sin A_S \\ \sin a_S \end{pmatrix}. \tag{6.23}$$

6.4.5. Heat Pump

The heat pump model is written in Matlab code and calls upon REFPROP to determine thermodynamic states of the refrigerant in the given states. This Matlab code is written as a "Matlab function" in Simulink to integrate it as part of the total system. All thermodynamic states are calculated as discussed in section 5.5.3.

The coefficient of performance of the heat pump is calculated for every time step and averaged over the number of operating hours. This results in the Seasonal COP (SCOP).

Cost of Components

The cost of components is an important factor to take into account when considering different technologies for a project. This section will give estimates on the cost of each component and finally an approximation of the total system costs will be presented. All cost indications are without taking into account any subsidies.

7.1. Cost of the USTES

The costs of the USTES are estimated at $150 \in /m^3$ based on a quotation from the company HoCoSto for a USTES from 800 m^3 . The costs of the USTES however do not increase linearly with size. The costs per cubic meter of buffer are decreasing with increasing USTES volume since some activities have to be performed regardless of the installed volume. These activities include for instance, permit approval, drainage, excavating costs, and logistics. Also, with increasing volume the need for insulation decreases and less building material per m^3 is required due to the surface area to volume ratio.

7.2. Cost of the Heat Pump

The heat pumps will be sourced from the Dutch heat pump manufacturer NRGTEQ. The costs of the different types of heat pumps are based on quotations by this company.

Air-Water Heat Pump

The air-water heat pump costs are determined at $450 \in /kW$ installed capacity. When installing multiple heat pumps for redundancy the total costs are expected to be slightly larger due to installation costs.

Water-Water Heat Pump

The water-water heat pump costs are quoted at $500 \in /kW$ installed capacity. This is slightly more expensive compared to the air-water heat pump since the rated capacity is in a lower range.

7.3. Cost of the Evacuated Tube Solar Collector Array

ETC costs are estimated at $450 \in /m^2$ based on a quotation from HoCoSto. The solar collector manufacturer is Kloben Industries. Installation costs can be lowered by installing the solar arrays centralised instead of scattered on rooftops.

7.4. Cost of the PV Array

PV panel costs have declined dramatically over the years. The cost for a pv panel with an efficiency of 19.5% is around $0.30 \le /Wp$. The cost for racking, inverter, and installation make up the rest of the cost at about 0.60 \le /Wp . The average combined costs are 0.90 euro per installed Wp. Since the standard size of a PV panel is $1.6m^2$ at 320Wp per panel the installed amount of Wp/m^2 is 200. At 0.90 euro per Wp this comes down to $180 \le /m^2$.

7.5. Cost of the DHN

The district heating network costs cannot be based on traditional district heating networks since it differs on many levels for instance that it uses smaller pipes. It is hard to give an exact figure since the costs depend on a lot of factors but costs are estimated to around $150 \in /m$.

Since both systems have a similar DHN the costs will not have a major influence on the overall conclusion. However, a good cost estimate is necessary to compare the systems to the current natural gas central heating systems.

The total length of the DHN is estimated at 700 meter. At a cost of 150 €/m this comes down to €105000, for the DHN. The costs contribute to the CAPEX of the system since it is installed during the first phase of the project.

7.6. Operation and Maintenance Costs

The operation and maintenance costs (O&M) imply all costs that are associated with keeping the system components in operating conditions. The costs are based on HoCoSto's O&M fee quotation at 1.2% of the CAPEX.

7.7. Weighted Average Cost of Capital

The weighted average cost of capital (WACC) describes the cost of capital. The WACC used during this study was based on earlier projects conducted by HoCoSto. The interest rate is based on a 20% allocation of private capital at 5% interest and an 80% capital raise through a bank/government loan at 1%, this results in the combined interest rate of 1.8%. This is based on interest rates for financing green energy projects in 2020. Future interest rates may differ from the rate used during this study.

7.8. Cost of Electricity

The cost of electricity is relevant when the PV array is not able to generate enough electricity. The costs are not constant since energy taxes decrease when a certain consumption threshold is reached. The first 10000 kWh are subject to $0.0997 {\in}/kWh$ tax while for every kWh above this threshold, until 2.5 million kWh, only $0.05083 {\in}/kWh$ tax is paid. The price per kWh for the electricity remains constant at $0.0783 {\in}/kWh$. Table 7.1 provides a summary of the costs.

Table 7.1: Cost overview of the system components. Costs are presented in the relevant units according to this study. In the final column it is noted whether the cost contribute to the initial capital expenses (CAPEX) or operating costs (OPEX).

Cost [€]	Capacity	CAPEX/OPEX
150	m ³	CAPEX
500	kW	CAPEX
450	kW	CAPEX
450	m^2	CAPEX
180	m^2	CAPEX
150	m	CAPEX
0.178	kWh	OPEX
0.150	kWh	OPEX
1.2% of CAPEX		OPEX
	150 500 450 450 450 180 150 0.178 0.150	150 m³ 500 kW 450 kW 450 m² 180 m² 150 m 0.178 kWh 0.150 kWh

7.9. Levelised Cost of Heat 69

7.9. Levelised Cost of Heat

The levelised cost of heat (LCOH) is defined as the total amount of heat delivered to the households divided by the initial investment or capital costs (CAPEX) of the system plus the operational costs (OPEX). The discount rate corrects future expenses as present value. Equation 7.1 presents a method to calculate the LCOH.

$$LCOH = \frac{CAPEX + \sum_{t=1}^{T} \frac{OPEX_t}{(1+r)^t}}{\sum_{t=1}^{T} \frac{E_t}{(1+r)^t}}$$
(7.1)

where T is the total life expectancy of the system, t is the time in years, t is the discount rate, $OPEX_t$ is the total operating costs in year t, and E_t is the total energy delivered in year t

The discount rate is assumed at 2% since sustainable energy projects generally are subject to low interest rates.

III

Evaluation



Validation per Component

8.1. Demand Validation

The energy demand of the users is based on the documented combined natural gas consumption of the users in 2018 as presented in table 4.1. The energy consumption was linked to the ambient temperature of that year according to the degree day method presented in chapter 4. The yearly energy consumption for the users corresponds to similar household size and building type and the annual energy demand after conversion to degree days corresponds to the initial energy demand of the users.

8.2. Solar Collector Validation

The solar radiation model is validated by comparing the tested power outputs defined by the solar collector manufacturer with the outputs of the Simulink model. The manufacturer Kloben provides the tested outputs in a summarised data sheet [18].

The solar collectors are modelled by the European standard EN 12975-2 as discussed in section 5.3 which has been extensively researched in laboratory experiments and in actual outdoor experiments. It acts as the primary standard for solar collectors sold in the European Union.

Manufacturer estimates compared to Simulink outputs

The datasheet provided by the manufacturer Kloben provides estimates of the energy output of the collector under different weather conditions. The parameter values used by Kloben to determine the power output per collector are given in table 8.1

Table 8.1: Test parameters and results for the 'ATON' solar collector type as presented by Kloben [18].

Parameter	Value	Unit
G_b	850	Wm^{-2}
G_d	150	$ m Wm^{-2}$
$T_m - T_{amb}$	50	K
Power output "ATON G 22-0" (4.71 m ²)	2739	W
Power output "ATON series" per m ²	582	W

The Simulink modelled power output for an ATON G 22-0 solar collector is 2749 W. The output for one m^2 is 583.6 W. This indicates the solar collector model accurately describes the manufacturers estimated power outputs. The model outputs deviate 3.6% and 2.7% respectively from the solar collector data sheet.

The solar collector efficiency is also tested according to CDR (EU) No 811/2013, resulting in a collector efficiency of 59% as presented by Kloben Industries [18]. The Simulink model constructed for this study cal-

8.3. PV Array 74

culated an efficiency of 59% based on the same parameters as presented by Kloben. From this it can be concluded the solar collector model is complying with the data provided by the manufacturer.

Based on this validation it can be concluded that the solar collector model is accurate in predicting the power and energy output of the solar collector with acceptable error margin.

8.3. PV Array

The photo-voltaic array consists of panels with an efficiency, as claimed by the manufacturer, of 19.7%. Throughout the year the efficiency of the PV module ranges around 20%, corrected for temperature changes of the module. The cumulative energy output for the year 2018 is 209 kWhm⁻² without taking into account the losses associated with the balance of systems. The cumulative solar irradiance incident on one square meter for the same year (2018) is 1071 kWhm⁻². This means the efficiency of the PV module simulation is 19.4% averaged over the year 2018. This is a 1.5% deviation from the manufacturers estimates which is likely to be the result of temperature variations.

The electricity production including the efficiency losses due to the balance of systems are lower. After incorporating these losses it follows that 17.6 % of the incident energy can be used as electricity or 188.5 kWhm $^{-2}$ in the year 2018. Averaged over a 5 year time period (Jan 2015 - Dec 2019) the annual electricity production is 193 kWhm $^{-2}$

8.4. USTES

The validation of the USTES is performed by validating the temperature decline due to heat losses and conduction over time. This is done without taking the charging and discharging into account since no data for validation are available on these processes. Instead it is assumed that as long as the energy balance of the USTES checks out with the in- and outflow of energy, all energy in the system is accounted for and no energy is lost to surroundings. Since the water-water heat pump increases the exergy and temperature operating range of the USTES, the effect of any misplaced energy (i.e. slight temperature differences between nodes) will be negligible.

The heat losses and the conduction in the USTES unfortunately cannot be validated on field experiments since no data are available on long term temperature declines. Instead the model is validated by comparison with a model currently used by the company HoCoSto. The model used by the company HoCoSto is less extensive compared to the model presented in this study. It could therefore only confirm that the heat losses are within the expected range.

Figures 8.1-8.3 show the cooling down of 3 different USTES sizes (500, 1000 and 3000 m³ respectively). It is expected that with increasing USTES size, heat losses will decline and therefore cooling down of the USTES nodes will take longer.

8.4. USTES 75

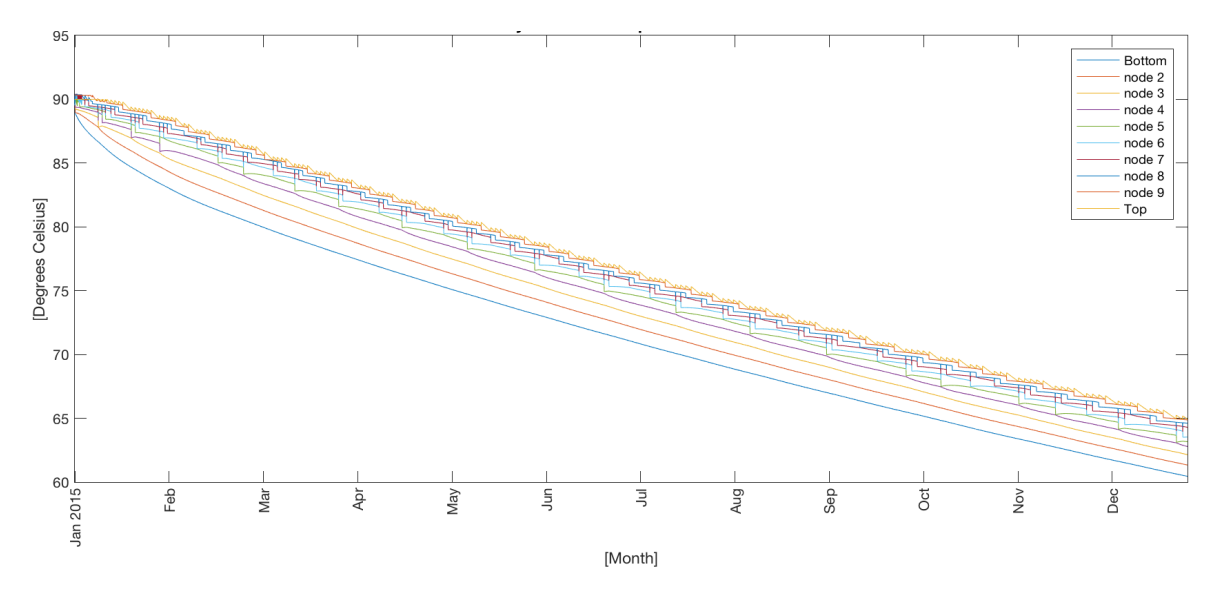


Figure 8.1: 1 year temperature decline for a USTES of 500 $\mathrm{m}^3.$

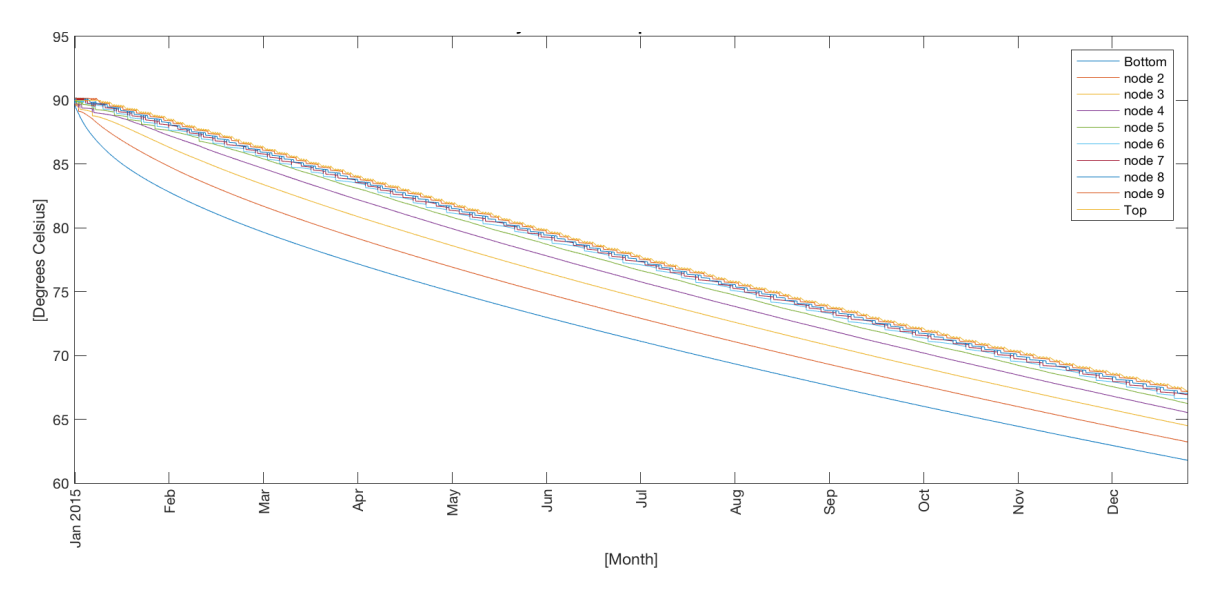


Figure 8.2: 1 year temperature decline for a USTES of 1000 m^3 .

8.4. USTES 76

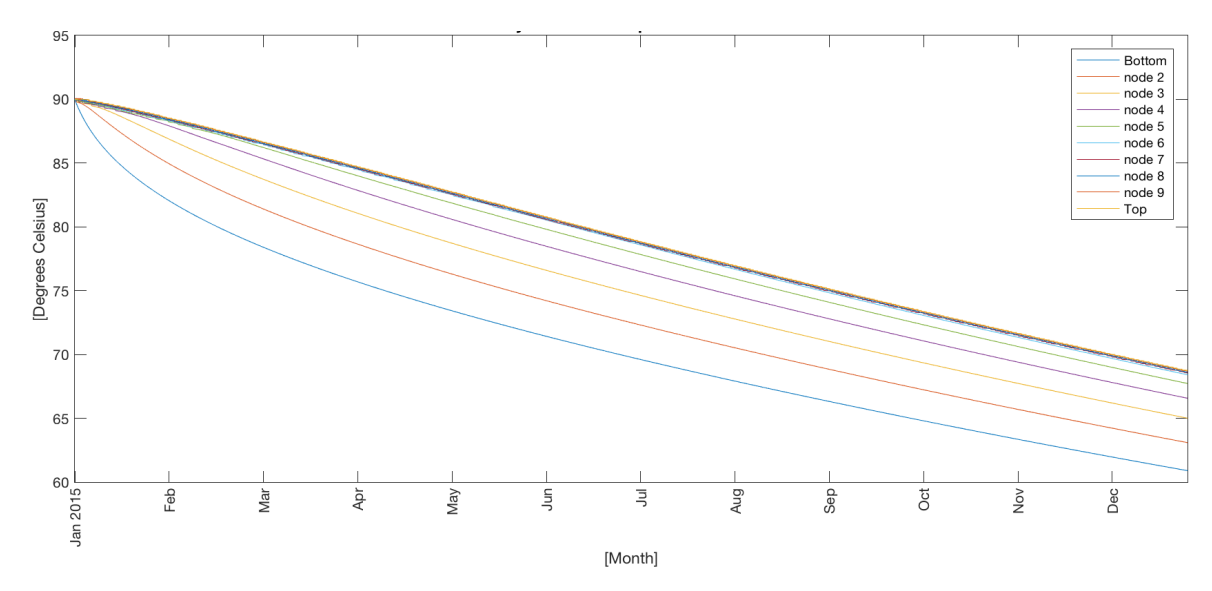


Figure 8.3: 1 year temperature decline for a USTES of 3000 m³.

However, it appears this effect is little since the USTES is constant in height at 4 meters. This results in that, from certain volumes, the heat losses at the top and bottom are prevalent and increase linearly with USTES size. Therefore, the temperature decline of the USTES is not affected majorly. In fact, between the USTES volumes of 1000 and 3000 m³ the heat losses through the bottom and top are prevalent, resulting in a constant average temperature after one year. The ΔT between the top and bottom node does increase slightly.

When comparing a smaller USTES size of 500 m^3 (figure 8.1) to a USTES with 1000 m^3 volume (figure 8.2) the difference in temperature decline becomes more clear. After one year the temperature of the 500 m^3 USTES is $1.5 \,^{\circ}\text{C}$ lower compared to the $1000 \,^{\circ}\text{m}^3$ USTES.

This effect becomes even more clear when the heat losses through the top, bottom and sides are evaluated separately. Figures 8.4 and 8.5 present the heat losses through the top, bottom and sides for different USTES sizes.

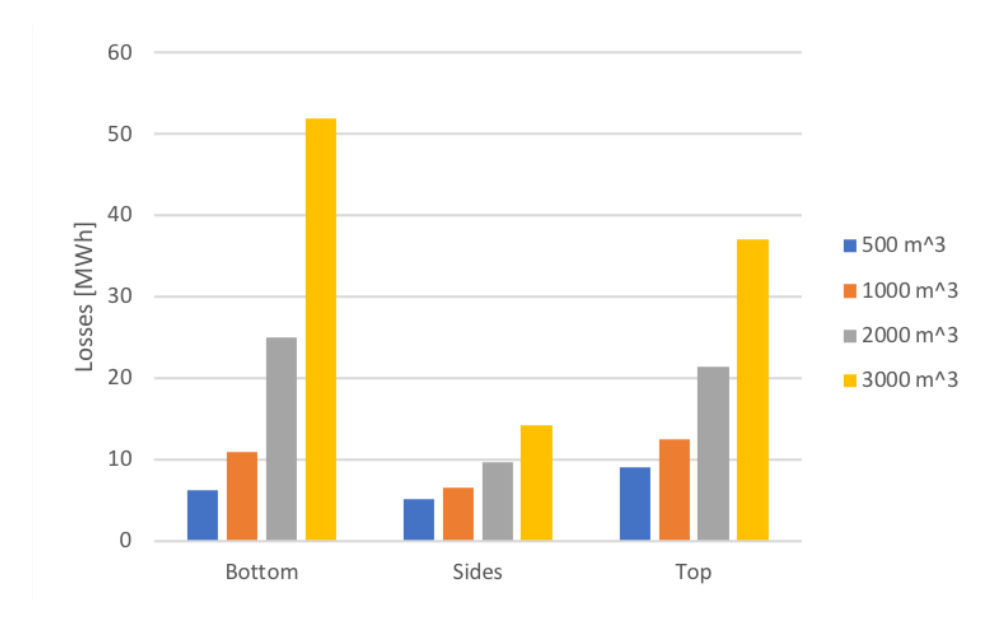


Figure 8.4: Heat losses for four different USTES volumes (500, 1000, 2000, and 3000 m^3) over a period of one year. From the graph it becomes clear that the heat losses through the top and bottom are prevalent and increase more with increasing USTES volume compared to heat losses to the sides. The higher heat losses through the bottom compared to the top are the result of better insulation at the top.

8.4. USTES 77

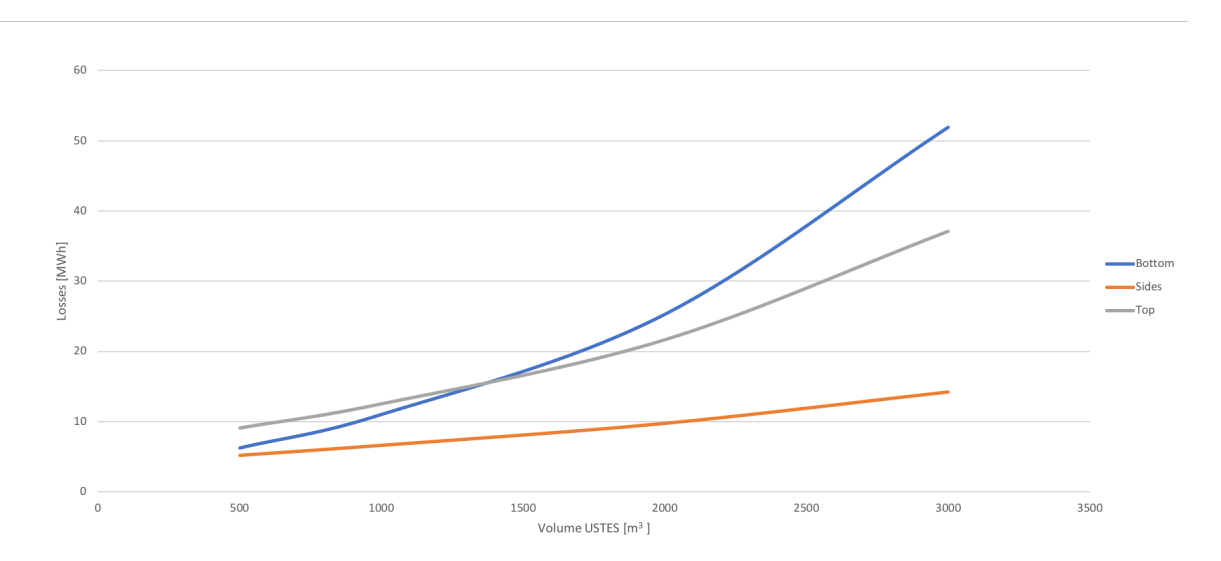


Figure 8.5: At small USTES sizes the bottom heat losses are smaller since the surface area of the bottom is significantly smaller compared to the top surface area. At larger volumes this effect decreases since the USTES has a fixed height of 4 meters and constant 45° sloped walls. This results in that from 1400 m³ the bottom heat losses surpass the top heat losses.

From these figures it is clear that the heat losses through the bottom and top increase faster compared to the heat losses through the sides. More surprising is the stronger heat loss increase in the bottom compared to the top. This is the result of the differences in insulation. The top is better insulated resulting in lower heat losses. However, due to the shape of the USTES the top surface area is larger compared to the bottom area. Since the height of the USTES is fixed at 4 meters and the walls are sloped at 45° the relative surface area increase of the bottom compared to the top is increasing with increasing volume. This results in that from 1400 m^3 the bottom heat losses surpass the top heat losses.

5 year time period

The temperature decline of an USTES of $1000~\text{m}^3$ volume over a time period of 5 years is presented in figure 8.6. The temperature decline is from 90~°C to 30~°C. This is a decline of 0.03~°C/day or 12~°C/year. However the temperature decline is not linear but is steeper at higher USTES temperatures. Looking at figure 8.2 it can be observed that for a $1000~\text{m}^3$ USTES during the first year the temperature decline is 25~°C from 90~°C to 65~°C. This is a decline of 0.07~°C/day.

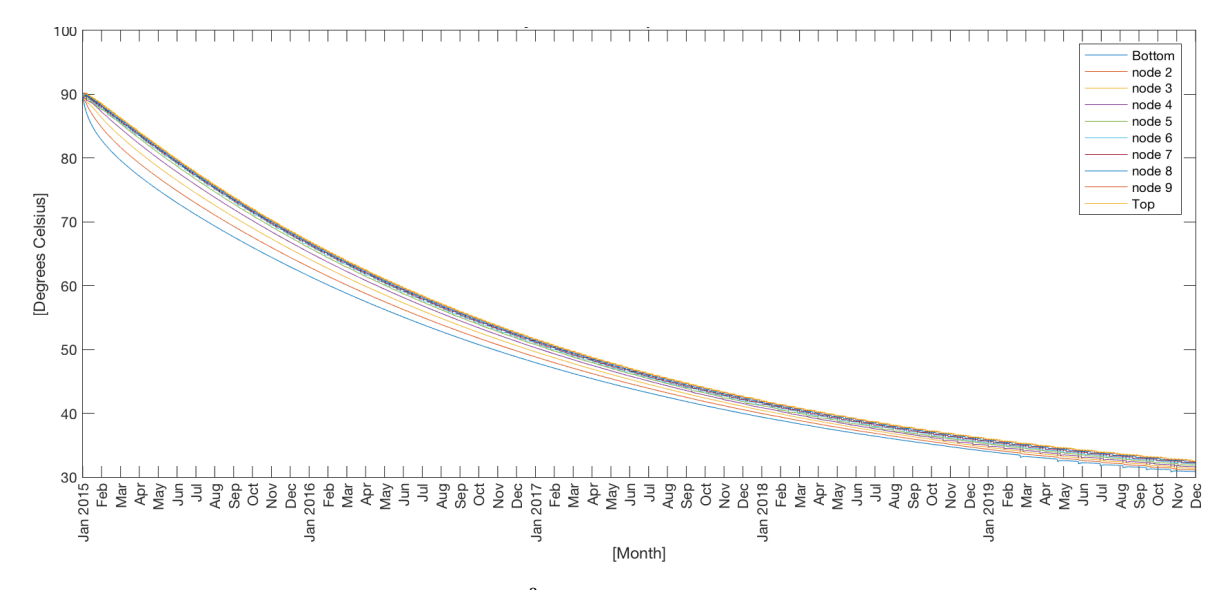


Figure 8.6: 5 year temperature decline of USTES of 1000 m^3

HoCOSto Comparison

HoCoSto quantifies the heat losses averaged over all sides of the USTES (top, bottom and sides) in Wm⁻² per day. According to the HoCoSto model at 40°C the heat loss totals 68 Wm⁻² for 24 hours. At 90°C this is 162 Wm⁻² for 24 hours. This is for a USTES volume of 800 m³ and a ground temperature of 16°C.

Comparing these values with the model presented in this study using the same parameters we see that at equal temperature the heat losses per square meter are 161 Wm^{-2} and 52 Wm^{-2} per 24 hours for a USTES at 90°C and 40°C respectively.

The modelled heat losses for a USTES at 90°C coincide with the heat losses estimated by HoCoSto. The heat losses of the USTES at 40°C are further off but still in the same range. The reason the heat losses are lower in the model presented in this study is thought to be due to the use of nodes instead of a uniform temperature.

8.5. Air-Water Heat Pump

The air-water heat pump will be validated through comparison with the theoretical Carnot cycle COP's. The theoretical Carnot cycle is calculated using equation 5.26 presented in section 5.5. However, as discussed in section 5.5 the practical COP is lower compared to the theoretical cycle. Generally the practical COP of a heat pump is around 0.4-0.5 of the theoretical cycle.

The air-water heat pump based system is modelled for both the theoretical Carnot and for the custom air-water heat pump modelled by using the REFPROP software.

Figure 8.7 shows the inverse (COP/COP $_{Carnot}$) of the theoretical Carnot COP of the air-water heat pump relative to the COP of the air-water heat pump modelled using the REFPROP software. The figure shows that the practical COP is around $0.48 \times COP_{Carnot}$ and therefore is considered in the expected range.

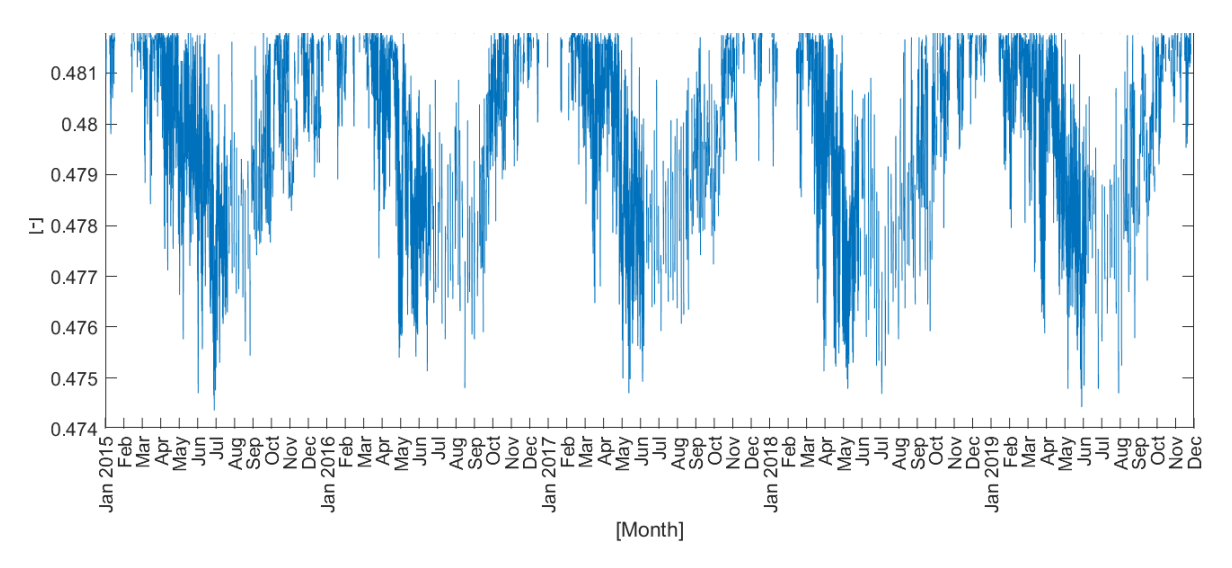


Figure 8.7: Ratio between the theoretical Carnot efficiency and the practical efficiency modelled using REFPROP software. The practical COP is around $0.48 \times COP_{Carnot}$. This is within the expected efficiency range.

Figure 8.8 presents the COP of the theoretical Carnot cycle and the practical COP.

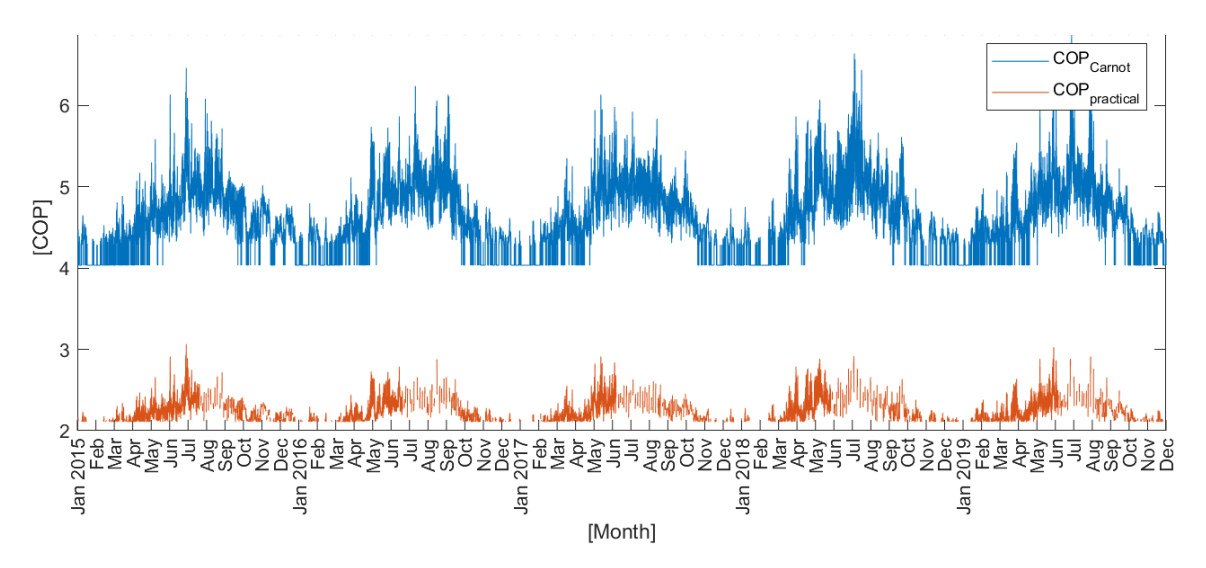


Figure 8.8: The theoretical COP and the practical COP.

9

Results

The model discussed in the previous chapters is used to run simulations on the two defined systems. The results of these simulations are presented in this chapter.

9.1. Demand

The energy demand for heating and hot tap water of the households is modelled for the year 2015 (figure 9.1) and for a five year time span 2015 - 2020 (figure 9.2).

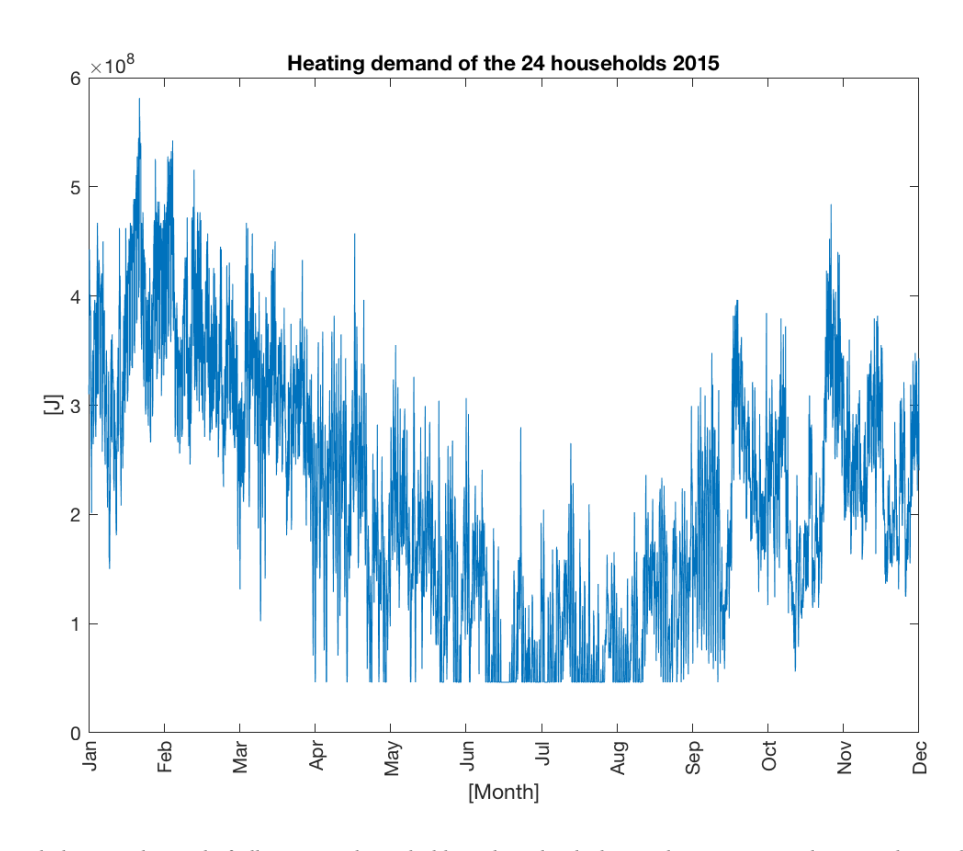


Figure 9.1: Hourly heating demand of all users (23 households and 1 school) during the year 2015. The annual cumulative heating demand is $1660 \, \mathrm{GJ}$.

9.1. Demand 82

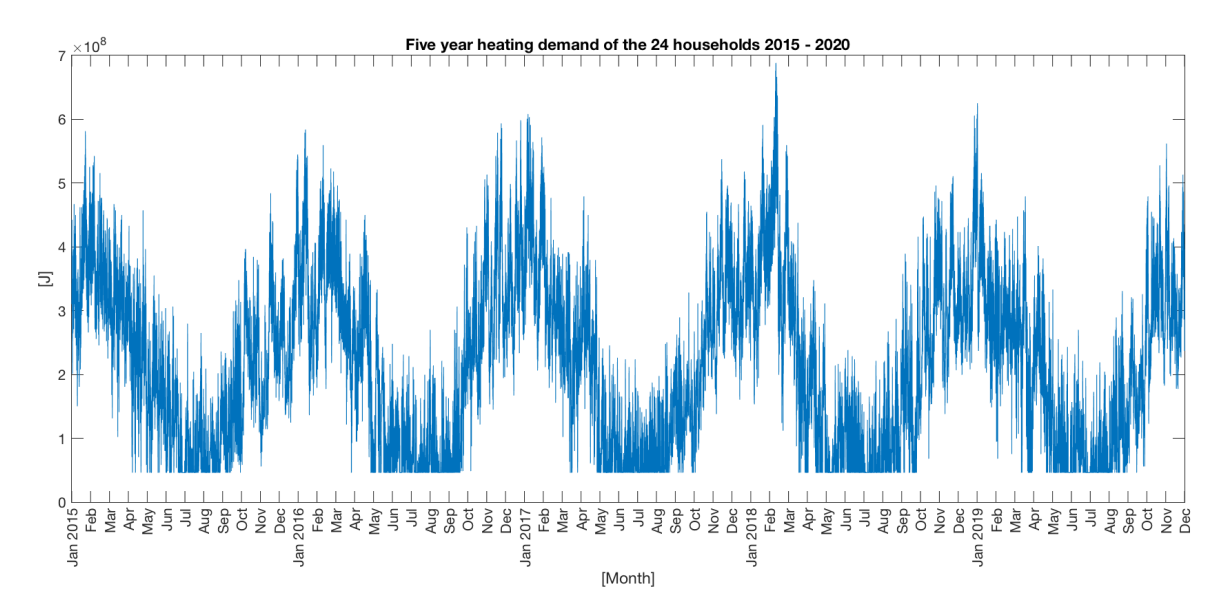


Figure 9.2: Hourly heating demand of users over the time period 2015 - 2020. Demand follows a sinusoidal pattern with a 12 month period. Peak demand occurs during November-March and off-peak during May-September.

From figure 9.2 can be seen that over the years the demand follows a rather stable sinusoidal shape with a period of 12 months. However, there are significant differences in the short term intensity of the heating demand. For instance, in February 2018 there was a significant increase in heating demand compared to other years. Every year the heating demand peaks between November-March.

9.2. Generation

This section presents the results from the energy generation models. The solar irradiance as presented in section 5.3.6 is the main parameter contributing to the yield of the solar collector and PV-panels. The ambient temperature as presented in chapter 4 is the main parameter determining the COP of the heat pump. The output results of these components are presented in this section. First the solar collector generation is given, second the electricity generation by PV-panels, and finally the air-water heat pump output and its coefficient of performance are presented.

9.2.1. Solar Collector Output

The solar collector output for a surface area of one square meter over time is presented in figure 9.3.

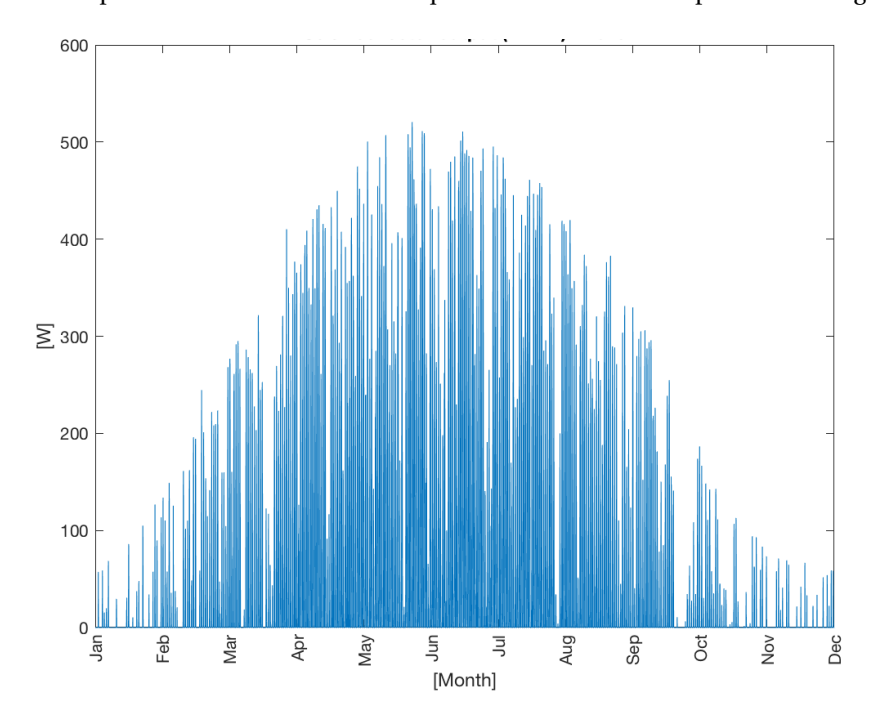


Figure 9.3: Hourly power output for one square meter of solar collector (KLOBEN ATON series) during the year 2015. The inlet temperature is constant at 40 $^{\circ}$ C with an outlet temperature of 90 $^{\circ}$ C.

The figure shows a sinusoidal output of energy from the solar collector. The peak output, in contrast to the peak demand, is during summer from May-July. Hence, the energy generation and the energy demand mismatch.

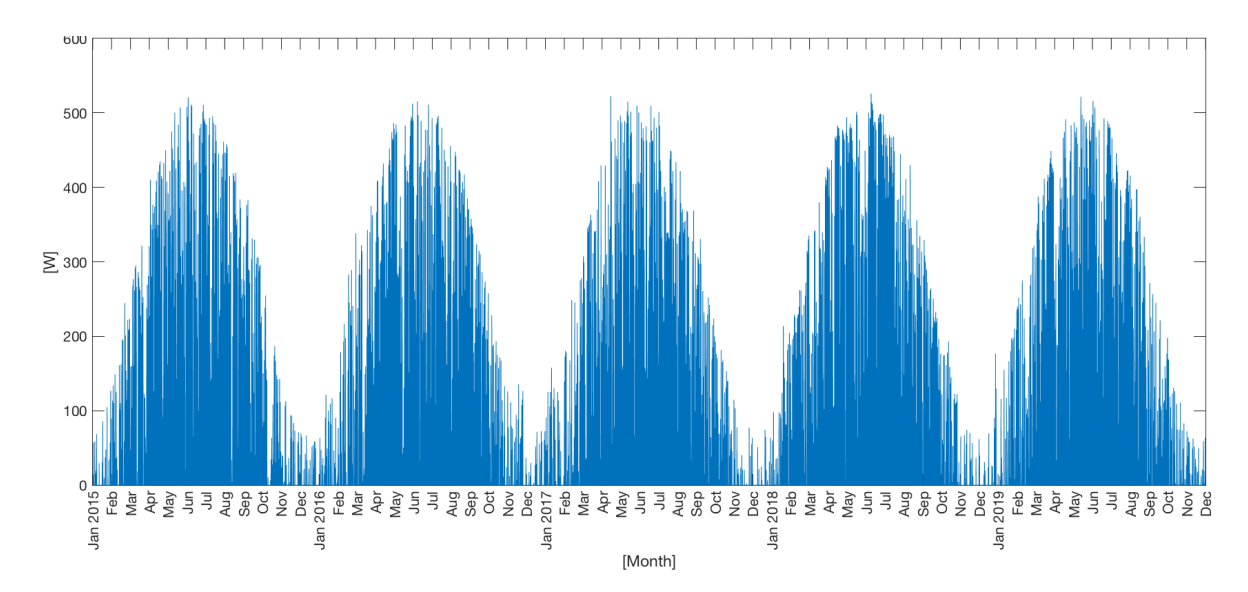


Figure 9.4: 5 year hourly power output for one square meter of solar collector (KLOBEN ATON series) 2015-2019. Peak output reaches 500 Watt/ $\rm m^2$. The inlet temperature is constant at 40 °C with an outlet temperature of 90 °C. Yearly average energy production over a 5 year time period is 376.6 kWhm $^{-2}$ year $^{-1}$

Figure 9.4 shows the output of the solar collector over a period of five years. Again note the sinusoidal shape as result of the seasonal irradiation fluctuations.

9.2.2. PV-panel Output

The electricity generation for the year 2015 by one square meter of Trina Solar PV-panel is presented in figure 9.5. The total annual electricity generation from 2015-2020 of this same square meter is shown in figure 9.6.

The graphs show a similar behaviour to the solar collector output. This was expected since both depend on many of the same parameters such as irradiance and ambient temperature.

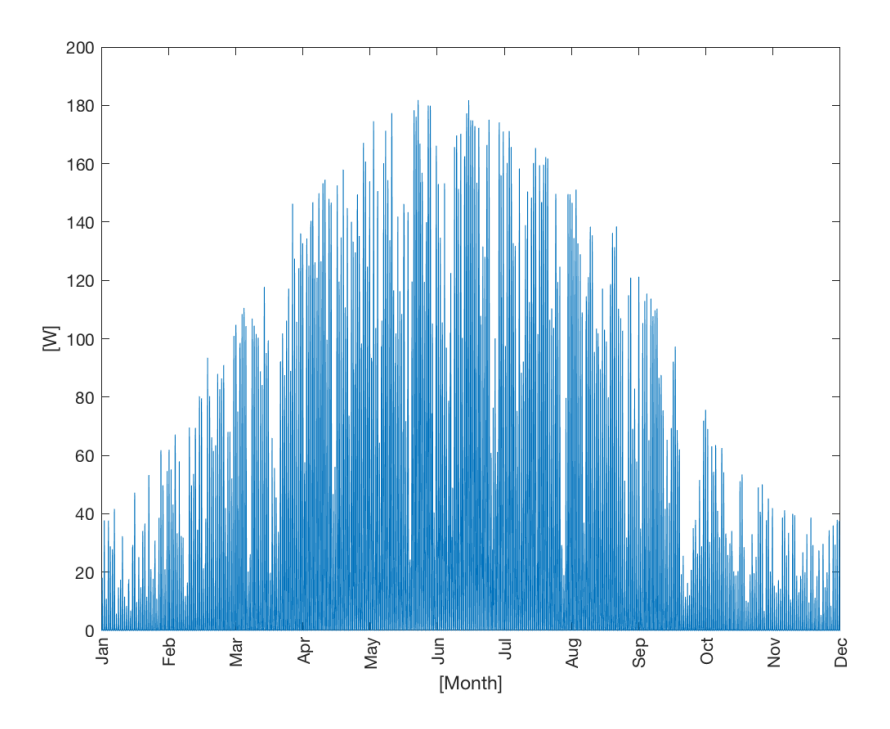


Figure 9.5: Power output of one square meter of Trina Solar photo-voltaic array during the year 2015. Peak electricity output is during summer months (May-July) at high solar irradiation.

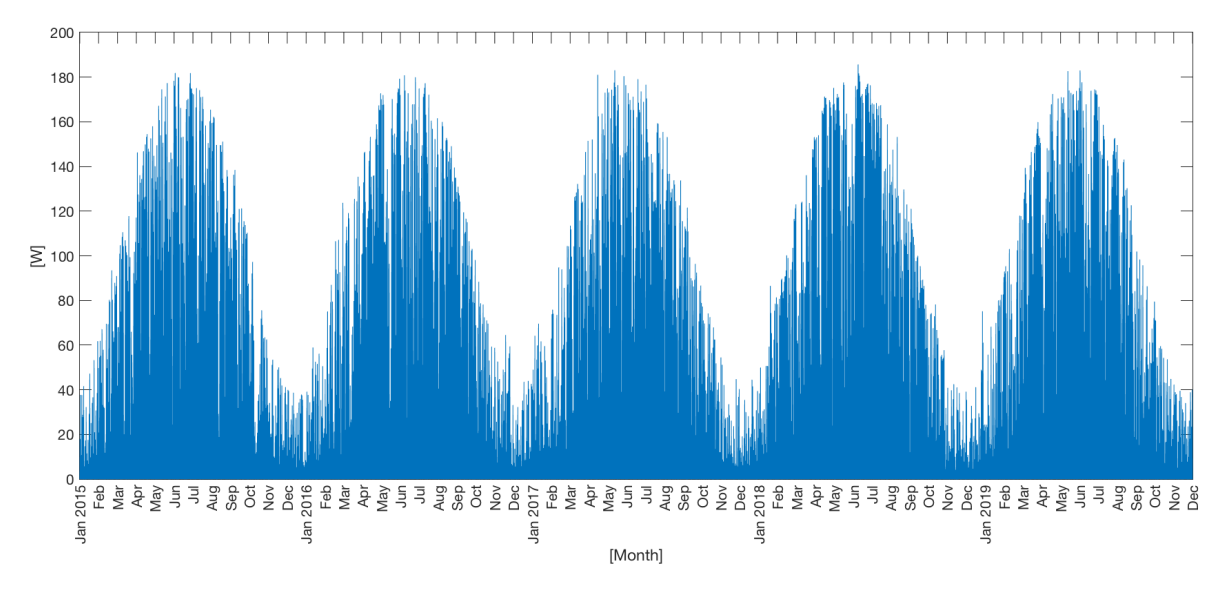


Figure 9.6: 5 year power output of one square meter of Trina Solar photo-voltaic panel. Yearly average electricity production over a 5 year time period is $193 \text{ kWhm}^{-2} \text{year}^{-1}$

9.2.3. Air-Water Heat Pump Output

The output of the air-water heat pump is controlled according to the control mechanism as described in chapter 6. The heat pump is only in operation during periods where the outdoor temperature reaches a temperature threshold and during times energy can be added to the USTES, i.e. when the USTES is at its maximum capacity the air-water heat pump is idle. The output of the air-water heat pump is visualised in figures 9.7 and 9.8.

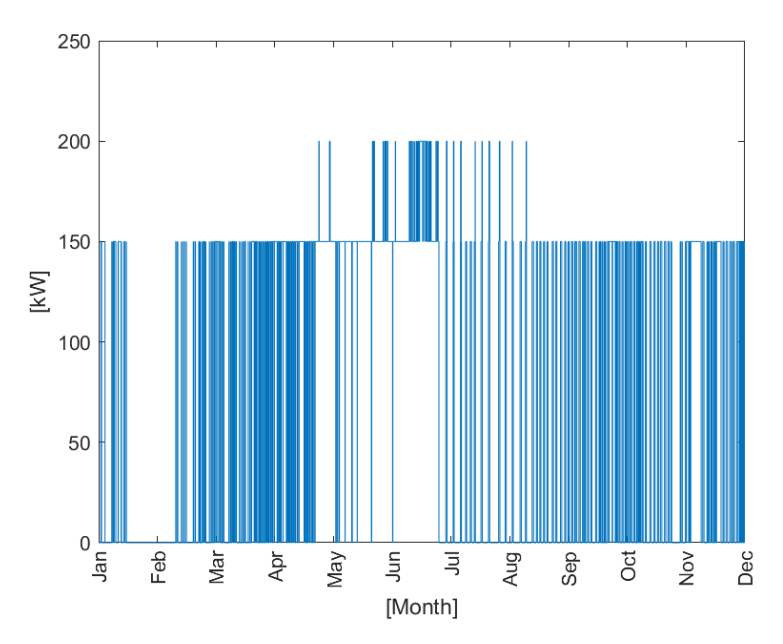


Figure 9.7: Power output in kW of a 200 kW air-water heat pump during the year 2015.

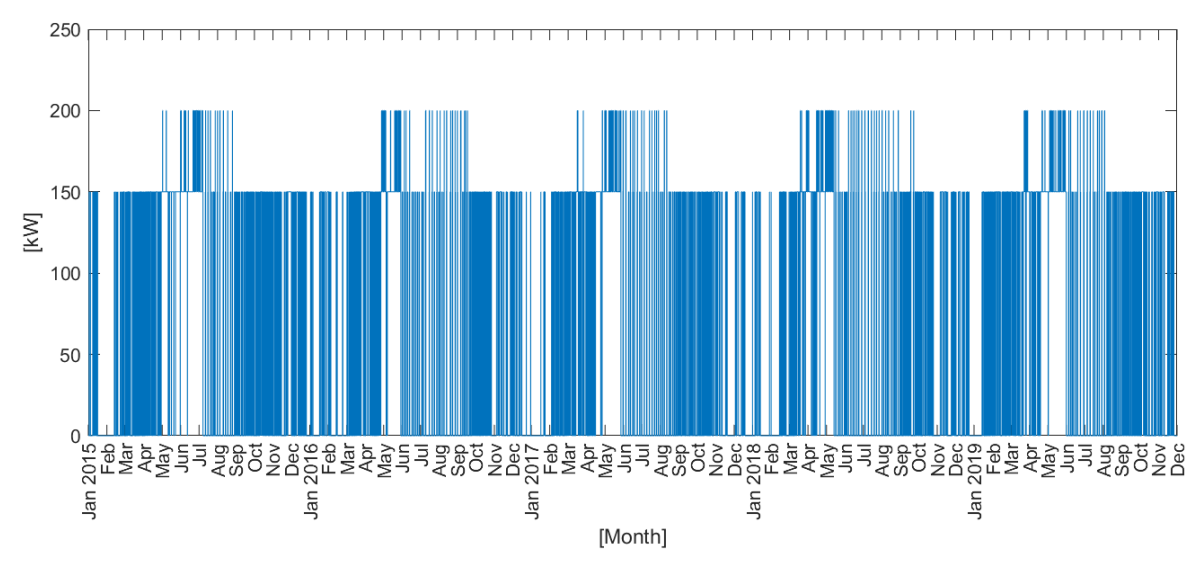


Figure 9.8: Power output in kW of the air-water heat pump over a 5 year time period.

Coefficient of Performance

The electricity consumption of the heat pump is dependent on the COP and subsequently the outdoor temperature. During colder periods the electricity consumption increases (low COP) while during warmer periods the electricity consumption decreases (high COP). Figure 9.9 shows the COP of the heat pump over a 5 year period.

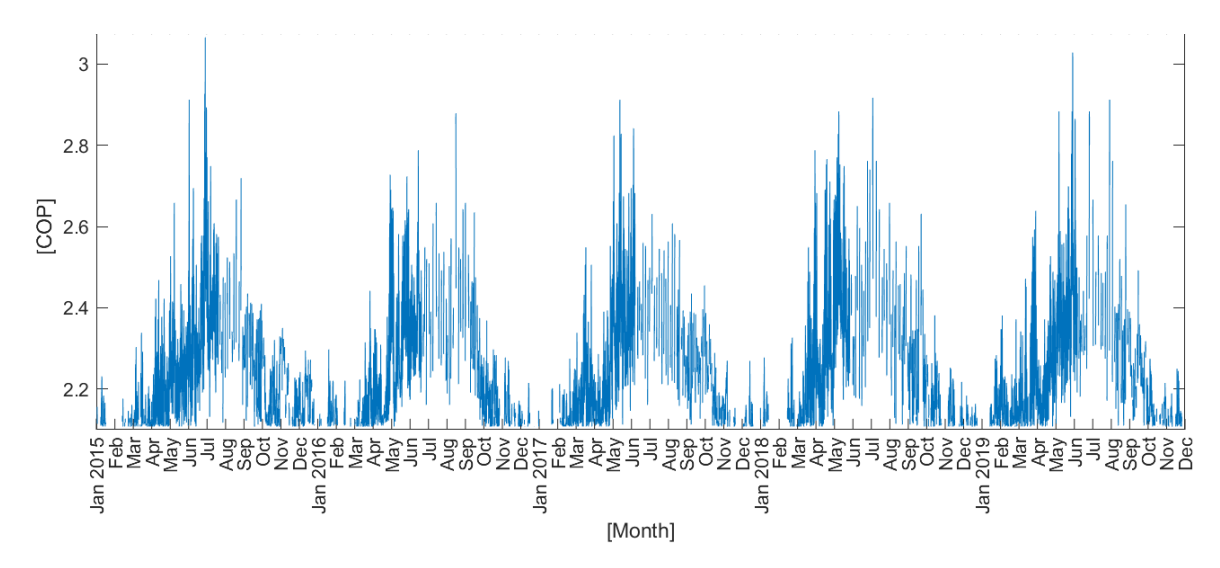


Figure 9.9: Coefficient of performance of the air-water heat pump over a 5 year time period.

9.3. Defining the System Optima

The sizing of the system is determined based on the key performance indicators as described in chapter 3. For every KPI a specific optimal sizing occurs. The optimal sizing for every KPI is determined through an iterative process.

The iterative process simulates a range of collector surface area/heat pump capacity and USTES volumes. From these simulations, optima occur for the KPI's. These optima are weighed based on the importance of the KPI to determine the final optimum system size configuration.

9.3.1. Optima of the Solar Collector Based System

The solar collector based system has two variable components. These are the USTES volume and the amount of solar collector surface area. In this section the results on the KPI's are presented.

LCOH Optimum

The primary KPI is the LCOH, its optimum occurs at the lowest value for the LCOH. Figure 9.10 shows the LCOH as function of the USTES volume for different surface areas of solar collector array. The lowest LCOH is \leq 0.128 which occurs at a USTES volume of 1600 m³ and a solar collector area of 800 m².

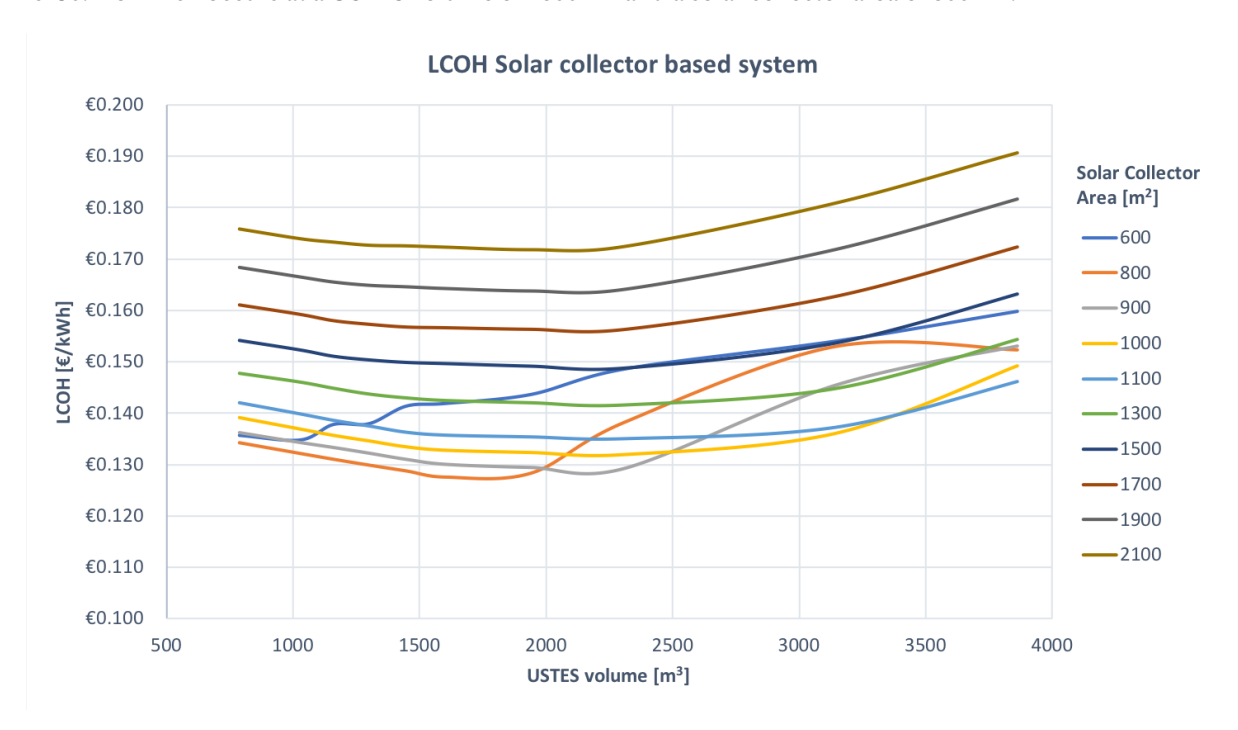


Figure 9.10: LCOH of the system configurations defining an optimum at the lowest point in the graph. Each line represents a certain solar collector array surface area. The x-axis shows the USTES volume while the y-axis presents the LCOH of the system.

Systems SCOP Optimum

The SCOP of the different system sizes are presented in figure 9.11. The SCOP increases with USTES volume and solar collector surface area since auxiliary heating and water-water heat pump operating hours decrease with increasing USTES volume and solar collector surface area.

The systems seasonal coefficient of performance is at an optimum when at a maximum value. This maximum SCOP is theoretically infinite since when no electricity is consumed by the system, no external energy is imported and the system operates fully autonomous. The lower the SCOP the worse the efficiency of the system is. Figure 9.11 shows an increasing SCOP with increasing USTES volume and solar collector area. This coincides with the fact that at larger solar collector area and higher USTES volume less energy is imported to the system resulting in the higher SCOP.

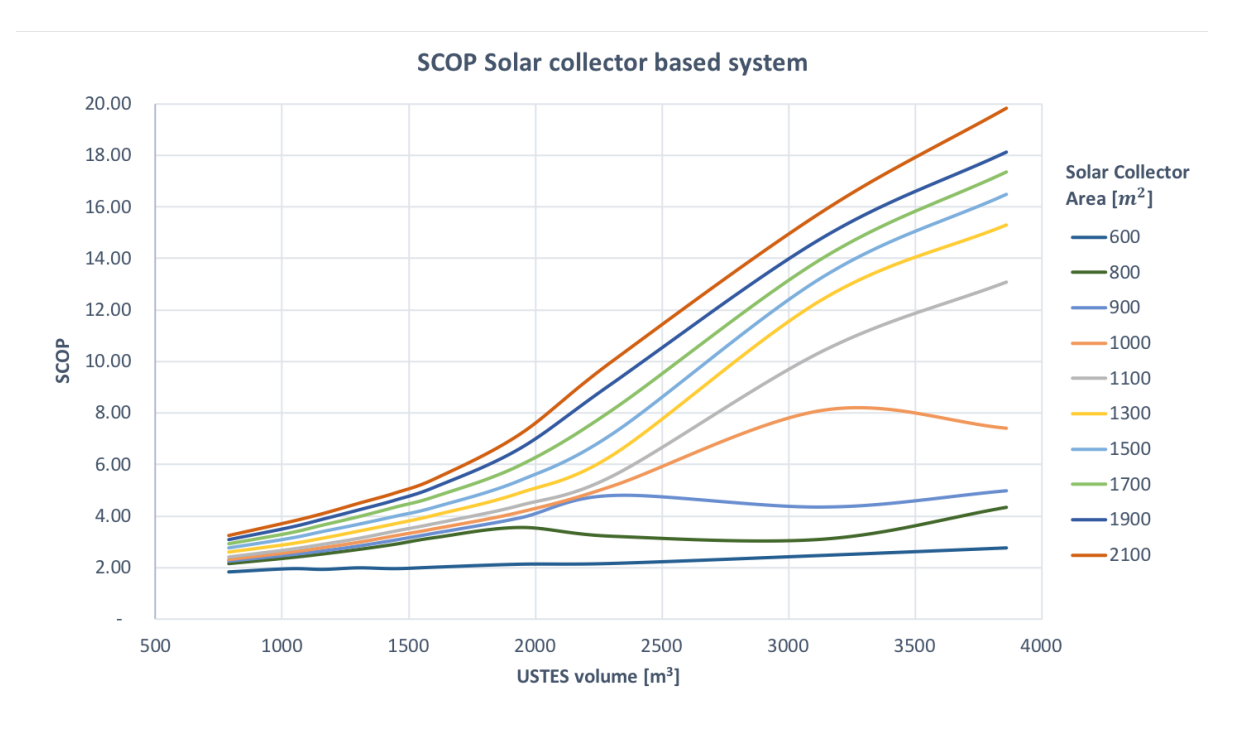


Figure 9.11: SCOP of the solar collector system configurations increasing with increasing size.

9.3.2. Optima of the Air-Water Heat Pump Based System

The sizing of the air-water heat pump is performed by iteration of two variables, the air-water heat pump capacity and the USTES volume.

LCOH Optimum

The LCOH of the air-water heat pump system is at a minimum of €0.118 at an USTES volume of 1300 m³ and a heat pump capacity of 175 kW. The graph in figure 9.12 shows the optimum for the air water heat pump based system.

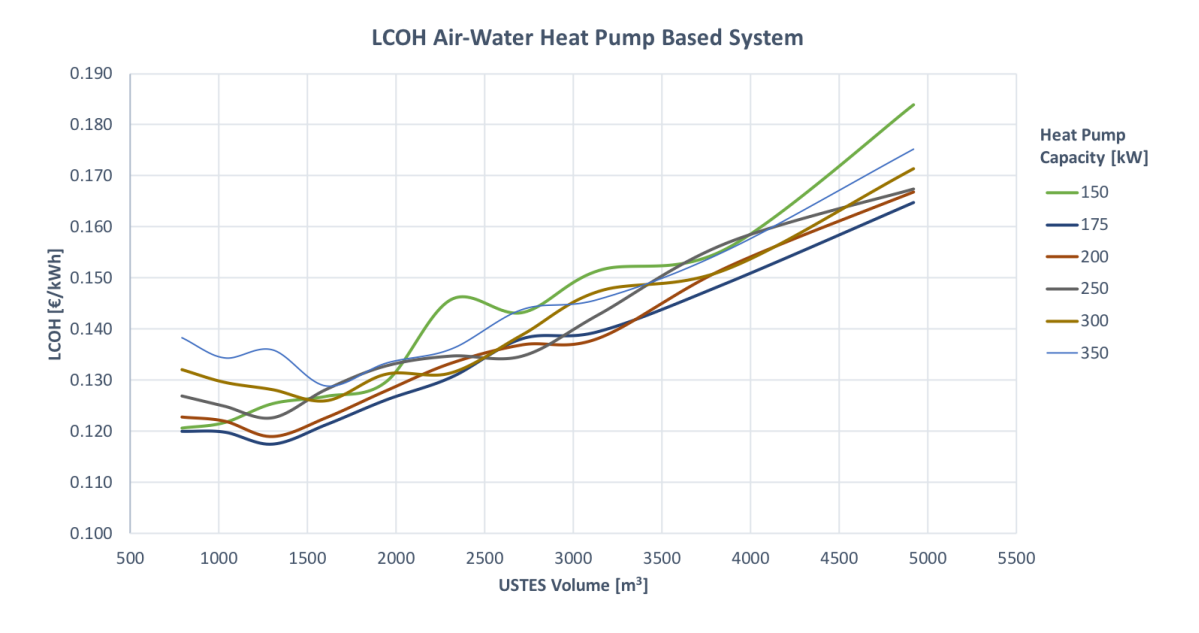


Figure 9.12: LCOH of the system capacities defining an optimum at the lowest point in the graph. Each line represents a certain heat pump capacity in kW.

SCOP Optimum

The SCOP optimum approaches a maximum with increasing USTES volume and increasing heat pump capacity. However, the SCOP has a limit related to the COP of the air-water heat pump. The maximum COP of the air-water heat pump based system is 3.1, this is the highest efficiency the system is able to achieve and subsequently the limit to the SCOP of the system. Figure 9.13 shows the SCOP of the different system sizes.

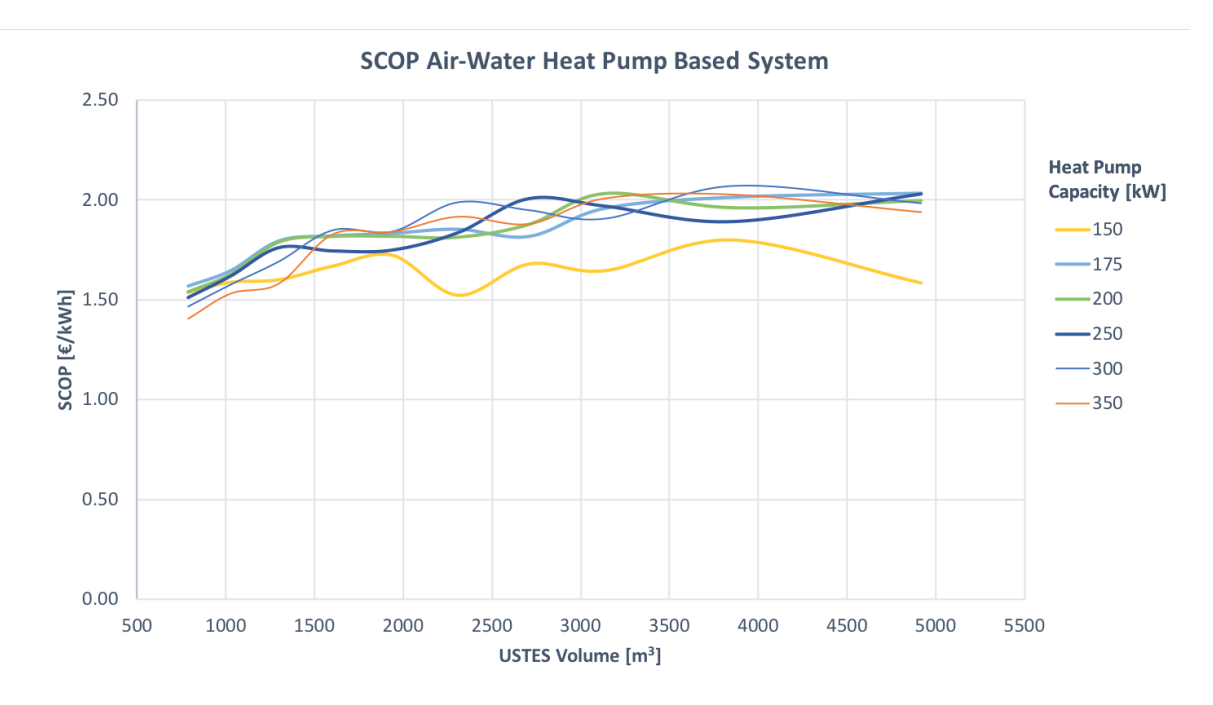


Figure 9.13: SCOP of the system configurations increasing with increasing system component sizes. Each line represents an installed heat pump capacity in kW.

9.4. CAPEX of the Systems

The CAPEX of the systems are based on the optimal system configuration as defined in section 10.1. The CAPEX of the solar collector based system is \leq 993.000,-. The pie chart in figure 9.15 breaks down the cost of components. The costs for the DHN is fixed for every configuration and makes up 10% of the total CAPEX.

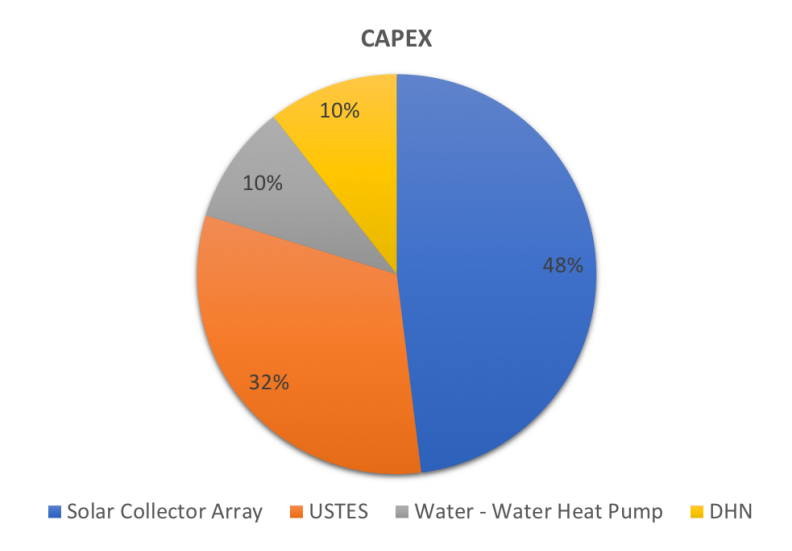


Figure 9.14: CAPEX cost share of the components for solar collector based system with 2100 m^3 USTES and 1060 m^2 solar collectors. Total costs are \leq 993.000,-.

The CAPEX of the air-water heat pump based system is €493.500,-. The pie chart in figure 9.15 breaks down the cost of components. From this chart it becomes clear that the USTES contributes the largest part of the total CAPEX. The costs for the DHN is fixed for every configuration and makes up 21% of the total CAPEX.

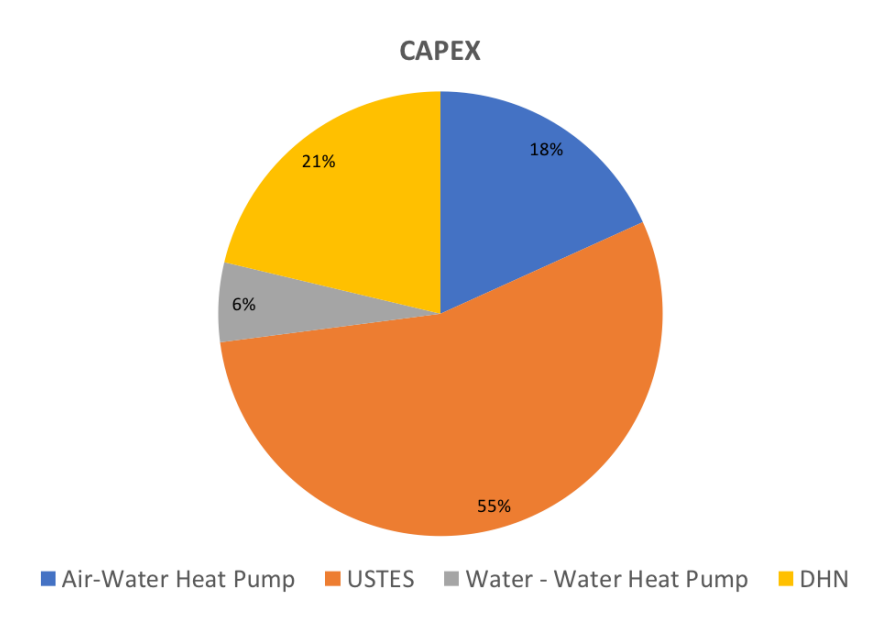


Figure 9.15: CAPEX cost share of the components for the heat pump based system with 1800 m^3 USTES and 200 kW air-water heat pump capacity. Total costs are \leq 493.500,-.

9.5. Autonomous Systems - Offsetting the Electricity Use

The systems both still depend on electricity sourced from the grid. To increase the autonomy and renewable share of the system, PV panels can be installed. The solar collector based system does not have the entire rooftop area left since the solar collectors are already taking up a large part of the available space. The heat pump based system does have the entire rooftop area available for additional PV panels.

One concern is the mismatch in time between consumption and generation. These systems are therefore not aimed to be fully autonomous but "zero on the meter", meaning the electricity generation is offset to the consumption using the general electricity grid as a "storage".

By installing a PV array the entire electricity use of the systems is compensated. Part of the effective rooftop area as described in section 5.3.7, totalling $1344~\mathrm{m}^2$ will be used for the placement of the PV array. This results in an increase of the SCOP to infinity since all energy consumed by the system is also generated within the system. The cost of the PV panels increase the CAPEX of the systems and subsequently the LCOH reaches a new optimum.

For the solar collector based system including PV the optimal LCOH is \leq 0.126 with a solar collector surface area of 1000 m², a PV surface area of 333 m² and a USTES volume of 3141 m³. Figure 9.16 presents the LCOH for different component configurations. The LCOH of this system is limited by the rooftop area available.

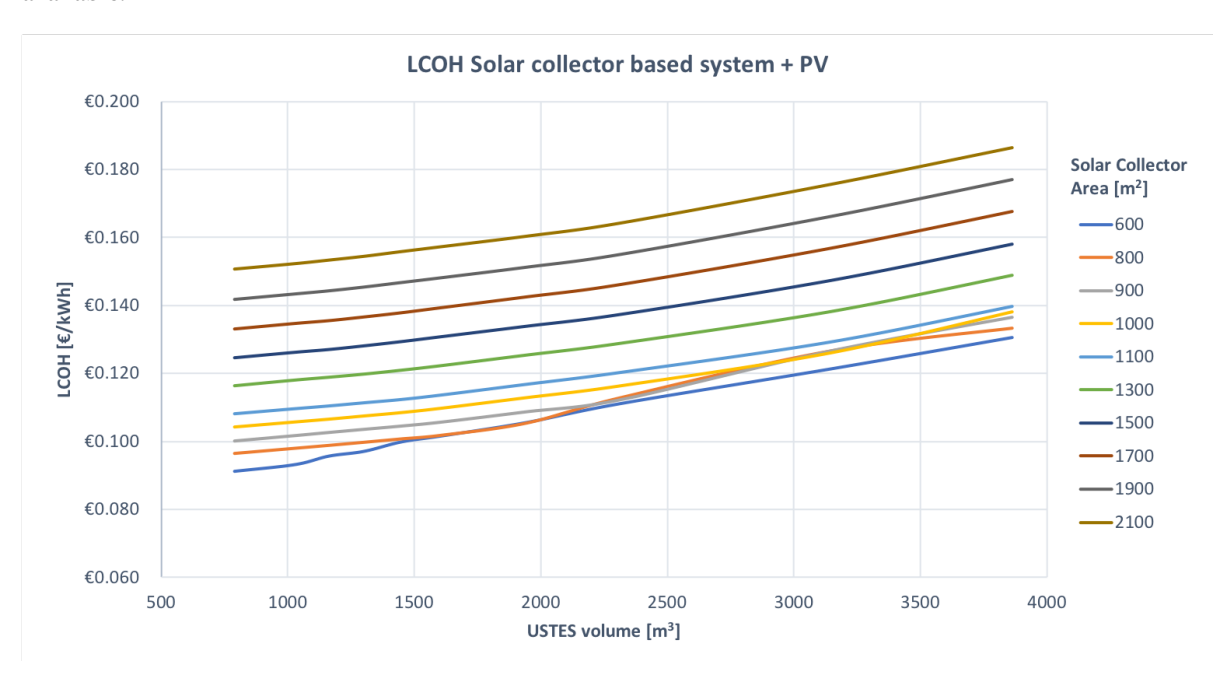


Figure 9.16: LCOH of the solar collector based system including a PV array. All electricity consumed by the system is generated by the PV array resulting in a "zero on the meter' autonomous system. The system is still communicating with the electricity grid.

The CAPEX share for each component of the system is presented in figure 9.17. The PV array entails 5% of the total CAPEX. The CAPEX totals \le 1.182.090,-.

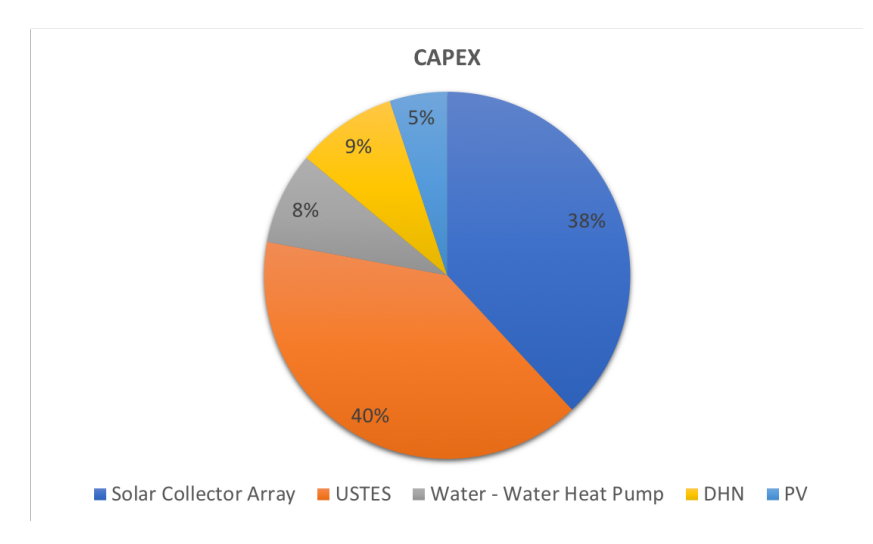


Figure 9.17: Pie chart of the CAPEX of the solar collector based system including PV. The system consists of 1000 m² of solar collectors, 333 m² of PV panels and 3141 m³ of USTES. The PV cost totals 5% of the total CAPEX. Total costs are \in 1.182.090,-.

The air-water heat pump system consumes more energy compared to the solar collector based system and therefore needs more surface area of PV panels to reach "zero on the meter" autonomy. Figure 9.18 presents the LCOH for the air-water heat pump system while all electricity use is offset by PV panels.

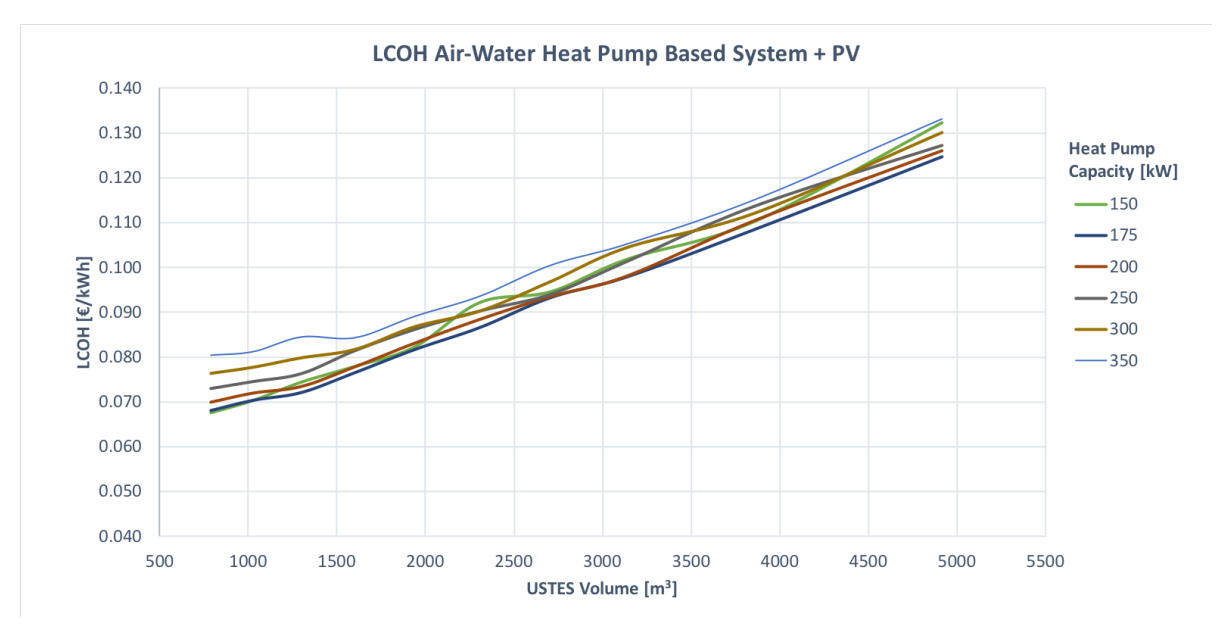


Figure 9.18: LCOH of the air-water heat pump system including a PV array. All electricity consumed by the system is generated by the PV array resulting in a "zero on the meter' autonomous system. The system is still communicating with the electricity grid.

The optimal LCOH for this system is ≤ 0.094 at a USTES volume of 2709 m³ and a heat pump capacity of 250 kW. To ensure all electricity is produced on site a PV array of 1343 m² is needed. This is considered the optimal configuration since the only relevant KPI is the LCOH. The autonomy of the system is equal for all configurations since all electricity is produced by the system. The system is constraint by the rooftop area available. With additional PV panels the LCOH can be reduced further.

The CAPEX of the system is €882.590,- and is presented in figure 9.19. The PV array entails 27% of the total CAPEX.

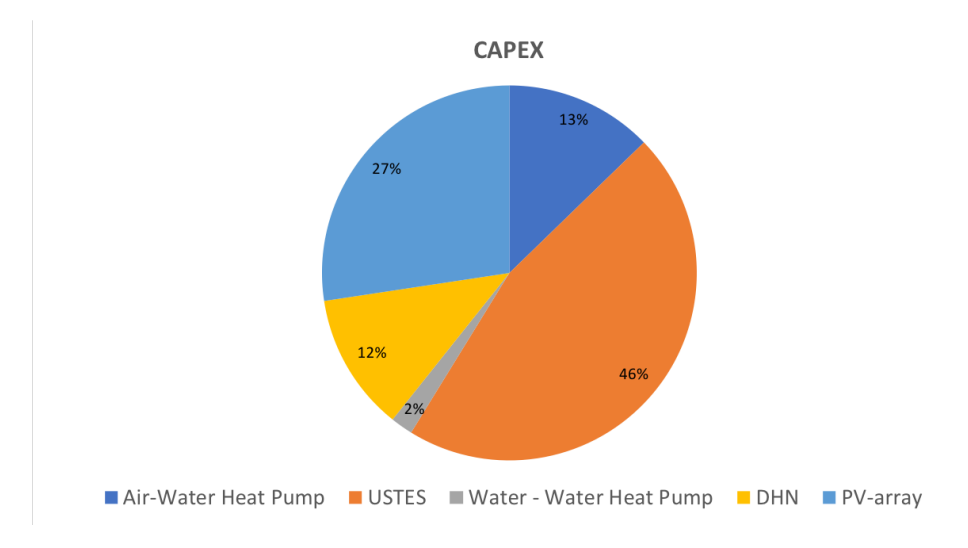


Figure 9.19: Pie chart of the CAPEX of the air-water heat pump system including PV. The system consists of a USTES of 2709 m 3 , a 250 kW air-water heat pump, and a 1343 m 2 PV array. The PV cost totals 27% of the total CAPEX. Total CAPEX is \leqslant 882.590,-.

9.6. Operating Expenditures

The systems LCOH is not only dependent on the CAPEX but also is affected by the operating expense (OPEX). The operating costs consist of two components, the first is the operating and management costs which are assumed at 1.2% of the CAPEX. The second is the electricity cost to run heat pumps and circulation pumps. The systems with a PV array installed are not subject to electricity costs but do have an increase in operating and management costs due to the increase in CAPEX. Table 9.1 provides an overview of the annual OPEX for the different systems.

Table 9.1: OPEX of the systems. Operating expenditures include cost of electricity use and operating and management costs.

	OPEX [€]
Solar collector based system	26.559,-
Air-water heat pump based system	43.986,-
Solar collector based system with PV	14.185,-
Air-water heat pump based system with PV	10.592,-

10

Discussion

This section will elaborate on the key performance indicators for both systems and present the optimal sizing of components for each KPI. Taking into account the weights determined for the KPI's, the optimal configuration for each system is determined.

The results of chapter 9 present the optima for the two KPI's. Table 10.1 gives the optimal KPI values and the corresponding sizing of components of the solar collector based system. Table 10.2 presents the same for the air-water heat pump system. From these optima the final system sizing is determined, which is believed to be the favourable combination for the Energiek Nagele project.

Table 10.1: Solar collector based system KPI evaluation. The weight represents the importance of the KPI in determining the eventual preferred system and its size. The total weight makes up 1.

KPI	Optimum Value	USTES Volume [m ³]	Volume [m ³] Solar Collector area [m ²]	
LCOH	0.122	1605	800	0.8
SCOP	19.83	3861	2100	0.2

Table 10.2: Heat pump based system KPI evaluation. The weight represents the importance of the KPI in determining the eventual preferred system and its size. The total weight makes up 1.

KPI	Optimum Value	USTES Volume [m ³]	Heat Pump Capacity [kW]	Weighing
LCOH	0.118	1300	175	0.8
SCOP	2.07	3861	300	0.2

10.1. Determining the Optimal System Configurations

The optimal system configuration and sizing for the solar collector based system without PV array is determined following equations 10.1 and 10.2 by weighing the KPI's. This results in a system with 2100 $\rm m^2$ of USTES volume and 1060 $\rm m^3$ of solar collector area.

$$V_{USTES}(system) = 0.8 * V_{USTES}(LCOH) + 0.2 * V_{USTES}(SCOP)$$
 (10.1)

$$A_{ETC}(system) = 0.8 * A_{ETC}(LCOH) + 0.2 * A_{ETC}(SCOP)$$

$$(10.2)$$

The optimal system configuration and sizing for the heat pump based system without PV array is determined following equations 10.3 and 10.4 by weighing the KPI's. However, the SCOP and subsequently the autonomy of the system is rather constant. This results in a system with 200 kW of air-water heat pump capacity and $1800 \, \mathrm{m}^3$ of USTES volume.

$$V_{USTES}(system) = 0.8 * V_{USTES}(LCOH) + 0.2 * V_{USTES}(SCOP)$$

$$(10.3)$$

$$P_{aw-HP}(system) = 0.8 * P_{aw-HP}(LCOH) + 0.2 * P_{aw-HP}(SCOP)$$
 (10.4)

The optimal system configuration and sizing for the solar collector based system with PV array is based on "Zero on the meter" at the lowest possible cost while taking into account the rooftop area constraint. This results in a system with $1000~\text{m}^2$ of solar collector area, $3141~\text{m}^3$ of USTES volume, and $333~\text{m}^2$ of PV panels. The LCOH of the system is 60.126. The LCOH can come down further by installing additional PV panels. However, the rooftop surface area constraints the PV array size.

The optimal system configuration and sizing for the heat pump based system with PV array is also determined to achieve "Zero on the meter" at lowest cost. This results in a system with 250 kW of air-water heat pump capacity, 2709 m³ of USTES volume, and 1343 m² of PV panels. This results in a LCOH of ≤ 0.094 . Again the LCOH can come down further if not for the rooftop area constraint.

Table 10.3 presents an overview of the optimal system configurations and the component sizes:

Table 10.3: Optimal component sizes of the different system configurations.

	USTES Volume [m ³]	Solar Collector [m ²]	Heat Pump Capacity [kW]	PV array [m ²]	LCOH	SCOP
Solar collector based system	2100	1060	-	-	0.134	4.76
Air-water heat pump based system	1800	-	200	-	0.126	1.82
Solar collector based system with PV	3141	1000	-	333	0.126	-
Air-water heat pump based system with PV	2709	-	250	1343	0.094	-

10.2. Simulation of the Optimal System Sizes

To be able to determine whether the system sizes presented in table 10.3 are feasible and to understand how they behave a full simulation of these systems is presented.

Solar Collector Based System

The optimal configuration for the solar collector based system consists of a solar collector array of 1060 m^2 and a USTES volume of 2100 m^3 . Figure 10.1 presents the solar collector output for the full simulation. This output differs from the output presented in figure 9.4 since the efficiency is dependent on the temperature of the bottom node of the USTES that acts as inlet fluid to the solar collector. The seasonal solar efficiency of the collectors as defined in section 3.4 is 40%. The solar fraction of the system is 86%.

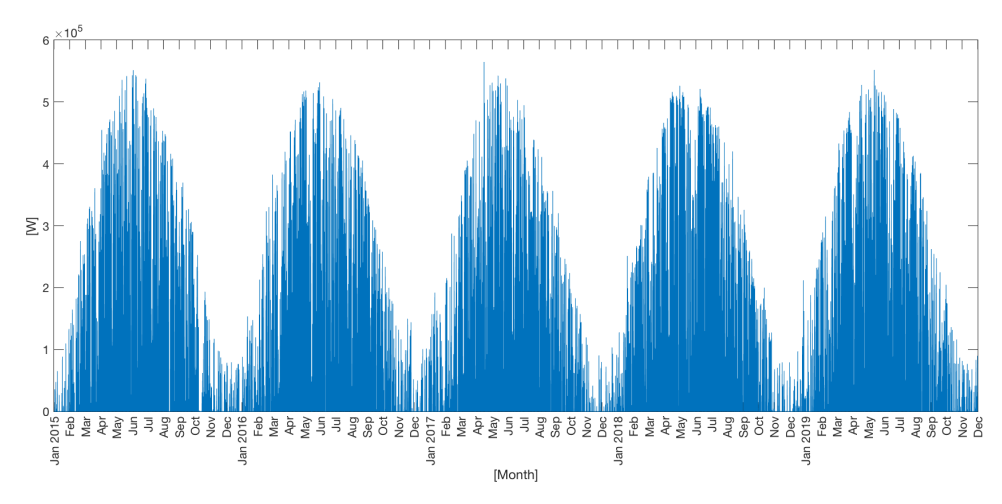


Figure 10.1: Output of the solar collector array during a five year time period.

The temperature of the nodes in the USTES over the years is presented in figure 10.2. From the graph can be seen that the temperature fluctuations are not the same every year but do follow a similar trend. From the

figure follows that not all energy comes from the solar collectors but some auxiliary heating is needed with this system sizing. This implies that using additional solar collectors and USTES volume to ensure demand are more expensive compared to the use of auxiliary heating. This is due to the low cost of electricity when a large amount of electricity is off taken and it results in a larger investment, operating and maintenance costs. By installing a PV array the auxiliary heating can also be considered renewable.

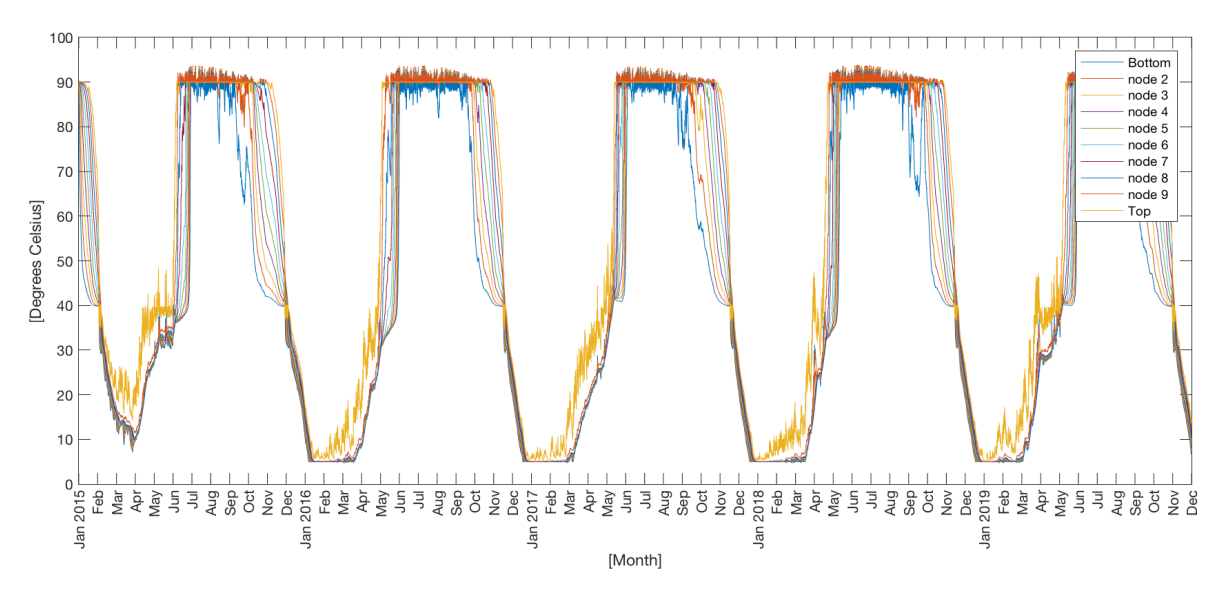


Figure 10.2: Temperature of the nodes in the USTES during a five year time period with 2100 m^3 USTES and 1060 m^2 solar collectors.

Air-Water Heat Pump System

The temperature profile of the USTES over a 5 year time period is presented in figure 10.3. To be certain the heat pump is only operating when energy can be added to the USTES, it only operates when the temperature of the bottom node of the USTES is below 80 $^{\circ}$ C and when there is a return mass flow from the DHN at 40 $^{\circ}$ C. This translates in the fact that the bottom node appears to be fluctuating between 80-90 $^{\circ}$ C.

From 10.3 also follows that in the years 2017 and 2018 some auxiliary heating is needed. This auxiliary heating can be prevented by installing more m^3 of USTES. However, based on the KPI's apparently it is favourable to have some auxiliary heating since it leads to a lower LCOH compared to installing additional USTES volume.

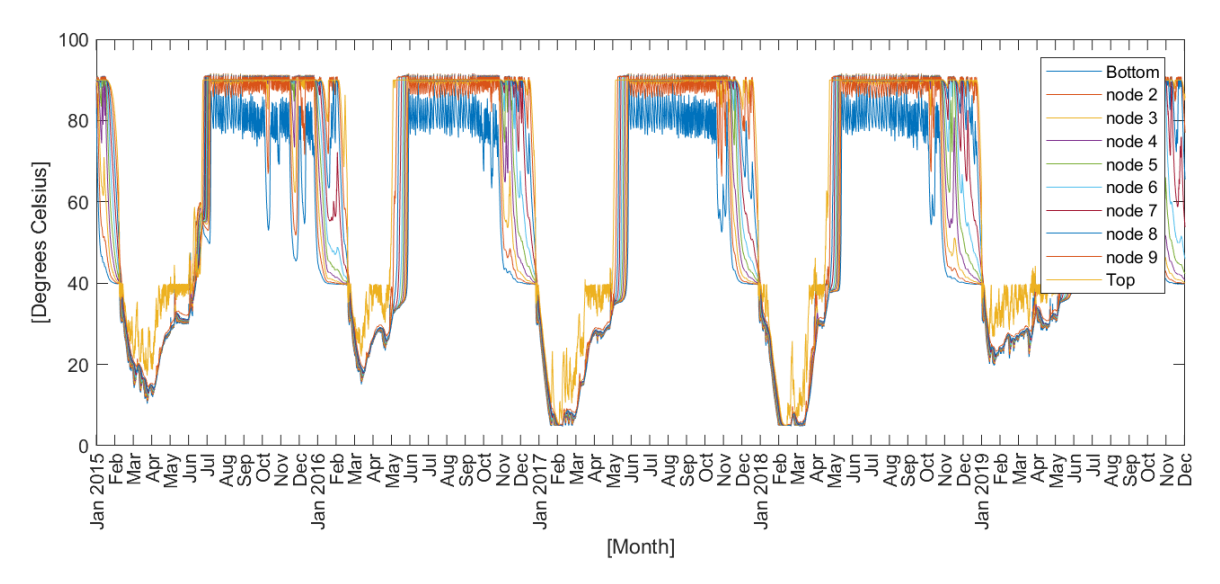


Figure 10.3: Temperature profile of the nodes in the USTES during a five year time period with 1800 m^3 USTES and 200 kW air-water heat pump capacity.

The graph in figure 9.12 presenting the LCOH does not show a consistent profile like the solar collector based system. This is due to the fact that the main parameter (the ambient air temperature) determining the output of the air-water heat pump does not follow consistent sinusoidal trends like the main parameter determining the solar collector output (the solar irradiance).

This effect is amplified by the fact that the control mechanism of the heat pump alters the power output depending on the ambient air temperature. Since it is impossible to predict what the ambient air temperature in the future will be the output of the heat pump can be too high or too low depending on the situation. This results in the fact that certain heat pump configurations perform better during certain situations that occur during the five year period. This may result in the slightly fluctuating LCOH.

However, this effect is small and does not have a large impact on the LCOH as can be seen from figure 9.12. It seems the air-water heat pump capacity does not majorly affect the levelised cost of heat. The USTES volume does have a more significant impact on the LCOH as the LCOH increases with increasing USTES volume.

The Autonomy of the system increases as the SCOP of the system increases. An increase in USTES volume enables the system to store more heat during periods the heat pump is operating at high COP. This heat collected at high efficiency can be used to serve demand during periods the heat pump operates at low COP. A volume increase of the USTES will essentially increase the heat pump output at high COP and lower its output at low COP, increasing the SCOP. An increase in heat pump capacity enables the system to reduce the total needed amount of operating hours and only operate at peak COP resulting in a higher SCOP. However, the increase in SCOP is small and likely does not outweigh the increase in investment costs.

The level of autonomy of the system is determined by the degree of electricity imported from the grid. Electricity used by the heat pump is imported from an external source and therefore, by increasing the heat pump operating hours the autonomy of the system decreases. The systems level of autonomy is closely related to the SCOP since they both depend on the amount of electricity imported from the grid.

The results show that it is feasible, both technically and economically, to have a small scale district heating network operate year round based on renewable energy combined with a local seasonal heat storage. To ensure the system is fully renewable a PV array is needed. However, whether or not these systems will be installed is not alone based on the LCOH and the renewable nature of the system. Another consideration is the impact on the users and the ease of installation. Also the cost competitiveness with the business as usual case is considered to be important. Below these additional factors are discussed.

Ease of Installation

Solar Collector

The ease of installation will increase as the system size decreases. The optimum occurs at the moment no system is installed at all. However, since the USTES is fully modular the effort for installing more USTES volume is lower compared to installing more solar collectors. Therefore, less solar collector area will have a larger impact on the ease of installation compared to the size of the USTES which will hardly be of impact. The impact on the users in the case of solar collectors is significant since a piping network needs to be installed to the rooftops of the buildings. This may be possible without entering the inside of the building reducing impact on the users.

Air-water heat pump

The ease of installation of the system is hardly affected by the sizing of components since the air-water heat pump installation is almost the same for different sizes of heat pump. The size of the heat pump does have an effect on the noise production of the heat pump. An increase in heat pump capacity will generally result in an increase in sound. This can lead to a decrease in living standard for the users. Measures need to be taken to reduce and minimise the noise of the air-water heat pump. Also a higher capacity heat pump needs a larger grid connection which may be a problem depending on the local electricity network. This may lead to constraints and the need for a lower heat pump capacity.

USTES

An increase in USTES volume will have some effect on the ease of installation but due to the modular nature of the USTES provided by HoCoSto an increase in volume has only a minor effect on the installation effort and time. The land utilisation of the USTES is also of minimal effect since the surface area can be used after installation.

PV array

The PV array is of low impact on the users buildings. Since it is a flat surface it is relatively easy to install and of low impact on the building.

10.3. Cost Competitiveness

Traditional heat generated by burning natural gas using a HR-boiler operating at a seasonal efficiency of 90% costs 0.088 €/kWh excluding capital costs (the initial costs of the HR-boiler) since the system is already in place. This is the business as usual in the Netherlands for the majority of households. Therefore, this price of heat is the benchmark for renewable heating systems.

The optimal configurations of the systems produce a LCOH of $0.134 \in /kWh$ and $0.126 \in /kWh$ for the solar collector based system and air-water heat pump based system, respectively. This indicates that without subsidies the alternative heating systems without PV presented in this study are not cost competitive with the business as usual case. However, although the LCOH is the most important indicator, the energy source is not mainly determined by this parameter. The value attributed to sustainability has been increasing over the years and therefore a premium on the energy price may be acceptable.

The systems including a PV array produce a LCOH of 0.126 €/kWh for the solar collector based system including PV and 0.094 €/kWh for the air-water heat pump based system including PV. The latter is the most competitive with the business as usual case of all system configurations but still cannot compete. With more rooftop area available the systems with PV are able to be cost competitive with the base case.

Table 10.4 presents the LCOH of all the systems optimal configurations. The costs for all systems is excluding subsidies and BTW.

10.4. Payback Period

The payback period of the systems is defined as the time it will take for the system to harvest enough energy to repay the CAPEX relative to the business as usual case, where natural gas is burned in the central heating boiler at a LCOH of $0.088 \in /kWh$. The systems proposed in this study are not able to payback the CAPEX. This is due to the fact that the LCOH for the proposed systems is higher than the business as usual case.

10.4. Payback Period

Table 10.4: LCOH optima of all systems considered during the study.

	LCOH [€/kWh
Natural gas boiler system	0.088
Solar collector based system	0.134
Air-water heat pump based system	0.126
Solar collector based system with PV	0.126
Air-water heat pump based system with PV	0.094

The systems including PV can be cost competitive if more rooftop area would be available. If more rooftop area would be available the LCOH of the air-water heat pump based system would be 0.068 €/kWh and 0.091 €/kWh for the solar collector based system. Still it is not believed the systems can be cost competitive since the cash flow saved on energy by the system is lower than the total interest paid on the investment. This results in the fact that the system will never repay itself when set off against the business as usual case.

The fact that the system cannot repay itself shows the systems are for now financially unattractive without subsidies. However, this is not the only metric the placement of green energy projects are decided on. The secondary benefits of the systems are socially relevant. Also, the expected lifetime of the system is about 30 years. It is not possible to account for the natural gas price fluctuations over the next 30 years. It is highly likely natural gas prices for domestic use will surge in the coming decades since, the Dutch government is actively discouraging the use of fossil fuels in the built environment by planning on increasing natural gas taxes and even forbidding new natural gas heating systems in new buildings.

10.5. Research Limitations

10.5. Research Limitations

The research presented in this study has its limitations as assumptions have been made. The limitations on the data analysis and the model are discussed in the following sections.

10.5.1. Limitations in the Data Analysis

The research is based on historic weather data (2015-2020) while the system will be built for a 30 year time period into the future for instance, from 2020-2050. Over a 30 year time period weather conditions and ambient temperatures may be affected due to climate change. The KNMI [5] notes that since the year 1906 the average temperature has increased by 1.9° C. During the last 30 years the average temperature has increased 0.04° C per annum. Figure 10.4 shows the average air temperatures since 1906 measured by the KNMI.

If this trend continues this could result in a significant decrease in heating demand. Over a 30 year time period the average temperature would increase $0.04 \times 30 = 1.2^{\circ}C$. This may not seem as much but it could significantly reduce the number of degree days and therefore the heating demand. An increase in the ambient temperature will also increase the COP of the air-water heat pump as well as the efficiency of the evacuated tube solar collectors.

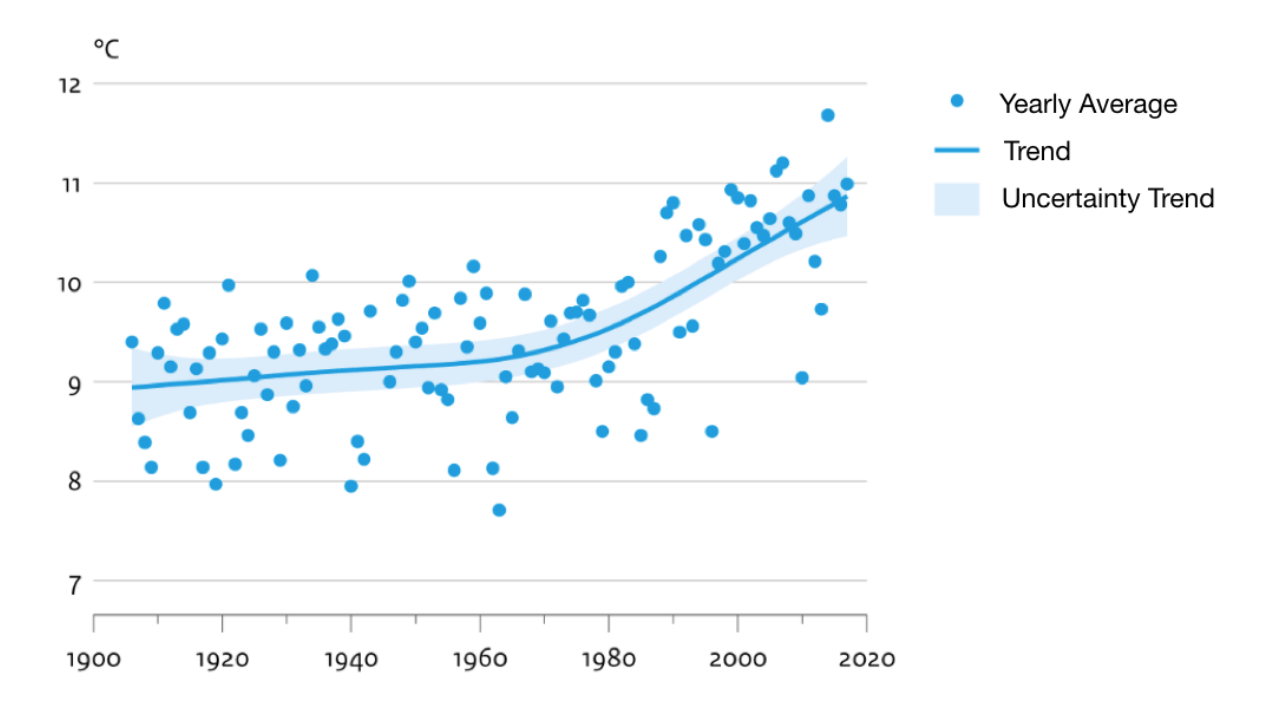


Figure 10.4: Average annual ambient air temperature since the year 1906. The measurements were taken by the KNMI at five different weather stations across the Netherlands. The figure shows an increase in average annual air temperature with an increase in warming rate from 1970-1980. The effect is believed to be caused by global warming due to the burning of fossil fuels. It is expected this trend will continue for some time into the future unless drastic measures are taken.

10.6. Recommendations

10.5.2. Limitations of the Model

The model is not perfect in every detail and is based on several assumptions mentioned during this study. Also certain control mechanisms can be improved for efficiency.

The control sequence that controls the air-water heat pump can be improved by detailing the operating moments. For instance, the heat pump should not operate at low ambient temperatures during late spring when the USTES is believed to contain enough energy to make it till warmer summer months where the heat pump will operate at higher COP's. This can increase the SCOP of the heat pump significantly. Also, in some years the USTES is at its maximum temperature in early summer. The heat losses throughout summer can be lowered when the reaching of the maximum energy capacity of the USTES is timed better at the end of summer. Finally it must be noted that it is not certain regulations allow for grid communications at zero cost. Further study is necessary to investigate the costs of a system that is heavily communicating with the grid as is the case with the air-water heat pump based system including PV.

10.6. Recommendations

The heat pump control mechanism introduced in this study is still very basic. It is believed that further studies on the control of the heat pump can drastically improve the efficiency of the entire system. With current control the USTES is already at its maximum capacity during early summer while it only needs to be at its maximum capacity at the end of the summer. A self learning algorithm can make the heat pump system more robust into the future considering the climate change and the ever increasing annual temperature fluctuations.

A system combining solar collectors and an air-water heat pump with a seasonal storage can perhaps utilise the best aspects of both systems proposed in this study. Further studies on this concept could especially be interesting for projects with limited rooftop area available.

Finally, the systems proposed in this study can have many secondary benefits. For instance, the air-water heat pump system can act as a peak shaver for the electricity grid. When an abundance of electricity is in the grid no curtailment is needed, instead the heat pump can be run under all conditions since the heat pump will always operate at a COP of at least 1. In the same way the auxiliary heating can be used to generate heat at very low, or even no cost.

Conclusion

The study shows that it is feasible, both technically and economically, to have a small scale district heating network operate year round based on renewable energy combined with a local seasonal heat storage.

For energy generation using solar thermal collectors evacuated tube solar collectors are the preferred choice over flat plate collectors in a cold climate like the Netherlands.

It was found that from a certain volume, the benefit of reduction in heat losses per m^3 due to the surface area to volume ratio disappears. This is due to the fact that the USTES is constant in height.

The air-water heat pump relying on R600a as refrigerant reaches COP's between 2.1-3.1 depending on the ambient air temperature at a sink inlet temperature of 40 °C and a sink outlet temperature of 90°C. This is about 0.48 the Carnot efficiency. It was found that the air-water heat pump capacity does not have a major impact on the LCOH as long as at least 150 kW capacity is installed. Less heat pump capacity results in insufficient heat collection where the USTES does not reach its full capacity.

Auxiliary heating in many cases is cheaper compared to installing additional system capacity. This is considered to be due to the low cost of electricity at high consumption and the increase in CAPEX and OPEX.

Both systems can reach "zero on the meter" when installing PV. The systems relying on PV are less expensive compared to grid imported electricity. For the "Energiek Nagele" project enough rooftop area is available although further reduction of the LCOH is possible since the area available does form a constraint. For future projects this might not be the case and needs to be taken into account.

The LCOH of the systems including PV can come down further if more rooftop area would be available. The rooftop area available used during this study is specific for the neighbourhood Karwijhof. In other projects this surface area may not be a constraint and lower LCOH may be obtained.

The cost of the district heating network is considerable compared to the total cost of the system. This is partly due to the layout of the DHN of project Nagele and can, in future system designs, be more efficient. This will lower the LCOH and increase the competitiveness to natural gas heating systems.

There is a difference in LCOH between the systems proposed during this study. Therefore a preferred system can be appointed, in this case the air-water heat pump system including a PV array is preferred. However, since for every project the conditions are different the solar collector based system may be more attractive in some cases. For instance, when a large central solar collector array can be installed, and noise disturbance is a major issue. While the air-water heat pump system will be more attractive in other situations for instance, projects with limited rooftop area or neighbourhoods where PV panels are already in place.

The systems including a PV array can compete with traditional heating systems based on the LCOH if rooftop area would not be a constraint. However, the systems cannot repay them self relative to the base scenario due to the financing costs making the deployment of these systems unattractive. By introducing subsidies (which currently are in place) and a more efficient DHN it will become more competitive when installing the

proposed systems in the real world. The likely scenario of higher natural gas prices in the future will increase the competitiveness of the systems proposed.

It can be concluded that the results presented can act as a starting point, a buildout of the model which incorporates subsidies and the social value for including seasonal storage in a shifting electricity system will show a more competitive LCOH which reflects the true value of USTES.

Acknowledgements

During my thesis I was supported by various people. First of all I would like to thank the company HoCoSto, and in particular Gerda and Rene Geerts for giving me the opportunity to do research on their innovative product.

I would like to thank prof. Carlos Infante Ferreira of the technical university of Delft for his effort as daily supervisor and reviewing my work.

Finally I would like to thank my fellow students Gijs Wolbert and Patriek Brouwer who helped me go through the, at times, stressful period of writing a thesis.

B.P. Ter Meulen Delft, May 2020

Bibliography

- [1] Cadafalch, J., and Carbonell, D., and Consul, R., and Ruiz R. (2015) Modelling of storage tanks with immersed heat exchangers. Solar Energy, Vol. 112 pp. 154-162, 2 2015. ISNN 0038-092X. doi: 10.1016/j.solener.2014.11.032. http://www.sciencedirect.com/science/article/pii/S0038092X14005763
- [2] Centraal Bureau van de Statistiek. Energie Cijfers. 2018. retrieved from https://longreads.cbs.nl/trends18/economie/cijfers/energie/#huishoudelijk-energieverbruik
- [3] Centraal Bureau van de Statistiek. Energieverbruik particuliere woningen. 2020. retrieved from https://opendata.cbs.nl/statline/#/CBS/nl/dataset/81528NED/table?fromstatweb
- [4] Centraal Bureau van de Statistiek. Energieverbruik van particuliere huishoudens. 2018. retrieved from https://www.cbs.nl/nl-nl/achtergrond/2018/14/energieverbruik-van-particuliere-huishoudens
- [5] Centraal Bureau van de Statistiek (CBS), and PBL Planbureau voor de Leefomgeving, and RIVM Rijksinstituut voor Volksgezondheid en Milieu, and Wageningen University and Research. (2018) Temperatuur in Nederland en mondiaal, 1906 2017. retrieved from https://www.clo.nl/indicatoren/nl0226-temperatuur-mondiaal-en-in-nederland
- [6] CED Greentech. Determining Module Inter-Row Spacing. retrieved from https://www.cedgreentech.com/article/\determining-module-inter-row-spacing
- [7] Chung, M., and Park, J., and Yoon, H., (1998) SIMULATION OF A CENTRAL SOLAR HEATING SYSTEM WITH SEASONAL STORAGE IN KOREA. Solar Energy, Vol 64(4-6), pp. 163-178, 12 1998. ISSN 0038-092X. doi: 10.1016/S0038-092X(98)00101-7. https://www.sciencedirect.com/science/ article/pii/S0038092X98001017
- [8] Cruickshank, A.C., and Baldwin, C. (2016) Sensible Thermal Energy Storage: Diurnal and Seasonal. Storing Energy, pp 291-311, 1 2016. doi: 10.1016/B978-0-12-803440-8.00015-4. https://www.sciencedirect.com/science/article/pii/B9780128034408000154#f0010
- [9] DINOloket. Data en Informatie van de Nederlandse Ondergrond. 1948. retrieved from https://www.dinoloket.nl/ondergrondgegevens
- [10] European Commission. (2019) The European Green Deal. page 9. retrieved from https://ec.europa.eu/info/sites/info/files/european-green-deal-communication_en.pdf
- [11] Eneco. Warmtepomp Rioolwater Zuivering Utrecht. retrieved from https://www.eneco.nl/over-ons/wat-we-doen/in-de-praktijk/warmtepomp-rwzi-utrecht/
- [12] Fischer, S., and Muller-Steinhagen, H., and Perers, B., and Bergquist, P. (2017) Collector test method under quasi-dynamic conditions according to European Standard EN 12975-2. retrieved from http://www.estif.org/solarkeymark/Links/Internal_links/wp1a/m3wp1ad3.pdf
- [13] Heller, A. (2000) 15 years of R&D in central solar heating in Denmark. Solar Energy, Vol. 69, pp 437-447. ISSN 0038-092X. doi: 10.1016/S0038-092X(00)00118-3.
- [14] Hydrosolar. How do vacuum tubes collector work. retrieved from https://hydrosolar.ca/blogs/news/how-do-vacuum-tubes-collector-work
- [15] Jazlan, A. (2014) Time Weighted Model Reduction of Flat Plate Solar Collectors. 11 2014.
- [16] Kalogirou, S.A. (2004) Solar thermal collectors and applications. Progress in Energy and Combustion Science, Vol. 30, pp. 231-295. ISSN 3601285. doi: 10.1016/j.pecs.2004.02.001.

Bibliography 110

[17] Kiss, A.A., and Infante Ferreira, C.A. (2017) Heat Pumps in Chemical Process Industry. CRC Press 2017. isbn 978-1-4987-1895-0.

- [18] Kloben Industries. Annex to Solar Keymark Certificate Summary of EN ISO 9806:2013 Test Results. DIN CERTCO, (25) 2 2019. retrieved from http://www.kloben.it/uploads/files/ProductAttachment/DB_0117S2904_R_Kloben_ATON_G_10121416182022__O_u__Natural_ATON_122000_163000_10COL943_20EM02_10COL\942_20EM02_10COL943Q_30EM02.pdf
- [19] KNMI. (2019) Weather data retrieved from KNMI (Dutch Meteorological Institute 2019. retrieved from http://projects.knmi.nl/klimatologie/uurgegevens/selectie.cgi
- [20] Lemmon, E.W., and Bell, I.H., and Huber, M.L., and McLinden, M.O. (2018) NIST Standard Reference Database 23: Reference Fluid Thermodynamic and Transport Properties-REFPROP, Version 10.0, National Institute of Standards and Technology. 2018. doi: http://dx.doi.org/10.18434/T4JS3C. https://www.nist.gov/srd/refprop
- [21] Mota-Babiloni, A., and Mateu-Royo, C., and Navarro-Esbrí, J., and Molés, F., and Amat-Albuixech, M., and Barragán-Cervera, Á. (2018) Optimisation of high-temperature heat pump cascades with internal heat exchangers using refrigerants with low global warming potential. Energy, Vol. 165(5), pp. 1248-1258, ISSN 0360-5442. doi: doi.org/10.1016/j.energy.2018.09.188. http://www.sciencedirect.com/science/article/pii/S0360544218319601.
- [22] Miltenburg van, R. (2016) Integration of decentralized solar collectors in Dutch district heating networks. Delft University of Technology. 4 2016.
- [23] Nash, A.L., and Badithela, A., and Jain, N. (2017) Dynamic modeling of a sensible thermal energy storage tank with an immersed coil heat exchanger under three operation modes. Applied Energy, Vol. 195, pp. 877-889, 6 2017. ISSN 0306-2619 doi: 10.1016/j.apenergy.2017.03.092 http://www.sciencedirect.com/science/article/pii/S0306261917303343.
- [24] Niessink, R.J.M. (2017) Temperature correction A Sensitivity Analysis. ECN Amsterdam 2017. https://publicaties.ecn.nl/PdfFetch.aspx?nr=ECN-N--17-039.
- [25] Novo, A.V., and Bayon, J.R., and Castro-Fresno, D., and Rodriguez-Hernandez, J. (2010) Review of seasonal heat storage in large basins: Water tanks and gravel—water pits. Applied Energy, Vol. 87(2), pp. 390-397, 22010. ISSN 0306-2619. doi: 10.1016/J.APENERGY.2009.06.033. https://www.sciencedirect.com/science/article/pii/S0306261909002694.
- [26] Rezaie, B., and Reddy, B.V., and Rosen, M.A. (2017) Assessment of the Thermal Energy Storage in Friedrichshafen District Energy Systems. Energy Procedia, Vol. 116, pp. 91-105, 6 2017. ISSN 876-6102. doi: 10.1016/J.EGYPRO.2017.05.058.https://www.sciencedirect.com/science/article/pii/ S1876610217322658.
- [27] Sarbu, I. and Sebarchievici, C. Chapter 3 Solar Collectors. 2017. isbn 9780128116623. doi: 10.1016/B978-0-12-811662-3.00003-7. http://dx.doi.org/10.1016/B978-0-12-811662-3.00003-7
- [28] Schmidt, T., and Mangold, D. (2009) Status of solar thermal seasonal storage in Germany. Steinbeis Research Insitute for Solar and Sustainable Thermal Energy Systems
- [29] Schmidt, T., and Mangold, D., and Müller-Steinhagen, H. (2003) SEASONAL THERMAL ENERGY STORAGE IN GERMANY. ISES Solar World Congress 2003.
- [30] Schmidt, T., and Mangold, D., and Müller-Steinhagen, H. (2004) Central solar heating plants with seasonal storage in Germany. Solar Energy, Vol. 76[1-3], pp. 165-174, 1 2004. ISSN 0038-092X. doi: 10.1016/J.SOLENER.2003.07.025. https://www.sciencedirect.com/science/article/pii/S0038092X03002937
- [31] Segers, R., and Oever van den, R., and Niessink, R., and Menkveld, m. (2017) Warmtemonitor 2017. CBS, TNO. retrieved from https://www.google.com/url?sa=t&rct=j&q=&esrc=s&source=web&cd=1&ved=2ahUKEwjT6cqIzsvnAhXNsaQKHZhHAGIQFjAAegQIBBAB&url=https%3A%2F%2Fwww.cbs.nl%2F-%2Fmedia%2F_pdf%2F2019%2F23%2Frapport%2520monitoring%2520warmte%25202017.pdf&usg=A0vVaw1_CNFJT_RgBLzunRnFZymT.

Bibliography 111

[32] Shelton, J. (1975) Underground storage of heat in solar heating systems. Solar Energy, Vol. 17(2), pp. 137-143, 5 1975. ISSN 0038-092X. doi: 10.1016/0038-092X(75)90070-5. https://www.sciencedirect.com/science/article/pii/0038092X75900705.

- [33] Sibbitt, B., and McClenahan, D., and Djebbar, R., and Thornton, J., and Wong, B., and Carriere, J., and Kokko, J. (2012) The Performance of a High Solar Fraction Seasonal Storage District Heating System Five Years of Operation. Energy Procedia, Vol. 30, pp. 856-865, 1 2012. ISSN 1876-6102. doi: 10.1016/J.EGYPRO.2012.11.097.https://www.sciencedirect.com/science/article/pii/S187661021201613X?via%3Dihub.
- [34] Smets, A., and Jager, K., and Isabella, O., and Swaaij van, R., and Zeman, M. (2016) Book Solar Energy 2016. UIT Cambridge Ltd. isbn: 9781906860325
- [35] Sorknæs, P. (2018) Simulation method for a pit seasonal thermal energy storage system with a heat pump in a district heating system. Energy, Vol. 152, pp. 533-538, 6 2018. ISSN 0360-5442. doi: 10.1016/J.ENERGY.2018.03.152. https://www.sciencedirect.com/science/article/pii/S0360544218305619.
- [36] SPF. SPF-Info User Manual Collector Catalogue. retrieved from https://www.spf.ch/index.php?id=17630
- [37] Sweet, M.L., and McLeskey, J.T. (2012) Numerical simulation of underground Seasonal Solar Thermal Energy Storage (SSTES) for a single family dwelling using TRNSYS. Solar Energy, Vol. 86(1), pp. 289-300, 1 2012. ISSN 0038-092X. doi: 10.1016/J.SOLENER.2011.10.002. https://www.sciencedirect.com/science/article/pii/S0038092X11003689.
- [38] Terziotti, L.T., and Sweet, M.L., and McLeskey, J.T. (2012) Modeling seasonal solar thermal energy storage in a large urban residential building using TRNSYS 16. Energy and Buildings, Vol. 45, pp. 28-31, 2 2012. ISSN 0378-7788. doi: 10.1016/J.ENBUILD.2011.10.023. https://www.sciencedirect.com/science/article/pii/S0378778811004671.
- [39] Trina Solar. Datasheet: Trina Solar DUOMAX dual glass 144 half-cell module. 2019. retrieved from https://static.trinasolar.com/sites/default/files/PS-M%20A%20Datasheet_Duomax_DEG15H.20%28II%29_NA_2019_A_0.pdf
- [40] Xu, J., and Wang, R.Z., and Li, Y.A. (2014) review of available technologies for seasonal thermal energy storage. Solar Energy, Vol. 103, pp. 610-638, 5 2014. ISSN 0038-092X. doi: 10.1016/J.SOLENER.2013.06.006. https://www.sciencedirect.com/science/article/pii/S0038092X13002272.